

Density-Functional Green Function Theory: Dynamical exchange-correlation field in lieu of self-energy

F. Aryasetiawan^{1,2}

¹*Department of Physics, Division of Mathematical Physics,
Lund University, Professorsgatan 1, 223 63, Lund, Sweden*

²*LINXS Institute of advanced Neutron and X-ray Science,
IDEON Building: Delta 5, Scheelevägen 19, 223 70 Lund, Sweden*

The one-particle Green function of a many-electron system is traditionally formulated within the self-energy picture. A different formalism was recently proposed, in which the self-energy is replaced by a dynamical exchange-correlation field, which acts on the Green function locally in both space and time. It was found that there exists a fundamental quantity, referred to as the dynamical exchange-correlation hole, which can be interpreted as effective density fluctuations induced in a many-electron system when a hole or an electron is introduced into the system, as in photoemission and inverse photoemission experiments. The dynamical exchange-correlation potential is simply the Coulomb potential of this exchange-correlation hole, which fulfils a sum rule and an exact constraint, identical to those satisfied by the static exchange-correlation hole in density-functional theory. The proposed formalism has been applied to a number of model systems such as the half-filled one-dimensional Hubbard model, the one-dimensional antiferromagnetic Heisenberg model, and the single-impurity Anderson model. The dynamical exchange-correlation hole and field of the homogeneous electron gas have also been studied with the view of constructing a density-functional approximation such as the local-density approximation. The availability of simple but accurate approximations for the exchange-correlation potential would circumvent costly computations of the traditional self-energy. The formalism may also provide new perspectives and insights into the many-body problem.

I. INTRODUCTION

The arrival of density-functional theory (DFT) in 1964-1965 [1, 2] witnessed one of the most important developments in condensed-matter theory and quantum chemistry [3–5]. The fundamental theorem of Hohenberg and Kohn [1] states that the ground-state density of a many-electron system uniquely determines the external potential. This seemingly simple theorem has far-reaching consequences: since the external potential uniquely determines the Hamiltonian it implies that *all* electronic properties of the system, ground-state as well as excited-state, are determined by the ground-state density, i.e., they are functionals of the ground-state density.

By itself, the Hohenberg-Kohn theorem has no immediate use, since the theorem provides no prescription on how to calculate electronic properties of the many-electron system. However, the ground-state energy possesses a special property in that it is minimised by the ground-state density. Were the ground-state energy as a functional of the ground-state density known, this variational property would yield, in principle, the Euler-Lagrange equation. An early example of this, long before the Hohenberg-Kohn theorem was known, is the Thomas-Fermi functional [6, 7], where the kinetic energy is approximated by that of a homogeneous electron gas in the spirit of the local-density approximation (LDA) [2]. However, the Thomas-Fermi energy functional is not sufficiently accurate for applications to real materials. It is too crude to reproduce, for example, the shell structure in the ground-state density of atoms.

The practical development of DFT was made possible by the Kohn-Sham scheme [2], which introduces the

concept of an auxiliary noninteracting system with the same density as that of the interacting system. The total ground-state energy is reshuffled into a sum of the noninteracting kinetic energy of the auxiliary system and the rest, which includes the difference between the interacting and the noninteracting kinetic energies, lumped into the exchange-correlation (xc) energy. The variational property of the total energy leads to the famous Kohn-Sham equation, which is a one-particle Schrödinger equation. Since the kinetic energy is calculated directly for the noninteracting system, the need for an explicit kinetic energy functional is avoided. There remains the problem of finding a good approximation for the xc functional, which fortunately can be approximated by explicit expressions of the density sufficiently accurate for making theoretical predictions. Starting with the LDA, more accurate functionals have been continuously developed over the years [8–11] (for reviews, see, for example, [4, 12]), and the recent use of machine learning [13, 14] may accelerate further development. The Kohn-Sham scheme is rather revolutionary, since the complicated many-electron problem of calculating the ground-state energy is reduced to solving the single-particle Kohn-Sham equation self-consistently.

Although the Kohn-Sham scheme has been very successful in calculating ground-state properties, the extension of DFT to calculations of excitation spectra remains an open challenge. The challenge of developing a density-functional formalism for excited states arose almost immediately after the birth of DFT. Almost 60 years ago, Sham and Kohn [15] addressed this challenge by considering the Green function approach with the associated self-energy. The self-energy of the homogeneous electron

gas, which can be calculated within the random-phase approximation (RPA) [16] or the *GW* approximation [17–20], is used as a reference. The LDA for the self-energy can then be applied. This approach was implemented by Wang and Pickett [21] and later improved by Godby *et al.* [22] to account for nonlocality of the self-energy. The applicability of this approach appears to be rather limited and has not found widespread use.

A promising approach to extend DFT to calculations of excited-state energies is via ensemble DFT [23–26]. By generalising DFT to mixtures of ground and excited states, it is possible to determine specifically chosen excitation energies at low cost. However, the method may not be suitable for calculating excitation spectra which are continuous such as those of solids.

An extension of DFT to time-dependent DFT (TDDFT) [27–32] provides a route for calculating excitation energies. TDDFT offers a rigorous formalism for describing the time evolution of an electron density under a time-varying external field [29]. This allows one to obtain the linear density-response function from which excitation energies can be extracted. However, the excitation energies correspond to the N -electron system, i.e., electron-number-conserving excitations. Excitations involving removal and addition of an electron resulting in $N \pm 1$ electrons corresponding to photoemission and inverse photoemission are difficult to simulate within TDDFT. To overcome this difficulty, a steady-state DFT was recently proposed [33, 34].

This article describes a recently proposed density-functional approach to determine the Green function [35] from which excitation spectra measured in angle-resolved photoemission and inverse photoemission can be extracted. This formalism replaces the self-energy by a dynamical xc field or potential, hereafter referred to as V_{xc} , which acts locally in both space and time on the Green function. V_{xc} is shown to be the Coulomb potential of a dynamical xc hole, which as the xc hole in DFT fulfils a sum rule and an exact constraint, providing a natural link to the ground-state density. This is analogous to the Slater exchange potential [36], which can in fact be seen as a special case of V_{xc} when correlations are neglected.

The dynamical xc hole can be thought of as density fluctuations induced when a hole or an electron is introduced into a many-electron system, as in photoemission and inverse photoemission experiments. The concept of xc hole offers a fundamentally different perspective of viewing the many-electron problem from the traditional self-energy. On the one hand, the xc hole connects the V_{xc} formalism to DFT and on the other hand opens a path to dynamical correlations not accessible in Kohn-Sham DFT. This duality allows for harnessing a wealth of DFT-inspired approximations while at the same time taking advantage of well-established approximations from many-body theory such as the RPA to incorporate dynamical correlations.

Since the formalism is exact, there is no restriction in

applying it to systems with strong electron correlations. This is illustrated in Sec. XVIII in which applications to the one-dimensional Hubbard and Heisenberg models as well as the single-impurity Anderson model are described. For weakly to moderately correlated systems, LDA-based approximations can be expected to work well, as in traditional DFT. A first step towards this direction is to calculate V_{xc} for the homogeneous electron gas elaborated in Sec. XVII with the aim of parametrising the resulting V_{xc} as a function of density.

A potentially important advantage of the V_{xc} formalism is in dealing with nonequilibrium systems. Due to the local character of V_{xc} in both space and time, the equation of motion of the Green function can be solved piecewise in time, in contrast to the traditional self-energy formalism, which requires knowledge of the self-energy for all time.

Although the present article is focused on fermions, the formalism can be extended to bosons and spin systems. An example of the latter is given in Sec. XVIII B, which describes an application to the one-dimensional antiferromagnetic Heisenberg model.

II. SLATER EXCHANGE HOLE AND POTENTIAL

In his attempt in the early 1950's [36] to simplify the Hartree-Fock equation by replacing the nonlocal exchange potential by a local one Slater discovered the exchange hole, a quantity of great importance in DFT, both from the conceptual and practical points of view. Slater's motivation was numerical; considering the state of computers at that time, it was not feasible to solve the Hartree-Fock equation for molecules and solids with a nonlocal exchange potential.

The nonlocal Fock exchange is given by

$$\Sigma_x(r, r') = -v(r - r') \sum_i^{\text{occ}} \phi_i(r) \phi_i^*(r'), \quad (1)$$

where the sum is over the lowest occupied (occ) orbitals and $v(r - r') = 1/|\mathbf{r} - \mathbf{r}'|$. The nonlocal exchange potential appears in the Hartree-Fock equation as

$$\int dr' \Sigma_x(r, r') \phi_k(r'). \quad (2)$$

Slater defined an orbital-dependent local potential

$$V_k(r) = \frac{1}{\phi_k(r)} \int dr' \Sigma_x(r, r') \phi_k(r') \quad (3)$$

so that

$$\int dr' \Sigma_x(r, r') \phi_k(r') = V_k(r) \phi_k(r). \quad (4)$$

Thus, the nonlocal Fock exchange when acting on a given orbital has been converted into a local potential, albeit orbital-dependent.

The local but orbital-dependent potential is in essence a rephrasing of the Fock exchange since orbital dependence implies nonlocality. Slater proceeded further and introduced an orbital-averaged potential:

$$\begin{aligned} V^S(r) &= \sum_k^{\text{occ}} \frac{|\phi_k(r)|^2}{\rho(r)} V_k(r) \\ &= - \int dr' v(r-r') \frac{1}{\rho(r)} \sum_{ik}^{\text{occ}} \phi_k^*(r) \phi_i(r) \phi_i^*(r') \phi_k(r'), \end{aligned} \quad (5)$$

where $\rho(r)$ is the ground-state density,

$$\rho(r) = \sum_k^{\text{occ}} |\phi_k(r)|^2. \quad (6)$$

The local orbital-independent potential $V^S(r)$ is known as the Slater $X\alpha$ exchange potential, which replaces the nonlocal Fock exchange potential:

$$\left[-\frac{1}{2} \nabla^2 + V_{\text{ext}}(r) + V^H(r) + V^S(r) \right] \phi_k(r) = \varepsilon_k \phi_k(r). \quad (7)$$

This equation is much more amenable to a numerical solution compared to the original Hartree-Fock equation.

Slater made an important observation: In any electronic system, the quantity

$$\rho_x(r, r') = -\frac{1}{\rho(r)} \sum_{ik}^{\text{occ}} \phi_k^*(r) \phi_i(r) \phi_i^*(r') \phi_k(r') \quad (8)$$

fulfils a sum rule and an exact constraint for *any* r :

$$\int d^3r' \rho_x(r, r') = -\delta_{\sigma\sigma'}, \quad \rho_x(r, r) = -\rho(r), \quad (9)$$

which can be readily verified. Note that the notation $r = (\mathbf{r}, \sigma)$ is used. Since the sum rule is independent of r one may write for $\sigma = \sigma'$,

$$\rho_x(\mathbf{r}, \mathbf{r}') = \rho_x(\mathbf{r}, \mathbf{r} + \mathbf{R}), \quad \mathbf{R} = \mathbf{r}' - \mathbf{r}, \quad (10)$$

so that

$$\int d^3R \rho_x(\mathbf{r}, \mathbf{r} + \mathbf{R}) = -1. \quad (11)$$

The above sum rule and the exact constraint motivate the interpretation of $\rho_x(r, r')$ as an exchange hole. For an electron at \mathbf{r} , the exchange-hole density at the position of the electron is the negative of the electron density. The exchange interaction (Pauli principle) pushes away electrons of the same spin, creating a hole around the given electron at \mathbf{r} , which as a function of \mathbf{R} integrates to a negative unit charge, *independent* of \mathbf{r} .

From Eq. (5), it is evident that the Slater potential can be regarded as the Coulomb potential generated by the exchange hole:

$$V^S(r) = \int dr' v(r-r') \rho_x(r, r'). \quad (12)$$

Because the exchange hole integrates to a negative unit charge, it is to be expected that the Slater potential is negative. The sum rule and the exact constraint have a very important consequence. As explained by Slater [37], if the exchange hole is approximated by a sphere with radius R_0 and assumed to have a constant density $\rho(r)$ as a function of r' one finds

$$\frac{4\pi}{3} R_0^3 \rho(r) = 1 \rightarrow R_0 = \left[\frac{3}{4\pi\rho(r)} \right]^{1/3}. \quad (13)$$

The Coulomb potential due to this exchange hole at \mathbf{r} , the centre of the sphere, is given by

$$\rho(r) \int d^3r' \frac{\theta(R_0 - |\mathbf{r}' - \mathbf{r}|)}{|\mathbf{r}' - \mathbf{r}|} = 2\pi\rho(r)R_0^2 \quad (14)$$

which is proportional to $\rho^{1/3}$, the well-known local-density dependence of the exchange potential. Note that this $\rho^{1/3}$ -dependence does not depend on the homogeneous electron gas. If the exchange hole of the homogeneous electron gas is used as a model, the Slater potential is given by

$$V^S(r) = -3 \left[\frac{3}{4\pi\rho(r)} \right]^{1/3}. \quad (15)$$

The finding that the exchange potential can be approximated by the local density and varies as $\rho^{1/3}$ can be regarded as the precursor of the LDA in DFT. The exchange potential in the LDA of DFT obtained by taking the functional derivative of the exchange energy of the homogeneous electron gas with respect to the density is equal to $\frac{2}{3}V^S(r)$.

The Slater local potential was meant to be an approximation to the non-local Fock exchange, but it was discovered that the bond energies of molecules obtained from the Slater potential were curiously superior to those calculated from the Hartree-Fock equation [4]. The bond energy of a molecule is the difference between the total energies of the molecule and the constituent atoms, which is a very important quantity in chemistry and physics.

Another indication of the significance of the Slater local potential is provided by prediction of the quasiparticle dispersion of the homogeneous electron gas. In this case, the Slater potential is simply constant, implying that the quasiparticle dispersion up to a constant shift is identical to that of the free-electron gas, namely, $\varepsilon(k) = \frac{1}{2}k^2$. This is in stark contrast to the dispersion calculated within the Hartree-Fock approximation, which widens the occupied band width by approximately a factor of two for $r_s \approx 3 \sim 4$ [38], representative of metallic systems. The logarithmic singularity of the derivative of the Hartree-Fock dispersion at the Fermi wave vector leads to a zero density of states at the Fermi level, which is nonphysical [38]. The exact dispersion is not known, but one can expect with confidence that the dispersion calculated within the *GW* approximation should be close to the exact one. The *GW* dispersion essentially resembles that

of the free-electron gas with $\approx 10\%$ narrowing of the occupied band [39]. This implies that the band widening resulting from a nonlocal exchange is cancelled to a great extent by correlations.

One can conclude that the Slater potential is actually a rather poor approximation to the nonlocal exchange since it yields a superior electron gas dispersion and bonding energy in molecules. This implies that the Slater potential contains to a large extent, in the sense of many-body perturbation theory, the effects of correlations. In systems where the valence electrons can be modelled by the electron gas, the combined effects of exchange and correlations may be better represented by a local potential.

There is a subtle difference between the Slater potential and the exchange potential in Kohn-Sham DFT. This difference can be understood by considering the exact expression for the exchange energy:

$$\begin{aligned} E_x &= \frac{1}{2} \int dr' dr'' \rho(r') v(r' - r'') \rho_x(r', r'') \\ &= \frac{1}{2} \int dr' dr'' \rho(r') v(r' - r'') [g_x(r', r'') - 1] \rho(r''), \end{aligned} \quad (16)$$

where

$$\rho_x(r, r') = [g_x(r, r') - 1] \rho(r'). \quad (17)$$

$g_x(r, r')$ is the exchange-only pair distribution function. The exchange potential in DFT is given by

$$\begin{aligned} V_x(r) &= \frac{\delta E_x}{\delta \rho(r)} \\ &= V^S(r) + \frac{1}{2} \int dr' dr'' \rho(r') v(r' - r'') \frac{\delta g_x(r', r'')}{\delta \rho(r)} \rho(r''). \end{aligned} \quad (18)$$

From the above equation it is clear that the Kohn-Sham exchange potential is not the Coulomb potential of the exchange hole. In addition to the Coulomb potential, there is a complicated term involving a three-point vertex function $\delta g_x(r', r'')/\delta \rho(r)$, which may be the origin of the pathology that is sometimes observed in the Kohn-Sham potential. In fact, this pathology was convincingly demonstrated for the beryllium atom by explicitly calculating the vertex function. The resulting vertex contribution exhibits a step structure, which is constant within the atomic shells and changes abruptly at the shell boundaries [40].

Slater's work anticipates much of the practical aspect of DFT. However, the idea that the local exchange potential is the Coulomb potential of the exchange hole has not been further developed. Development in DFT has followed the Kohn-Sham scheme of having an auxiliary noninteracting system. For example, an extension to nonequilibrium systems in the presence of a time-dependent potential also employs a Kohn-Sham noninteracting auxiliary system [29, 30].

III. TRADITIONAL SELF-ENERGY FORMALISM

The time-ordered Green function is defined as [41–43]

$$iG(rt, r't') = \langle T[\hat{\psi}(rt)\hat{\psi}^\dagger(r't')] \rangle, \quad (19)$$

where the expectation value is taken with respect to the interacting many-electron ground state. T is the time-ordering symbol and $\hat{\psi}(rt)$ is the field operator in the Heisenberg picture,

$$\hat{\psi}(rt) = \hat{U}(0, t)\hat{\psi}(r)\hat{U}(t, 0), \quad (20)$$

where the time-evolution operator is given by

$$\hat{U}(t, 0) = T e^{-i \int_0^t dt' \hat{H}(t')}. \quad (21)$$

For systems in equilibrium, the time-evolution operator simplifies to $\hat{U}(t, 0) = \exp(-i\hat{H}t)$, in which the many-electron Hamiltonian is given by

$$\begin{aligned} \hat{H} &= \int dr \hat{\psi}^\dagger(r) h_0(r) \hat{\psi}(r) \\ &+ \frac{1}{2} \int dr dr' \hat{\psi}^\dagger(r) \hat{\psi}^\dagger(r') v(r - r') \hat{\psi}(r') \hat{\psi}(r), \end{aligned} \quad (22)$$

where

$$h_0(r) = -\frac{1}{2} \nabla^2 + V_{\text{ext}}(r). \quad (23)$$

In this case, the Green function depends only on the time difference $t - t'$ so that t' can be set to zero. For a Hamiltonian without a spin-flip term such as the one above, the Green function is diagonal in spin space, that is, $\sigma = \sigma'$. The equation of motion of the Green function is obtained from the Heisenberg equation of motion of the field operator:

$$\begin{aligned} i\partial_t \hat{\psi}(rt) &= [\hat{\psi}(rt), \hat{H}] \\ &= \left(h_0(r) + \hat{V}_H(rt) \right) \hat{\psi}(rt), \end{aligned} \quad (24)$$

where

$$\hat{V}_H(rt) = \int dr' v(r - r') \hat{\rho}(r't). \quad (25)$$

Here, $\hat{\rho}(rt) = \hat{\psi}^\dagger(rt)\hat{\psi}(rt)$ is the density operator. Constructing two equations by multiplying Eq. (24) from the left and right by $\hat{\psi}^\dagger(r')$ ($t' = 0$) leads to the equation of motion of the Green function,

$$\begin{aligned} [i\partial_t - h_0(r)] G(r, r'; t) \\ + i \int dr'' v(r - r'') \langle T[\hat{\rho}(r''t) \hat{\psi}(rt) \hat{\psi}^\dagger(r')] \rangle \\ = \delta(r - r') \delta(t). \end{aligned} \quad (26)$$

The interaction term with the Coulomb potential contains the following,

$$iG^{(2)}(r, r', r''; t) = \langle T[\hat{\rho}(r''t)\hat{\psi}(rt)\hat{\psi}^\dagger(r't)] \rangle, \quad (27)$$

which is a special case of the two-particle Green function. (Note that the definition of $G^{(2)}$ in this article differs from the one in Ref. [44] by a factor $-i$.) The equation of motion of the two-particle Green function in turn contains the three-particle Green function, and so forth. Traditionally, this hierarchy of equations is truncated by introducing the self-energy Σ defined as [18]

$$\begin{aligned} & \int dr'' dt'' \Sigma(r, r''; t - t'') G(r'', r'; t'') \\ &= \int dr'' v(r - r'') G^{(2)}(r, r', r''; t) - V_H(r) G(r, r'; t), \end{aligned} \quad (28)$$

where the Hartree mean-field V_H has been subtracted from $G^{(2)}$. The equation of motion becomes

$$\begin{aligned} & [i\partial_t - h_0(r) - V_H(r)] G(r, r'; t) \\ & - \int dr'' dt'' \Sigma(r, r''; t - t'') G(r'', r'; t'') = \delta(r - r') \delta(t). \end{aligned} \quad (29)$$

The self-energy then accounts for the effects of exchange and correlations of the many-electron system. It is also a natural quantity that emerges when the Green function is calculated using the many-body perturbation theory based on Wick's theorem [41, 42].

IV. DYNAMICAL XC HOLE

In this section, it is shown that there is a universal quantity, referred to as the dynamical xc hole, which fulfils a sum rule and a strict constraint independent of the particular systems. It will be shown later in Sec. VII A that its static ($t = 0$) and equal-space ($r' = r$) limit in the absence of correlations is identical with the Slater exchange hole. The Coulomb potential of this dynamical xc hole generates V_{xc} , formally replacing the nonlocal self-energy. Thus, it may be seen that the Slater exchange potential is a special case of static V_{xc} without correlations.

In the proposed framework, a correlation function g , which correlates the electron density and the Green function, is introduced [35]:

$$\begin{aligned} G^{(2)}(r, r', r''; t) &= -i \langle T[\hat{\rho}(r''t)\hat{\psi}(rt)\hat{\psi}^\dagger(r't)] \rangle \\ &= G(r, r'; t) g(r, r', r''; t) \rho(r''). \end{aligned} \quad (30)$$

$G^{(2)}$ can be rewritten as

$$G^{(2)}(r, r', r''; t) = [\rho(r'') + \rho_{xc}(r, r', r''; t)] G(r, r'; t), \quad (31)$$

where

$$\rho_{xc}(r, r', r''; t) = [g(r, r', r''; t) - 1] \rho(r'') \quad (32)$$

can be interpreted as an xc hole since it integrates to -1 for $t < 0$ as will be shown below.

To show the sum rule, consider integrating $G^{(2)}$ over the space variable \mathbf{r}'' . For $t < 0$ one finds

$$\begin{aligned} & i \int d^3 r'' G^{(2)}(r, r', r''; t < 0) \\ &= - \int d^3 r'' \langle \hat{\psi}^\dagger(r') \hat{\rho}(r''t) \hat{\psi}(rt) \rangle \\ &= - \langle \hat{\psi}^\dagger(r') \hat{N}_{\sigma''}(t) \hat{\psi}(rt) \rangle, \end{aligned} \quad (33)$$

where

$$\hat{N}_\sigma = \int d^3 r \hat{\rho}(r) \quad (34)$$

is the number operator that counts the number of electrons with spin σ in the system. It then follows that

$$\begin{aligned} & \int d^3 r'' G^{(2)}(r, r', r''; t < 0) \\ &= i(N_{\sigma''} - \delta_{\sigma\sigma''}) \langle \hat{\psi}^\dagger(r') \hat{\psi}(rt) \rangle \\ &= (N_{\sigma''} - \delta_{\sigma\sigma''}) G(r, r'; t < 0). \end{aligned} \quad (35)$$

From Eq. (31),

$$\begin{aligned} & \int d^3 r'' G^{(2)}(r, r', r''; t) \\ &= \left[N_{\sigma''} + \int d^3 r'' \rho_{xc}(r, r', r''; t) \right] G(r, r'; t), \end{aligned} \quad (36)$$

which when compared with Eq. (35) yields the sum rule,

$$\int d^3 r'' \rho_{xc}(r, r', r''; t < 0) = -\delta_{\sigma\sigma''} \quad (37)$$

for any r, r' , and $t < 0$. This justifies the interpretation of ρ_{xc} as an xc hole.

A similar derivation can be carried out for $t > 0$ and one finds

$$\int d^3 r'' G^{(2)}(r, r', r''; t > 0) = N_{\sigma''} G(r, r'; t > 0). \quad (38)$$

The sum rule for $t > 0$ is therefore

$$\int d^3 r'' \rho_{xc}(r, r', r''; t > 0) = 0. \quad (39)$$

The sum rule for any r, r' , and t can be summarised as

$$\int d^3 r'' \rho_{xc}(r, r', r''; t) = -\delta_{\sigma\sigma''} \theta(-t). \quad (40)$$

It can also be seen from the definition of $G^{(2)}$ in Eq. (30) that

$$\begin{aligned} iG^{(2)}(r, r', r; t) &= \langle T[\hat{\rho}(rt)\hat{\psi}(rt)\hat{\psi}^\dagger(r')] \rangle \\ &= \langle T[\hat{\psi}^\dagger(rt)\hat{\psi}(rt)\hat{\psi}(rt)\hat{\psi}^\dagger(r')] \rangle = 0 \end{aligned} \quad (41)$$

since $\hat{\psi}(rt)\hat{\psi}(rt) = 0$ so that

$$g(r, r', r; t) = 0. \quad (42)$$

It follows from Eq. (32) that the xc hole fulfils a strict constraint,

$$\rho_{xc}(r, r', r; t) = -\rho(r), \quad (43)$$

for any r, r' , and t .

V. VXC AND THE EQUATION OF MOTION OF THE GREEN FUNCTION

Using the expression for $G^{(2)}$ in Eq. (31), the equation of motion of the Green function in Eq. (26) becomes

$$[i\partial_t - h(r) - V_{xc}(r, r'; t)] G(r, r'; t) = \delta(r - r')\delta(t), \quad (44)$$

where

$$h(r) = h_0(r) + V_H(r), \quad (45)$$

and

$$V_{xc}(r, r'; t) = \int dr'' v(r - r'') \rho_{xc}(r, r', r''; t), \quad (46)$$

which is simply the classical Coulomb potential of the xc hole. Mathematically it can also be viewed as the Lagrange parameter which ensures that the Green function is correctly reproduced. This potential may in general be complex so that the Hamiltonian is nonhermitian. The form of the equation of motion of the Green function is identical to the time-dependent Schrödinger equation. Treating r' as a parameter, the Green function is analogous to the wave function but it can decay due to the potential V_{xc} being complex. This property is elaborated further in Sec. XIV.

The xc hole may be interpreted as effective density fluctuations induced in a many-electron system when a hole ($t < 0$) or an electron ($t > 0$) is added. The added hole or electron experiences the Coulomb potential arising from the density fluctuations (xc hole) as it propagates through the system. However, these density fluctuations are in general complex and therefore not experimentally observable.

An important feature that distinguishes Vxc from the self-energy is its local character in time. Due to this feature, the Green function can be propagated point-wise in time since its value at time t can be used to calculate the value at an infinitesimal time later without knowing its previous values at earlier time than t . In this sense, as with the time-dependent Schrödinger equation, the equation of motion has no memory. This is in contrast to the self-energy approach which requires knowledge of the Green function at all time due to the time convolution between the self-energy and the Green function.

Vxc and the self-energy differ in a fundamental way in that the former is local whereas the latter is nonlocal in space. The nonlocality in space renders expressing the self-energy as a functional of the density difficult, which is illustrated by the nonlocal exchange self-energy. The form of the nonlocal exchange in terms of products of orbitals permits no simple approximation in terms of the density. The problem is akin to the kinetic energy, which is also nonlocal. The kinetic energy expressed as a density functional such as the Thomas-Fermi functional [6, 7] and its improvements has not been particularly successful. This problem is avoided in the Kohn-Sham DFT [2] by directly calculating the kinetic energy using orbitals. In contrast, the Slater local exchange potential can be naturally approximated in terms of the density, as described in Sec. II. However, the local exchange potential is not a good approximation to the nonlocal one, as illustrated by the electron-gas dispersion, for which the local exchange potential and the nonlocal Fock exchange give very different results. The Slater local exchange potential performs much better than the nonlocal Fock exchange.

A. Equation of motion in orbital basis

Expressed in a set of base orbitals $\{\varphi_i\}$, the Green function can be written as

$$G(r, r'; t) = \sum_{ij} \varphi_i(r) G_{ij}(t) \varphi_j(r'). \quad (47)$$

In the orbital basis, the equation of motion in Eq. (44) takes the form

$$i \frac{\partial}{\partial t} G_{ij}(t) - \sum_k h_{ik} G_{kj}(t) - \sum_{kl} V_{ik,lj}^{xc}(t) G_{kl}(t) = \delta_{ij} \delta(t), \quad (48)$$

where G_{ij} and h_{ik} are the matrix elements of G and h in the orbitals and

$$V_{ik,lj}^{xc}(t) = \int d^3r d^3r' \varphi_i^*(r) \varphi_k(r) V_{xc}(r, r'; t) \varphi_l^*(r') \varphi_j(r'). \quad (49)$$

The presence of four orbital indices is indicative of the two-particle bosonic character of V_{xc} , in contrast to the self-energy which is fermionic.

B. Spectral representation of V_{xc}

Although Vxc is naturally expressed in the time domain, its spectral properties may provide useful information when constructing approximations. To analyse the spectral representation of V_{xc} , it is necessary to investigate the spectral representation of $G^{(2)}$. This is achieved by inserting in the definition of $G^{(2)}$ a complete set of eigenstates of the $N \pm 1$ -system,

$$\hat{H} |\Psi_m^{N\pm 1}\rangle = E_m^{N\pm 1} |\Psi_m^{N\pm 1}\rangle. \quad (50)$$

For $t > 0$

$$\begin{aligned}
iG^{(2)} &= \langle \Psi_0 | \hat{\rho}(r'') \hat{\psi}(r, t) \hat{\psi}^\dagger(r') | \Psi_0 \rangle \\
&= \langle \Psi_0 | e^{i\hat{H}t} \hat{\rho}(r'') \hat{\psi}(r) e^{-i\hat{H}t} | \Psi_m^{N+1} \rangle \langle \Psi_m^{N+1} | \hat{\psi}^\dagger(r') | \Psi_0 \rangle \\
&= \sum_m \langle \Psi_0 | \hat{\rho}(r'') \hat{\psi}(r) | \Psi_m^{N+1} \rangle \langle \Psi_m^{N+1} | \hat{\psi}^\dagger(r') | \Psi_0 \rangle \\
&\quad \times e^{-i(E_m^{N+1} - E_0)t}.
\end{aligned} \tag{51}$$

For $t < 0$

$$\begin{aligned}
iG^{(2)} &= -\langle \Psi_0 | \hat{\psi}^\dagger(r') \hat{\rho}(r'') \hat{\psi}(r, t) | \Psi_0 \rangle \\
&= -\sum_m \langle \Psi_0 | \hat{\psi}^\dagger(r') | \Psi_m^{N-1} \rangle \langle \Psi_m^{N-1} | \hat{\rho}(r'') \hat{\psi}(r) | \Psi_0 \rangle \\
&\quad \times e^{i(E_m^{N-1} - E_0)t}.
\end{aligned} \tag{52}$$

This spectral decomposition shows that $G^{(2)}$ shares the same spectral structure as G in terms of the excitation energies of the $N \pm 1$ system but with different spectral weights. Since G is fermionic, it follows that $G^{(2)}$ is also fermionic.

From the relation

$$\begin{aligned}
V_{xc}(r, r'; t) G(r, r'; t) &= \int dr'' v(r - r'') G^{(2)}(r, r', r''; t) \\
&\quad - V_H(r) G(r, r'; t)
\end{aligned} \tag{53}$$

it is clear that the spectral property of the left-hand side must be fermionic since the Coulomb potential v and the Hartree potential V_H are static and do not alter the spectral property of $G^{(2)}$ and G , which are both fermionic.

To find out the spectral property of V_{xc} , it is useful to make comparison with the self-energy in the GW approximation,

$$\Sigma(r, r'; t) = iG(r, r'; t)W(r, r'; t). \tag{54}$$

Here, the screened interaction W is bosonic whereas Σ is fermionic. Since $V_{xc}G$ is fermionic and G itself is fermionic, it can be conjectured that analogous to W , V_{xc} should be bosonic. V_{xc} consists of static and dynamic terms:

$$V_{xc}(r, r'; t) = V_{xc}^S(r, r') + V_{xc}^D(r, r'; t). \tag{55}$$

Similarly to the dynamic part of the screened interaction W [18, 19], the dynamic part of V_{xc} has a bosonic spectral representation,

$$-iV_{xc}^D(\omega) = \int_{-\infty}^0 d\omega' \frac{B(\omega')}{\omega - \omega' - i\delta} + \int_0^\infty d\omega' \frac{B(\omega')}{\omega - \omega' + i\delta}, \tag{56}$$

where the chemical potential is absent.

VI. FORMAL EXPRESSION FOR THE XC HOLE

The xc hole is a fundamental quantity, since its Coulomb potential generates V_{xc} . The xc hole is expressible as a linear response of the Green function with

respect to an external probing field $\varphi(rt)$. This can be understood by considering the two-particle Green function $G^{(2)}$ which can be expressed as a functional derivative of the Green function with respect to the probing field $\varphi(rt)$. It is convenient to use the notation $1 = (r_1 t_1)$ etc. With this notation, the equation of motion is given by

$$\begin{aligned}
&[i\partial_1 - h_0(1)]G(1, 2) \\
&+ i \int d3 v(1 - 3) \langle T[\hat{\rho}(3) \hat{\psi}(1) \hat{\psi}^\dagger(2)] \rangle = \delta(1 - 2).
\end{aligned} \tag{57}$$

From the Schwinger functional derivative method [18, 19]

$$G^{(2)}(1, 2, 3) = \rho(3)G(1, 2) + i \frac{\delta G(1, 2)}{\delta \varphi(3)}. \tag{58}$$

It follows immediately from the definition of the xc hole in Eq. (31) that [44]

$$\rho_{xc}(1, 2, 3)G(1, 2) = i \frac{\delta G(1, 2)}{\delta \varphi(3)} \tag{59}$$

or more compactly

$$\rho_{xc}(1, 2, 3) = i \frac{\delta}{\delta \varphi(3)} \ln G(1, 2). \tag{60}$$

It is understood that the probing field is set to zero once the derivative is taken.

The identity

$$GG^{-1} = 1 \rightarrow \delta G = -G\delta G^{-1}G \tag{61}$$

yields

$$\frac{\delta G(1, 2)}{\delta \varphi(3)} = - \int d4d5 G(1, 4) \frac{\delta G^{-1}(4, 5)}{\delta \varphi(3)} G(5, 2). \tag{62}$$

Together with

$$G^{-1}(1, 2) = (i\partial_1 - h(1) - \varphi(1))\delta(1 - 2) - \Sigma(1, 2), \tag{63}$$

which follows from the equation of motion of G in the presence of the probing field, one arrives at [44, 45]

$$\begin{aligned}
&\rho_{xc}(1, 2, 3)G(1, 2) \\
&= i \int d4 G(1, 4) \left\{ \delta(3 - 4) + \frac{\delta V_H(4)}{\delta \varphi(3)} \right\} G(4, 2) \\
&\quad + i \int d4d5 G(1, 4) \frac{\delta \Sigma(4, 5)}{\delta \varphi(3)} G(5, 2).
\end{aligned} \tag{64}$$

The first term on the right-hand side, $iG(1, 3)G(3, 2)$, corresponds to the exchange contribution. The second term involving $\frac{\delta V_H}{\delta \varphi}$ will be referred to as the density-response contribution, and the last term with $\frac{\delta \Sigma}{\delta \varphi}$ as the vertex correction. The second and third terms together constitute the correlation contribution and neglecting the third term (vertex correction) amounts to RPA.

The quantity in the curly brackets can be identified as the inverse dielectric function:

$$\epsilon^{-1}(4, 3) = \delta(4 - 3) + \frac{\delta V_H(4)}{\delta \varphi(3)}. \quad (65)$$

It is convenient to define

$$K(4, 3) = \frac{\delta V_H(4)}{\delta \varphi(3)} = \int d5 v(4 - 5) \chi(5, 3), \quad (66)$$

where χ is the linear density-response function

$$\chi(5, 3) = \frac{\delta \rho(5)}{\delta \varphi(3)}. \quad (67)$$

and

$$v(1 - 2) = v(r_1 - r_2) \delta(t_1 - t_2), \quad (68)$$

reflecting the instantaneous nature of the Coulomb interaction in the nonrelativistic case.

VII. EXCHANGE HOLE

Considering only the exchange contribution in Eq. (64) yields the exchange hole ρ_x :

$$\rho_x(1, 2, 3) G(1, 2) = i G(1, 3) G(3, 2). \quad (69)$$

Keeping in mind that $t_2 = 0$ and $t_1 = t_3 = t$, due to the presence of the instantaneous Coulomb interaction $v(1 - 3)$ in the equation of motion in Eq. (57), the substitutions

$$1 \rightarrow (rt), \quad 2 \rightarrow (r'0), \quad 3 \rightarrow (r''t), \quad (70)$$

lead to a more explicit expression for the exchange hole:

$$\rho_x(r, r', r''; t) G(r, r'; t) = i G(r, r''; 0^-) G(r'', r'; t). \quad (71)$$

On the right-hand side the rule governing an equal-time Green function,

$$G(rt, r''t) = G(rt, r''t^+) = G(r, r''; t - t^+ = 0^-), \quad (72)$$

has been used. Since

$$iG(r, r; 0^-) = -\rho(r), \quad (73)$$

the exact constraint in Eq. (43) is already fulfilled by the exchange hole. This implies that the correlation hole fulfils the following condition,

$$\rho_c(r, r', r; t) = 0. \quad (74)$$

For a noninteracting G ,

$$\begin{aligned} iG_0(r, r'; t) &= -\theta(-t) \sum_k^{\text{occ}} \phi_k(r) \phi_k^*(r') e^{-i\varepsilon_k t} \\ &+ \theta(t) \sum_k^{\text{unocc}} \phi_k(r) \phi_k^*(r') e^{-i\varepsilon_k t}, \end{aligned} \quad (75)$$

so that for $t < 0$

$$i \int dr'' G_0(r, r''; 0^-) G_0(r'', r'; t < 0) = -G_0(r, r'; t < 0). \quad (76)$$

This result can be shown as follows:

$$\begin{aligned} i \int dr'' G_0(r, r''; 0^-) G_0(r'', r'; t < 0) \\ &= -i \int dr'' \sum_k^{\text{occ}} \phi_k(r) \phi_k^*(r'') \sum_{k'}^{\text{occ}} \phi_{k'}(r'') \phi_{k'}^*(r') e^{-i\varepsilon_{k'} t} \\ &= -i \sum_k^{\text{occ}} \phi_k(r) \phi_k^*(r') e^{-i\varepsilon_k t} \\ &= -G_0(r, r'; t < 0). \end{aligned} \quad (77)$$

For $t > 0$

$$i \int dr'' G_0(r, r''; 0^-) G_0(r'', r'; t > 0) = 0 \quad (78)$$

since in this case $k' > k_F$. With $G = G_0$, it follows from Eq. (71) that the exchange hole fulfils the sum rule:

$$\int dr'' \rho_x(r, r', r''; t) = -\theta(-t). \quad (79)$$

In general, if $G \neq G_0$

$$-i \int dr'' G(r, r''; 0^-) G(r'', r'; t < 0) \neq G(r, r'; t < 0) \quad (80)$$

and

$$i \int dr'' G(r, r''; 0^-) G(r'', r'; t > 0) \neq 0. \quad (81)$$

This implies that if a renormalised G is used and only the exchange part is considered, then in general the sum rule is not fulfilled.

A. Relationship with the Slater exchange hole

The relationship with the Slater exchange hole can be seen by taking the limit $t \rightarrow 0^-$, $r' \rightarrow r$, and using the noninteracting Green function in Eq. (71). Since

$$iG_0(r, r''; 0^-) = -\sum_k^{\text{occ}} \phi_k(r) \phi_k^*(r'') \quad (82)$$

one finds

$$\rho_x(r, r, r''; 0^-) = -\frac{1}{\rho(r)} \sum_{ik}^{\text{occ}} \phi_k^*(r) \phi_i(r) \phi_i^*(r'') \phi_k(r''), \quad (83)$$

which is identical with the Slater exchange hole in Eq. (8).

VIII. CORRELATION HOLE

It can be shown that there is no density-response contribution to the sum rule. Consider the change in charge density under a perturbation $\delta\varphi$:

$$\delta\rho(1) = \int d2 \chi(1,2)\delta\varphi(2), \quad (84)$$

where χ is the linear density-response function as defined in Eq. (67). Since a constant perturbation, $\delta\varphi = c$, does not affect the density, it follows that

$$\int d2 \chi(1,2) = 0. \quad (85)$$

The RPA response function fulfils this condition when calculated using G_0 , as shown below.

The response function can be expanded in powers of polarisation P ,

$$\chi = P + PvP + \dots \quad (86)$$

One observes that if the polarisation fulfils the condition

$$\int d2 P(1,2) = 0, \quad (87)$$

then the response function χ also fulfils the condition in Eq. (85).

The polarisation in RPA is given by

$$P(r, r'; t) = -iG(r, r'; t)G(r', r; -t). \quad (88)$$

If a noninteracting G_0 in Eq. (75) is used, Eq. (87) and consequently Eq. (85) are satisfied. This can be shown by considering

$$\begin{aligned} G_0(r, r'; t)G_0(r', r; -t) &= \theta(-t) \sum_{k \leq k_F} \varphi_k(r) \varphi_k^*(r') e^{-i\varepsilon_k t} \sum_{k' > k_F} \varphi_{k'}(r') \varphi_{k'}^*(r) e^{i\varepsilon_{k'} t} \\ &+ \theta(t) \sum_{k > k_F} \varphi_k(r) \varphi_k^*(r') e^{-i\varepsilon_k t} \sum_{k' \leq k_F} \varphi_{k'}(r') \varphi_{k'}^*(r) e^{i\varepsilon_{k'} t}. \end{aligned} \quad (89)$$

When integrating over r' one finds

$$\int dr' \varphi_k^*(r') \varphi_{k'}(r') = 0, \quad (90)$$

since φ_k and $\varphi_{k'}$ are occupied and unoccupied, respectively, or vice versa. Hence, the condition in Eq. (87) is fulfilled.

However, it is not immediately evident that the conditions in Eq. (87) and Eq. (85) are satisfied when a renormalised G is used. To see this, consider

$$G(r, r'; t) = \int \frac{d\omega}{2\pi} e^{-i\omega t} G(r, r'; \omega). \quad (91)$$

Using the spectral representation,

$$G(r, r'; \omega) = \int_{-\infty}^{\mu} d\omega' \frac{A(r, r'; \omega')}{\omega - \omega' - i\eta} + \int_{\mu}^{\infty} \frac{A(r, r'; \omega')}{\omega - \omega' + i\eta}, \quad (92)$$

where μ is the chemical potential and

$$A(r, r'; \omega) = -\frac{1}{\pi} \text{sign}(\omega - \mu) \text{Im} G(r, r'; \omega), \quad (93)$$

one arrives at

$$\begin{aligned} &\int dr' dt' P(r, r'; t - t') \\ &= -i \int dr' dt' G(r, r'; t - t') G(r', r; t' - t) \\ &= \int_{-\infty}^{\mu} d\omega_1 \int_{\mu}^{\infty} d\omega_2 \int dr' \\ &\quad \left\{ \frac{A(r, r'; \omega_1) A(r', r; \omega_2) + A(r, r'; \omega_2) A(r', r; \omega_1)}{\omega_1 - \omega_2} \right\}. \end{aligned} \quad (94)$$

The spectral function for a noninteracting G_0 is given by

$$A_0(r, r'; \omega) = \sum_k \varphi_k(r) \varphi_k^*(r') \delta(\omega - \varepsilon_k). \quad (95)$$

It is quite evident that the integral over r' is zero since it leads to integrals between occupied and unoccupied orbitals, as in Eq. (90). However, it is not clear if this holds for an interacting G . If the integral in Eq. (94) is nonzero then the sum rule is not fulfilled by the exchange and density-response terms individually. It is not impossible that the sum of these two terms would fulfill the sum rule, but this seems unlikely. This conjecture might explain the known fact that a self-consistent GW yields poor spectral functions [39]. When a renormalised G is used, inclusion of the vertex seems necessary to preserve the sum rule.

IX. SPHERICAL AVERAGE OF THE XC HOLE

The fact that the Coulomb interaction depends only on the spatial separation between two point charges has a very important consequence for the xc hole: only the spherical average of the xc hole is needed to determine V_{xc} . This follows from the well-known result in DFT, which partially explains the success of LDA [46].

The change of variable $\mathbf{R} = \mathbf{r}'' - \mathbf{r}$ in Eq. (46) leads to

$$\begin{aligned} V_{xc}(r, r'; t) &= \sum_{\sigma_R} \int d^3R v(R) \rho_{xc}(r, r', \mathbf{r} + \mathbf{R}; t) \\ &= \int dR R \bar{\rho}_{xc}(r, r', R; t), \end{aligned} \quad (96)$$

where

$$\bar{\rho}_{xc}(r, r', R; t) = \sum_{\sigma_R} \int d\Omega_R \rho_{xc}(r, r', \mathbf{r} + \mathbf{R}; t) \quad (97)$$

is the spherical average of the exchange-correlation hole for given r , r' , and t . This result is very appealing, since it implies that the many-electron problem of determining the Green function is reduced to finding a spherical charge distribution, and only its first radial moment is required. The second radial moment is known since it corresponds to the sum rule. This means that there are an infinite number of xc holes that yield the exact V_{xc} since all radial moments higher than two need not be exact. This property is a consequence of the Coulomb interaction being dependent only on the spatial separation. This property is not utilised in the self-energy approach in which the Coulomb interaction is lumped into the definition of the self-energy as can be seen in Eq. (28).

A. Local-density approximation (LDA)

The reasoning by Slater described in Sec. II that leads to the LDA for the exchange potential can be readily carried over to V_{xc} . As in the case of the static exchange hole, the sum rule and the exact constraint $\rho_{xc}(r, r', r; t) = -\rho(r)$ have a very important implication, namely V_{xc} behaves approximately as $\rho^{1/3}(r)$, independent of r' and t . Following Slater [37], if the xc hole is approximated by a sphere of radius R_0 and assumed to be constant, one finds that the Coulomb potential due to the exchange hole at r , the centre of the sphere, is proportional to $1/R_0$ and hence V_{xc} is proportional to $\rho(r)^{1/3}$ in the lowest approximation, as in Eq. (15). It must be emphasised again that the $\rho(r)^{1/3}$ -dependence does not rely on the homogeneous electron gas since it is solely based on the exact constraint which is valid in general. The dependence of V_{xc} on local density may be regarded as a manifestation of nearsightedness advocated by Walter Kohn [47–49].

As will be described in a later section, the xc hole and potential of the homogeneous electron gas can be calculated within RPA. The results can be parametrised as a function of density and applied within LDA to real systems. For the homogeneous electron gas (HEG) the spherical average of the xc hole of a given spin σ and density ρ has the form

$$\bar{\rho}_{xc}(r, r', R; t) = \bar{\rho}_{xc}(\rho, |\mathbf{r}' - \mathbf{r}|, R; t). \quad (98)$$

A possible LDA for the xc hole is

$$\bar{\rho}_{xc}^{\text{LDA}}(r, r', R; t) = \bar{\rho}_{xc}^{\text{HEG}}(\rho(r), |\mathbf{r}' - \mathbf{r}|, R; t), \quad (99)$$

where $\rho(r)$ is the local density at r .

A more direct route is to apply LDA on V_{xc} directly:

$$V_{xc}^{\text{LDA}}(r, r'; t) = V_{xc}^{\text{HEG}}(\rho(r), |\mathbf{r}' - \mathbf{r}|; t). \quad (100)$$

This approximation could be improved by taking into account the density dependence at r' as in the weighted LDA [50, 51].

X. CONNECTION WITH KOHN-SHAM V_{xc}

To establish the connection between the Kohn-Sham (KS) xc potential V_{xc}^{KS} and the dynamical xc field consider the equations of motion satisfied by the two corresponding Green functions, G^{KS} and G . From these two equations,

$$\begin{aligned} & \left(i \frac{\partial}{\partial t} - h(r) - V_{xc}(r, r'; t) \right) [G(r, r'; t) - G^{\text{KS}}(r, r'; t)] \\ &= [V_{xc}(r, r'; t) - V_{xc}^{\text{KS}}(r)] G^{\text{KS}}(r, r'; t). \end{aligned} \quad (101)$$

Using the property that the diagonal components of both G^{KS} and G give the ground-state density [52], and evaluating the equation with $r' \rightarrow r$ and $t \rightarrow 0^-$ yields the relationship between $V_{xc}(r, r; 0^-)$ and $V_{xc}^{\text{KS}}(r)$:

$$\begin{aligned} & \lim_{r' \rightarrow r, t \rightarrow 0^-} \left(\frac{\partial}{\partial t} - \frac{i}{2} \nabla^2 \right) [G(r, r'; t) - G^{\text{KS}}(r, r'; t)] \\ &= [V_{xc}(r, r; 0^-) - V_{xc}^{\text{KS}}(r)] \rho(r). \end{aligned} \quad (102)$$

There does not seem to be any immediate reason that the left-hand side vanishes so that under this assumption in general $V_{xc}(r, r; 0^-) \neq V_{xc}^{\text{KS}}(r)$. The first term on the left-hand side with time derivative can be understood as the difference in the first moment of the occupied densities of states after integration over r . The second term is the difference in the kinetic energies of the true interacting and noninteracting systems, which is contained in the Kohn-Sham E_{xc} .

Note that

$$g(r, r, r''; t = 0^-) \neq g^{\text{KS}}(r, r''), \quad (103)$$

since g^{KS} is defined as the average of g_λ , which is the static correlation function corresponding to a scaled Coulomb interaction, λv [46, 53].

The xc energy in the Kohn-Sham scheme is given by

$$E_{xc}^{\text{KS}} = \frac{1}{2} \int dr dr' \rho(r) v(r - r') \rho_{xc}^{\text{KS}}(r, r'), \quad (104)$$

where

$$\rho_{xc}^{\text{KS}}(r, r') = [g^{\text{KS}}(r, r') - 1] \rho(r') \quad (105)$$

is the static Kohn-Sham xc hole. It can then be seen that the Kohn-Sham xc potential is given by

$$\begin{aligned} V_{xc}^{\text{KS}}(r) &= \frac{\delta E_{xc}^{\text{KS}}}{\delta \rho(r)} \\ &= \int dr' v(r - r') \rho_{xc}^{\text{KS}}(r, r') \\ &+ \frac{1}{2} \int dr' dr'' \rho(r') v(r' - r'') \frac{\delta g^{\text{KS}}(r', r'')}{\delta \rho(r)} \rho(r''). \end{aligned} \quad (106)$$

Thus, in addition to the Coulomb potential of the xc hole, there is an additional contribution arising from the dependence of the distribution function g^{KS} on the density.

This is in contrast to V_{xc} , which is purely the Coulomb potential of the xc hole. Since the xc hole in finite systems such as atoms and molecules integrates to -1 , V_{xc} behaves asymptotically as $-\frac{1}{r}$ automatically. On the other hand, approximate Kohn-Sham xc potentials can violate this asymptotic behaviour [54] even though the xc hole fulfils the sum rule, due to the presence of $\delta g^{KS}/\delta \rho$, which can give a spurious asymptotic contribution.

It is well-known that band gaps in semiconductors and insulators are systematically underestimated within Kohn-Sham DFT. The presence of a derivative discontinuity of the xc potential is usually invoked to explain this underestimation [55]. The V_{xc} formalism offers a natural explanation for this underestimation. The xc field arises as the Coulomb potential of the xc hole, which integrates to -1 for the hole and 0 for the electron. This implies that the xc field for the hole (occupied state) should be more negative than that for the electron (unoccupied state), whereas in Kohn-Sham DFT, both hole and electron experience the same potential. The Kohn-Sham xc potential is designed for occupied states only to reproduce the ground-state density.

XI. CONNECTION WITH THE SELF-ENERGY

It is quite evident from comparison of the equations of motion in Eqs. (29) and (44) that V_{xc} and the self-energy are related according to

$$V_{xc}(1, 2)G(1, 2) = \int d3 \Sigma(1, 3)G(3, 2). \quad (107)$$

However, this relation by itself is too general and rather superficial since it appears as a mere redefinition of the self-energy. It is more insightful to consider the relationship between the xc hole and the density response of the system and how this relationship gives rise to Eq. (107).

From Eq. (64) with the vertex $\delta \Sigma / \delta \varphi$ neglected and using the definition of the inverse dielectric function in Eq. (65) one finds

$$\begin{aligned} & \int d3 v(1-3)\rho_{xc}(1, 2, 3)G(1, 2) \\ &= i \int d3 v(1-3) \int d4 G(1, 4)\epsilon^{-1}(4, 3)G(4, 2). \end{aligned} \quad (108)$$

The quantity $W = \epsilon^{-1}v$ is the screened interaction, and one obtains

$$\begin{aligned} V_{xc}(1, 2)G(1, 2) &= i \int d4 G(1, 4)W(4, 1)G(4, 2) \\ &= \int d4 \Sigma_{GW}(1, 4)G(4, 2), \end{aligned} \quad (109)$$

which yields V_{xc} corresponding to the GW approximation for the self-energy.

A. Dyson-like equation

The equation of motion of the Hartree Green function G^H is given by

$$[i\partial_t - h(r)]G^H(r, r'; t) = \delta(r - r')\delta(t). \quad (110)$$

It then follows from the equation of motion in Eq. (44) that

$$\begin{aligned} G(r, r'; t) &= G^H(r, r'; t) \\ &+ \int dr'' dt' G^H(r, r''; t - t')V_{xc}(r'', r'; t')G(r'', r'; t'), \end{aligned} \quad (111)$$

which can be verified by operating $i\partial_t - h(r)$ on both sides of the equation. The above equation may be regarded as the analogue of the Dyson equation in the self-energy framework. If the Kohn-Sham Green function, G^{KS} , which satisfies

$$[i\partial_t - h(r) - V_{xc}^{KS}(r)]G^{KS}(r, r'; t) = \delta(r - r')\delta(t), \quad (112)$$

is used as a reference instead of the Hartree Green function, the same Dyson-like equation is fulfilled with G^H replaced by G^{KS} and V_{xc} replaced by $V_{xc} - V_{xc}^{KS}$.

The Dyson equation in the V_{xc} formalism is difficult to solve, since it is not in the form of a matrix equation. This is in contrast to the self-energy approach, in which the Dyson equation is in matrix form. Due to its local nature in both space and time, the V_{xc} formalism is well suited for solving the Green function by point-wise propagation in time of the equation of motion. On the other hand, the Green function in the self-energy approach is difficult to propagate since the self-energy acts as a time convolution on the Green function. Knowledge of the Green function for all time is a prerequisite before it can be propagated.

XII. TOTAL SPECTRAL FUNCTION

The Fourier transform of the Green function into the frequency domain provides information on the momentum-resolved spectra. For many purposes, it is often sufficient to know the total spectral function corresponding to the trace of the Green function. In this case, one can take advantage of the local nature of V_{xc} and as shown below only its diagonal component is needed. A related approach is the work by Gatti *et al.* [56] who introduced an effective potential, local in space but energy dependent, defined to reproduce the diagonal component of the Green function from which the total spectral function can be calculated. Another related approach is the work of Savrasov and Kotliar [57], who introduced the concept of spectral-density functional theory, in which the key variable is given by the local Green function rather than the electron density.

A. Temporal density

The temporal density is defined as the diagonal component of the Green function:

$$\rho(r, t) = -iG(r, r; t). \quad (113)$$

For $t = 0^-$ it is equal to the electron density. The Fourier transform of the integral over space gives the spectral function or density of states:

$$\rho(\omega) = \frac{1}{\Omega} \int dr \int dt e^{i\omega t} \rho(r, t). \quad (114)$$

The nomenclature "temporal density" arises from its interpretation as the probability amplitude that a hole or an electron created at r is annihilated at the same position at a later time t .

Note that the temporal density is *not* the same as the density fluctuation arising from the addition of a hole or an electron [58]. Consider an electron addition ($t > 0$) at r . The density corresponding to the time-evolved state,

$$|\Psi(r, t)\rangle = e^{-i\hat{H}t} \hat{\psi}^\dagger(r) |\Psi_0\rangle, \quad (115)$$

is given by

$$\begin{aligned} \rho_{\text{fluc}}(r, t) &= \langle \Psi(r, t) | \hat{\rho}(r) | \Psi(r, t) \rangle \\ &= \langle \Psi_0 | \hat{\psi}(r) e^{i\hat{H}t} \hat{\rho}(r) e^{-i\hat{H}t} \hat{\psi}^\dagger(r) | \Psi_0 \rangle. \end{aligned} \quad (116)$$

This density fluctuation is real whereas the temporal density

$$\begin{aligned} \rho(r, t) &= -\langle \Psi_0 | \hat{\psi}(rt) \hat{\psi}^\dagger(r) | \Psi_0 \rangle \\ &= -e^{iE_0 t} \langle \Psi_0 | \hat{\psi}(r) e^{-i\hat{H}t} \hat{\psi}^\dagger(r) | \Psi_0 \rangle \end{aligned} \quad (117)$$

is generally complex. The temporal density is also different from the time-dependent density in TDDFT [29, 32], which corresponds to the real density that varies in time when an external time-dependent field is applied. In the case of the temporal density, the addition and subsequent annihilation of an electron or a hole is performed on a system initially in its ground state in the absence of a time-dependent external field.

Consider now the equation of motion for the Green function in Eq. (44) calculated at $r' = r$ and $t \neq 0$ [58]:

$$\begin{aligned} [i\partial_t - V_{\text{MF}}(r) - V_{\text{xc}}(r, t)] \rho(r, t) \\ - \frac{i}{2} \nabla^2 G(r, r'; t) \Big|_{r'=r} = 0, \end{aligned} \quad (118)$$

where

$$V_{\text{xc}}(r, t) := V_{\text{xc}}(r, r; t) \quad (119)$$

and

$$V_{\text{MF}}(r) = V_{\text{ext}}(r) + V_{\text{H}}(r). \quad (120)$$

For each r' the temporal current density is defined according to

$$\mathbf{j}(r, r'; t) := -\frac{1}{2} \nabla G(r, r'; t). \quad (121)$$

Note that the temporal current density should be regarded as a construct and does not necessarily correspond to a physical current density. The equation of motion becomes

$$\partial_t \rho(r, t) + \nabla \cdot \mathbf{j}(r, t) = S(r, t), \quad (122)$$

where

$$\nabla \cdot \mathbf{j}(r, t) = \nabla \cdot \mathbf{j}(r, r'; t) \Big|_{r'=r} = -\frac{1}{2} \nabla^2 G(r, r'; t) \Big|_{r'=r} \quad (123)$$

and

$$S(r, t) = -i [V_{\text{MF}}(r) + V_{\text{xc}}(r, t)] \rho(r, t). \quad (124)$$

The divergence of the temporal current density can be illustrated more concretely by expanding $G(r, r'; t)$ in a complete set of orbitals $\{\varphi_i\}$,

$$G(r, r'; t) = \sum_{ij} \varphi_i(r) G_{ij}(t) \varphi_j^*(r'). \quad (125)$$

The divergence of the temporal current density for a given r is then given by

$$\nabla \cdot \mathbf{j}(r, t) = -\frac{1}{2} \sum_i [\nabla^2 \varphi_i(r)] \psi_i^*(r, t), \quad (126)$$

where

$$\psi_i^*(r, t) = \sum_j G_{ij}(t) \varphi_j^*(r). \quad (127)$$

The equation of motion, Eq. (122), has the form of the continuity equation in electrodynamics with a source/sink term S on the right-hand side. Eq. (123) implies that only the diagonal component, $G(r, r; t)$, and the neighbouring components, $G(r \pm \delta r, r; t)$, are needed to calculate the divergence of the temporal current density. This is substantially less information than that needed to calculate the momentum-resolved spectral function. The temporal current density is not explicitly required; only its divergence is relevant. Note that no auxiliary system has been introduced, and all quantities are defined in terms of exact quantities whose existence is guaranteed.

B. Practical scheme à la Kohn-Sham

It is useful to introduce a kinetic potential V_{K} defined as [58]

$$V_{\text{K}}(r, t) := -i \frac{\nabla \cdot \mathbf{j}(r, t)}{\rho(r, t)}. \quad (128)$$

With this definition, the continuity equation can be rewritten as

$$i\partial_t \ln \rho(r, t) = V_{\text{MF}}(r) + V_{\text{xc}}(r, t) + V_{\text{K}}(r, t) \quad (129)$$

with the formal solution

$$\rho(r, t) = \rho(r, 0^\pm) \exp[-iV_{\text{MF}}(r)t] \times \exp\left\{-i \int_0^t dt' [V_{\text{xc}}(r, t') + V_{\text{K}}(r, t')]\right\}. \quad (130)$$

Alternatively,

$$\rho(r, t) = \rho(r, 0^\pm) + \int_0^t dt' [S(r, t') - \nabla \cdot \mathbf{j}(r, t')]. \quad (131)$$

$\rho(r, 0^\pm)$ is the initial electron or hole density obtained from, for example, density-functional calculation. To practically solve for $\rho(r, t)$ approximations for V_{xc} and V_{K} are required. V_{xc} is expected to be amenable to a local-density type of approximation, but the kinetic potential V_{K} is associated with the kinetic energy. Sufficiently accurate approximations for the kinetic energy as an explicit functional of the electron density are not yet available.

A practical scheme analogous to the Kohn-Sham DFT [2–5] can be constructed by defining ΔV_{K} as

$$\Delta V_{\text{K}} = -i \left\{ \frac{\nabla \cdot \mathbf{j}}{\rho} - \frac{\nabla \cdot \mathbf{j}^{\text{KS}}}{\rho^{\text{KS}}} \right\} = V_{\text{K}} - V_{\text{K}}^{\text{KS}}. \quad (132)$$

Here, ρ^{KS} and \mathbf{j}^{KS} are, respectively, the temporal density and the temporal current density associated with the Kohn-Sham Green function. With this definition, the continuity equation becomes

$$\partial_t \rho(r, t) + \frac{\nabla \cdot \mathbf{j}^{\text{KS}}(r, t)}{\rho^{\text{KS}}(r, t)} \rho(r, t) = \tilde{S}(r, t), \quad (133)$$

where

$$\tilde{S}(r, t) = -i [V_{\text{MF}}(r) + \tilde{V}_{\text{xc}}(r, t)] \rho(r, t), \quad (134)$$

$$\tilde{V}_{\text{xc}} = V_{\text{xc}} + \Delta V_{\text{K}}. \quad (135)$$

The difference in kinetic potentials is incorporated into the xc field. The formal solution given by

$$\rho(r, t) = \rho(r, 0^\pm) \exp[-iV_{\text{MF}}(r)t] \times \exp\left\{-i \int_0^t dt' [\tilde{V}_{\text{xc}}(r, t') + V_{\text{K}}^{\text{KS}}(r, t')]\right\}. \quad (136)$$

Note that Eq. (133) is the equation of motion of the *true* interacting temporal density. Unlike the Kohn-Sham scheme, there is no auxiliary system.

XIII. TOTAL ENERGY: RELATIONSHIP TO GALITSKII-MIGDAL FORMULA

The Galitskii-Migdal formula provides a way to calculate from the Green function the total ground-state energy, and is given by [41]

$$E_0 = -\frac{i}{2} \int dr \lim_{r' \rightarrow r} \lim_{t \rightarrow 0^-} (i\partial_t + h_0(r)) G(r, r'; t), \quad (137)$$

where $h_0(r) = -\frac{1}{2}\nabla^2 + V_{\text{ext}}(r)$. Within the Vxc formalism the time derivative of the Green function can be calculated from the equation of motion:

$$i\partial_t G(r, r'; t)|_{t=0^-} = (h_0(r) + V_{\text{H}}(r) + V_{\text{xc}}(r, r'; 0^-)) G(r, r'; 0^-). \quad (138)$$

Substituting the above expression into the Galitskii-Migdal formula results in

$$E_0 = -\frac{i}{2} \int dr \lim_{r' \rightarrow r} (2h_0(r) + V_{\text{H}}(r) + V_{\text{xc}}(r, r'; 0^-)) \times G(r, r'; 0^-) \\ = -\frac{1}{2} \int dr \lim_{r' \rightarrow r} \nabla^2 \Gamma^{(1)}(r, r') + \int dr V_{\text{ext}}(r) \rho(r) \\ + \frac{1}{2} \int dr (V_{\text{H}}(r) + V_{\text{xc}}(r, r; 0^-)) \rho(r), \quad (139)$$

where

$$\Gamma^{(1)}(r, r') = -iG(r, r'; 0^-) \quad (140)$$

is the one-particle reduced density matrix whose diagonal element is the ground-state density. One notes that

$$E_{\text{H}} = \frac{1}{2} \int dr V_{\text{H}}(r) \rho(r) = \frac{1}{2} \int dr dr' \rho(r) v(r - r') \rho(r'), \quad (141)$$

is the Hartree energy. The last term in E_0 containing V_{xc} is the xc energy,

$$E_{\text{xc}} = \frac{1}{2} \int dr V_{\text{xc}}(r, r; 0^-) \rho(r) \\ = \frac{1}{2} \int dr dr'' \rho(r) v(r - r'') \rho_{\text{xc}}(r, r, r''; 0^-). \quad (142)$$

$\rho_{\text{xc}}(r, r, r''; 0^-)$ is the static xc hole in many-body theory. It is different from the xc hole in Kohn-Sham DFT since the kinetic energy in Eq. (139) is that of the interacting system rather than the noninteracting Kohn-Sham system. The above xc energy does not incorporate the contribution from the kinetic energy.

The formula in Eq. (139) offers an interesting possibility of calculating the ground-state energy using the variational principle. The reduced density matrix $\Gamma^{(1)}$ can be diagonalised and expressed in terms of its eigenfunctions (natural orbitals) according to

$$\Gamma^{(1)}(r, r') = \sum_i n_i \phi_i(r) \phi_i^*(r'), \quad (143)$$

where ϕ_i is an eigenfunction with eigenvalue n_i :

$$\int dr' \Gamma^{(1)}(r, r') \phi_i(r') = n_i \phi_i(r). \quad (144)$$

The eigenfunctions are orthonormal, and the eigenvalues fulfil the conditions

$$\sum_i n_i = N, \quad 0 \leq n_i \leq 1, \quad (145)$$

where N is the number of electrons in the system. The ground-state density is given by

$$\rho(r) = \Gamma^{(1)}(r, r) = \sum_i n_i |\phi_i(r)|^2. \quad (146)$$

Note that the sum is over all orbitals, not restricted to the lowest N as in the case of the Kohn-Sham system.

The ground-state energy can be regarded as a functional of the occupation numbers $\{n_i = \cos^2 \theta_i\}$ and natural orbitals $\{\phi_i^*, \phi_i\}$. Varying with respect to these parameters under the conditions in Eq. (145) and the requirement of orthonormality of the orbitals would lead to a set of coupled equations, which must be solved self-consistently. This approach is known as reduced density matrix functional theory (RDMFT) [59–62], regarded as a promising way to improve the standard Kohn-Sham DFT. In this approach, the basic variable is the one-particle reduced density matrix, and the corresponding Hohenberg-Kohn theorem is proven by Gilbert [63]. There is no auxiliary system, and the kinetic energy corresponds to the true interacting one, as indicated earlier.

XIV. QUASIPARTICLE WAVE FUNCTION IN THE VXC FORMALISM

In his famous phenomenological Fermi liquid theory from the mid 1950s, Landau introduced the concept of a quasiparticle [41, 64, 65]. Landau quasiparticles are restricted to those long-lived excitations at the Fermi level. This concept was generalised in a later development of Green function theory to include quasiparticles away from the Fermi level. In metals a quasiparticle at the Fermi level does indeed have an infinite lifetime as predicted by Landau, but away from the Fermi level it acquires a finite lifetime and decays with time. This phenomenon is observed in angle-resolved photoemission spectra of a large number of materials, which typically exhibit a main quasiparticle peak close to the chemical potential. In addition, there are usually incoherent features (satellites) at higher binding energies arising from the coupling of electrons to collective excitations such as plasmons. In magnetic systems the electrons can be coupled to spin excitations or magnons giving rise to features at low binding energies such as kinks in the band dispersion.

Traditionally, the quasiparticle is defined as an eigenfunction of the quasiparticle equation [18] involving the

self-energy Σ :

$$\left[-\frac{1}{2} \nabla^2 + V_H(r) + V_{\text{ext}}(r) \right] \Psi_k(r, E_k) + \int dr' \Sigma(r, r'; E_k) \Psi_k(r', E_k) = E_k \Psi_k(r, E_k). \quad (147)$$

Since the Hamiltonian is not Hermitian, quasiparticles with different energies are not in general orthonormal. In the language of self-energy, the lifetime is inversely proportional to the imaginary part of the self-energy. The many-electron system in Landau's phenomenological theory is qualitatively viewed as a set of quasiparticles interacting with residual interactions.

A. Quasiparticle wave function

A different concept of a quasiparticle wave function can be constructed from the definition of the Green function [66]. In contrast to the traditional one defined in Eq. (147), the proposed quasiparticle wave function decays in time and contains not only the quasiparticle mode, but also other modes arising from the coupling to collective excitations such as plasmons.

Consider expanding the Green function in a complete set of orbitals $\{\varphi_k\}$:

$$\begin{aligned} G(r, r'; t) &= \sum_{kk'} \varphi_k(r) G_{kk'}(t) \varphi_{k'}^*(r') \\ &= \sum_k \varphi_k(r) \psi_k^*(r', t), \end{aligned} \quad (148)$$

where

$$\psi_k^*(r', t) = \sum_{k'} G_{kk'}(t) \varphi_{k'}^*(r'). \quad (149)$$

It will be shown that $\sum_{k'} |G_{kk'}(t)|^2 \leq 1$, so that $G_{kk'}(t)$ can be regarded as a coefficient of expansion of ψ_k^* in orbital $\varphi_{k'}^*$. This leads to the interpretation of ψ_k^* as a quasiparticle wave function.

For a noninteracting system, $G_{kk'}(t) = G_k^0(t) \delta_{kk'}$ so that

$$G^0(r, r'; t) = \sum_k \varphi_k(r) G_k^0(t) \varphi_k^*(r'), \quad (150)$$

where

$$G_k^0(t) = i\theta(-t)\theta(\mu - \varepsilon_k)e^{-i\varepsilon_k t} - i\theta(t)\theta(\varepsilon_k - \mu)e^{-i\varepsilon_k t}. \quad (151)$$

Here, ε_k is the eigenvalue corresponding to orbital φ_k . The noninteracting quasiparticle wave function is then

$$\psi_k^{0*}(r, t) = G_k^0(t) \varphi_k^*(r). \quad (152)$$

It is quite evident that

$$|G_k^0(t)|^2 = 1, \quad (153)$$

which implies that the noninteracting quasiparticle does not decay, as expected.

We wish to prove that

$$\sum_{k'} |G_{kk'}(t)|^2 \leq 1. \quad (154)$$

Consider the case $t < 0$

$$\begin{aligned} |G_{kk}(t)|^2 &= \left| \langle \Psi_0 | \hat{c}_k^\dagger \hat{c}_k(t) | \Psi_0 \rangle \right|^2 \\ &= \left| \langle \Psi_0 | \hat{c}_k^\dagger e^{i\hat{H}t} \hat{c}_k | \Psi_0 \rangle \right|^2 \end{aligned} \quad (155)$$

Let $|\phi_k\rangle = \hat{c}_k |\Psi_0\rangle$. For fermions, the occupation number of a given orbital cannot exceed 1 so that

$$\langle \phi_k | \phi_k \rangle = \langle \Psi_0 | \hat{n}_k | \Psi_0 \rangle \leq 1. \quad (156)$$

Since the operator $e^{i\hat{H}t}$ is unitary,

$$|G_{kk}(t)|^2 = \left| \langle \phi_k | e^{i\hat{H}t} | \phi_k \rangle \right|^2 \leq 1. \quad (157)$$

This follows from the fact that the operator $e^{i\hat{H}t}$ is unitary. The overlap of the rotated state $|e^{i\hat{H}t}\phi_k\rangle$ with $|\phi_k\rangle$ must be less than or equal to $|\langle \phi_k | \phi_k \rangle|$.

For a given t let S be the unitary matrix that diagonalises G :

$$G_{kk'}(t) = \sum_{k_1} S_{kk_1} \tilde{G}_{k_1}(t) S_{k_1 k'}^\dagger, \quad (158)$$

$$\chi_k(r) = \sum_{k'} \varphi_{k'}(r) S_{k' k}, \quad (159)$$

$$G(r, r'; t) = \sum_k \chi_k(r) \tilde{G}_k(t) \chi_k^*(r'). \quad (160)$$

One finds

$$\begin{aligned} \sum_{k'} |G_{kk'}(t)|^2 &= \sum_{k'} \sum_{k_1 k_2} S_{kk_1} \tilde{G}_{k_1}(t) S_{k_1 k'}^\dagger S_{k' k_2} \tilde{G}_{k_2}^*(t) S_{k_2 k}^\dagger \\ &= \sum_{k_1} S_{kk_1} |\tilde{G}_{k_1}(t)|^2 S_{k_1 k}^\dagger. \end{aligned} \quad (161)$$

Since $|\tilde{G}_{k_1}(t)|^2 \leq 1$ it follows that

$$\sum_{k'} |G_{kk'}(t)|^2 \leq 1. \quad (162)$$

This result shows that

$$\int dr |\psi_k(r, t)|^2 = \sum_{k'} |G_{kk'}(t)|^2 \leq 1 \quad (163)$$

and provides a justification for interpreting $\psi_k^*(r, t)$ in Eq. (149) as a quasiparticle wave function. $G_{kk'}(t)$ can be understood as an expansion coefficient of the quasiparticle

wave function $\psi_k^*(r, t)$ in the base orbital $\varphi_{k'}^*$. A similar analysis can be performed for $t > 0$. The result in Eq. (163) could be seen from a different point of view [67]. The extension to nonequilibrium Green function can be found in a recent publication [66].

This definition of a quasiparticle wave function is general and is unrelated to the Vxc formalism. Unlike the standard definition, which corresponds only to the main quasiparticle peak, the proposed definition also contains possible excitations arising from the coupling to collective modes. The quasiparticle wave functions and the Green function are equivalent since they can be constructed from the knowledge of the other.

B. Quasiparticle equation in the Vxc formalism

The quasiparticle equation of motion can be derived from the equation of motion of the Green function in the Vxc formalism. It is useful to choose a mean-field xc potential $V_{xc}^0(r)$ and define a deviation potential,

$$\Delta V(r, r'; t) = V_{xc}(r, r'; t) - V_{xc}^0(r). \quad (164)$$

V_{xc}^0 may be chosen as the Kohn-Sham xc potential. Choosing the orbitals to be those of the mean-field Hamiltonian,

$$\left[-\frac{1}{2} \nabla^2 + V_{\text{ext}} + V_H + V_{xc}^0 \right] \varphi_k = \varepsilon_k \varphi_k, \quad (165)$$

it follows from the equation of motion for the Green function in Eq. (44) with $t \neq 0$

$$\sum_k [i\partial_t - \varepsilon_k - \Delta V(r, r'; t)] \varphi_k(r) \psi_k^*(r', t) = 0. \quad (166)$$

Multiplying on the left by $\varphi_q^*(r)$ and integrating over r yields (renaming r' as r after integration),

$$(i\partial_t - \varepsilon_q) \psi_q^*(r, t) - \sum_k \Delta V_{qk}(r, t) \psi_k^*(r, t) = 0. \quad (167)$$

where

$$\Delta V_{qk}(r, t) = \int dr' \varphi_q^*(r') \varphi_k(r') \Delta V(r', r; t). \quad (168)$$

This equation provides a quantitative description of a many-electron system as a set of quasiparticles, which interact with the (residual) interactions ΔV_{qk} , as in Landau phenomenological quasiparticle theory.

The quasiparticle equation of motion can be recast as

$$[i\partial_t - \varepsilon_q - \Xi_q(r, t)] \psi_q^*(r, t) = 0, \quad (169)$$

where

$$\Xi_q(r, t) = \frac{1}{\psi_q^*(r, t)} \sum_k \Delta V_{qk}(r, t) \psi_k^*(r, t) \quad (170)$$

acts as a q -dependent effective field. Each quasiparticle wave function experiences its own potential. The formal solution is given by

$$\psi_q^*(r, t) = \psi_q^*(r, 0^\pm) e^{-i\varepsilon_q t - i \int_0^t dt' \Xi_q(r, t')}. \quad (171)$$

The formal solution displays a clear physical meaning: when the residual effects of exchange and correlations encapsulated in $\Xi_q(r, t)$ are removed, the quasiparticle wave function returns to its mean-field reference orbital. Since $\Xi_q(r, t)$ is generally complex, which is a consequence of having a nonhermitian V_{xc} , its imaginary part causes the quasiparticle wave function to decay with time in an interacting many-electron system.

Once $\psi_q^*(r, t)$ is solved for all q , the Green function can be constructed from Eq. (148). Although the quasiparticle wave functions and the Green function are equivalent, the former can provide a useful description of the effects of the electron-electron interactions and a tool for analysing these effects. $|G_{kk'}(t)|^2$ gives the weight of the quasiparticle ψ_k^* in orbital $\varphi_{k'}^*$. It provides information on how the quasiparticle is distributed among the orbitals and how much weight has been lost from the reference orbital φ_k^* due to residual exchange-correlation effects as a function of time.

From the formal solution of the quasiparticle wave function in Eq. (171) it is physically suggestive to decompose the effective field into a static (S) and a dynamic (D) term as

$$\Xi_q(r, t) \approx \Xi_q^S(r) + \Xi_q^D(r) e^{i\Omega t}, \quad (172)$$

where Ω is the energy of the main collective excitation of the system that is coupled to the electrons. The static term corrects the reference orbital energy ε_q while the dynamic term induces an incoherent or satellite feature in the spectral function.

Examples of the effective potential Ξ_q are given for the Hubbard dimer and the homogeneous electron gas in Secs. XVI C and XVII E, respectively.

C. Quasiparticle-averaged effective potential

The effective potential $\Xi_q(r, t)$ depends on the quasiparticle states. A possible simplification is to take a quasiparticle average (avg) following Slater's idea of orbital averaging,

$$\begin{aligned} \Xi^{\text{avg}}(r, t) &= \sum_q \frac{|\psi_q(r, t)|^2}{\rho_{QP}(r, t)} \Xi_q(r, t) \\ &= \frac{1}{\rho_{QP}(r, t)} \sum_{qk} \psi_q(r, t) \Delta V_{qk}(r, t) \psi_k^*(r, t), \end{aligned} \quad (173)$$

where

$$\rho_{QP}(r, t) = \sum_q |\psi_q(r, t)|^2. \quad (174)$$

The equation of motion with the q -independent effective potential reduces to the following,

$$[i\partial_t - \varepsilon_q - \Xi^{\text{avg}}(r, t)] \psi_q^*(r, t) = 0. \quad (175)$$

However, for a homogeneous system, such as an electron gas, the q -dependence is important because without it there will be no band narrowing of the free-electron dispersion.

D. Self-consistency

The dependence of the quasiparticle states on the choice of orbitals raises an interesting question as to whether it is possible to remove this orbital dependency by means of a self-consistency procedure. By definition, the quasiparticle wave functions are intrinsically dependent on the reference orbitals. However, the reference orbitals can be defined self-consistently with respect to some given conditions. One possible condition is to require the reference orbitals to reproduce the ground-state density. The new ground-state density obtained from the quasiparticle wave functions is given by

$$\rho(r) = -iG(r, r; 0^-) = -i \sum_k \varphi_k(r) \psi_k^*(r, 0^-), \quad (176)$$

which can be used to redefine V_H and V_{xc} . The new reference mean-field Hamiltonian delivers an updated set of reference orbitals, yielding a new set of quasiparticle wave functions.

XV. EXTENSION TO THERMAL AND NONEQUILIBRIUM GREEN FUNCTION

The Vxc formalism can be readily extended to the thermal or Matsubara Green function:

$$G_M(r\tau, r'\tau') = -\text{Tr} \left\{ \hat{\rho}_K T[\hat{\psi}(r\tau) \hat{\psi}^\dagger(r'\tau')] \right\}, \quad (177)$$

where $\hat{K} = \hat{H} - \mu\hat{N}$ and τ is an imaginary time. Its equation of motion is given by

$$\begin{aligned} &\left[\frac{\partial}{\partial \tau} + h_0(r) - \mu \right] G_M(r\tau, r'\tau') \\ &- \int dr'' v(r - r'') \langle T[\hat{\rho}(r''\tau) \hat{\psi}(r\tau) \hat{\psi}^\dagger(r'\tau')] \rangle \\ &= -\delta(\tau - \tau') \delta(r - r'), \end{aligned} \quad (178)$$

where the thermal averaging is defined as

$$\langle \hat{O} \rangle = \text{Tr}(\hat{\rho}_K \hat{O}). \quad (179)$$

Since G_M depends only on $\tau - \tau'$ it is permissible to set τ' to zero,

$$\begin{aligned} &\langle T[\hat{\rho}(r''\tau) \hat{\psi}(r\tau) \hat{\psi}^\dagger(r')] \rangle \\ &= -G_M(r, r'; \tau) [\rho(r'') + \rho_{xc}(r, r', r''; \tau)] \end{aligned} \quad (180)$$

leading to

$$\left[\frac{\partial}{\partial \tau} + h(r) + V_{xc}(r, r'; \tau) - \mu \right] G_M(r, r'; \tau) = -\delta(\tau)\delta(r - r'), \quad (181)$$

where $h = h_0 + V_H$ and

$$V_{xc}(r, r'; \tau) = \int dr'' v(r - r'') \rho_{xc}(r, r', r''; \tau). \quad (182)$$

The sum rule as well as the exact constraint for the exchange-correlation hole in Eqs. (40) and (43) are still fulfilled.

An extension to nonequilibrium systems can also be made. In systems in which the Hamiltonian is time dependent, the field operator in the Heisenberg picture is given by

$$\hat{\psi}(rt) = \hat{U}(0, t) \hat{\psi}(r) \hat{U}(t, 0). \quad (183)$$

The time-evolution operator fulfils the Schrödinger equation:

$$i\partial_t \hat{U}(t, 0) = \hat{H}(t) \hat{U}(t, 0), \quad (184)$$

with the formal solution

$$\hat{U}(t, 0) = T e^{-i \int_0^t dt_1 \hat{H}(t_1)}. \quad (185)$$

The conjugate equation is given by

$$-i\partial_t \hat{U}^\dagger(t, 0) = \hat{U}^\dagger(t, 0) \hat{H}(t). \quad (186)$$

From the group and unitary properties,

$$\hat{U}(t, 0) \hat{U}(0, t) = 1, \quad \hat{U}(t, 0) \hat{U}^\dagger(t, 0) = 1, \quad (187)$$

and the definition of the Heisenberg operator, it follows that

$$\begin{aligned} i\partial_t \hat{\psi}(rt) &= \hat{U}(0, t) [\hat{\psi}(r), \hat{H}(t)] \hat{U}(t, 0) \\ &= \hat{U}(0, t) [h_0(rt) + \hat{V}_H(r)] \hat{\psi}(r) \hat{U}(t, 0) \\ &= [h_0(rt) + \hat{V}_H(rt)] \hat{\psi}(rt), \end{aligned} \quad (188)$$

where

$$h_0(rt) = -\frac{1}{2} \nabla^2 + V_{\text{ext}}(rt), \quad (189)$$

$$\hat{V}_H(rt) = \int dr'' v(r - r'') \hat{\rho}(r''t). \quad (190)$$

Multiplying on the right and on the left by $\hat{\psi}^\dagger(r't')$, and after a simple manipulation one obtains

$$\begin{aligned} [i\partial_t - h_0(rt)] G(rt, r't') \\ + i \int dr'' v(r - r'') \langle T [\hat{\rho}(r''t) \hat{\psi}(rt) \hat{\psi}^\dagger(r't')] \rangle \\ = \delta(r - r') \delta(t - t'). \end{aligned} \quad (191)$$

The derivation of the xc hole and field is rather similar to the equilibrium case. A correlator g is introduced,

$$\begin{aligned} G^{(2)}(rt, r't', r'') &= -i \langle T [\hat{\rho}(r''t) \hat{\psi}(rt) \hat{\psi}^\dagger(r't')] \rangle \\ &= G(rt, r't') g(rt, r't', r'') \rho(r''t). \end{aligned} \quad (192)$$

As in the equilibrium case, $G^{(2)}$ can be rewritten as

$$G^{(2)}(rt, r't', r'') = [\rho(r''t) + \rho_{xc}(rt, r't', r'')] G(rt, r't'), \quad (193)$$

where

$$\rho_{xc}(rt, r't', r'') = [g(rt, r't', r'') - 1] \rho(r''t). \quad (194)$$

The sum rule and the exact constraint are given by, respectively,

$$\int dr'' \rho_{xc}(rt, r't', r'') = -\theta(t' - t) \delta_{\sigma\sigma'}, \quad (195)$$

$$\rho_{xc}(rt, r't', r) = -\rho(rt), \quad (196)$$

for any r, r', t , and t' .

The equation of motion of the Green function is given by

$$[i\partial_t - h(rt) - V_{xc}(rt, r't')] G(rt, r't') = \delta(r - r') \delta(t - t'), \quad (197)$$

where $h(rt)$ contains the Hartree potential and

$$V_{xc}(rt, r't') = \int dr'' v(r - r'') \rho_{xc}(rt, r't', r''). \quad (198)$$

XVI. EXAMPLES OF V_{xc}

After elaborating the theoretical aspects of the V_{xc} formalism, some examples will now be described to illustrate some salient features of V_{xc} .

A. Hydrogen atom

The hydrogen atom provides a simple illustration for the sum rule Eq. (40) and the exact constraint Eq. (43). It also illustrates the well-known difficulty with LDA.

For the hydrogen atom, the hole Green function is given by

$$G(r, r'; t < 0) = i\varphi_s(r) \varphi_s(r') \exp(-i\varepsilon_s t) \theta(-t), \quad (199)$$

where φ_s and ε_s are the 1s-orbital and its energy. The electron Green function is not considered here since it requires eigenfunctions of the two-electron problem. For $t < 0$ V_{xc} acts to cancel the spurious self-interaction:

$$V_{xc}(r, r'; t < 0) = -V_H(r) = - \int dr'' v(r - r'') |\varphi_s(r'')|^2, \quad (200)$$

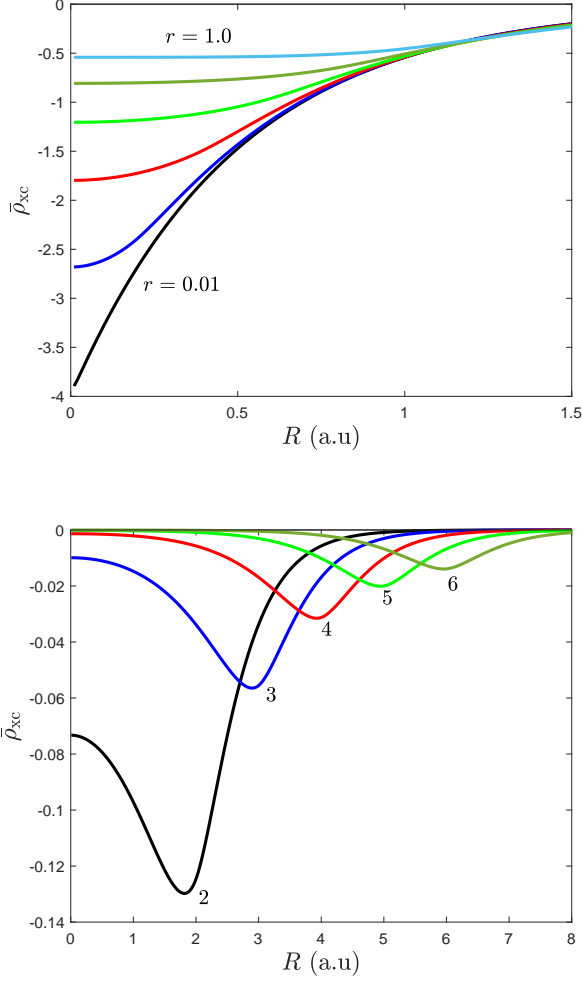


FIG. 1. Top: The spherical average of the xc hole of the hydrogen atom centred at \mathbf{r} for several values of $r = 0.01$ (black), 0.2 (blue), 0.4 (red), 0.6 (green), 0.8 (olive), and 1.0 (light blue), as indicated in the figure in progression from $r = 0.01$ to 1.0. Bottom: The same as the top figure but for $r > 1$, beyond the Bohr radius ($r = 1$) as indicated in the figure. For large r the xc hole is dipped around the nucleus rather than at \mathbf{r} , the location where the hole is created ($R = 0$).

independent of r' and t . The corresponding xc hole is given by

$$\rho_{xc}(r, r', r''; t < 0) = -|\varphi_s(r'')|^2 = -\frac{1}{\pi}e^{-2r''}. \quad (201)$$

The exact constraint in Eq. (43),

$$\rho_{xc}(r, r', r; t < 0) = -\rho(r), \quad (202)$$

as well as the sum rule in Eq. (40),

$$\int dr'' \rho_{xc}(r, r', r''; t < 0) = -\int dr'' |\varphi_s(r'')|^2 = -1, \quad (203)$$

are clearly fulfilled.

Only the spherical average of the xc hole is needed. Taking \mathbf{r} as the centre of the hole independent of \mathbf{r}' and t the spherical average as defined in Eq. (97) is given by

$$\begin{aligned} \bar{\rho}_{xc}(r, R) &= \int d\Omega_R \rho_{xc}(\mathbf{r} + \mathbf{R}) \\ &= -2\pi \int_{-1}^1 dy \frac{1}{\pi} e^{-2\sqrt{r^2 + R^2 + 2rRy}}. \end{aligned} \quad (204)$$

The change of variable $x = \sqrt{r^2 + R^2 + 2rRy}$ yields

$$\bar{\rho}_{xc}(r, R) = -\frac{1}{2rR} \left\{ (2a + 1)e^{-2a} - (2b + 1)e^{-2b} \right\}, \quad (205)$$

where

$$a = |r - R|, \quad b = r + R. \quad (206)$$

In the limit $R \rightarrow 0$,

$$\bar{\rho}_{xc}(r, R \rightarrow 0) = -4\pi \frac{e^{-2r}}{\pi} = 4\pi\rho(r), \quad (207)$$

and in the limit $r \rightarrow 0$,

$$\bar{\rho}_{xc}(r \rightarrow 0, R) = -4\pi \frac{e^{-2R}}{\pi} = 4\pi\rho(R). \quad (208)$$

Fig. 1 shows the spherical average of the xc hole centred at several values of \mathbf{r} . For small r it approaches $4\pi\rho(R)$ and is peaked around its centre at \mathbf{r} , that is, around $R = 0$, whereas for large r beyond the Bohr radius ($r = 1$) the xc hole is dipped around the nucleus rather than around its centre as can be seen in the lower figure of Fig. 1. Note that R is the distance from the centre at \mathbf{r} . Thus, for large r away from the nucleus, the xc hole is left behind around the nucleus, whereas in LDA the hole is always centred around \mathbf{r} , a well-known shortcoming of LDA. For large r the LDA is a poor approximation for the xc hole.

B. The Holstein model

The Holstein Hamiltonian describes a coupling between electrons and a set of bosons, such as plasmons or phonons. In its simplified version, where there is only one electron, it is given by [68]

$$\hat{H} = \varepsilon \hat{c}^\dagger \hat{c} + \sum_q \hat{c}^\dagger \hat{c} g_q (\hat{b}_q + \hat{b}_q^\dagger) + \sum_q \omega_q \hat{b}_q^\dagger \hat{b}_q, \quad (209)$$

where ε is the core electron energy, ω_q is the boson energy with wave vector q , and \hat{c} and \hat{b}_q are the core electron and boson operators, respectively. Under the assumption that the boson has no dispersion with an average energy

ω_p , the exact solution for the core-electron removal spectra is given by [68]

$$A(\omega) = \sum_{n=0}^{\infty} f_n \delta(\omega - \varepsilon - \Delta\varepsilon + n\omega_p), \quad (210)$$

where

$$f_n = \frac{e^{-a} a^n}{n!}, \quad a = \sum_q \left(\frac{g_q}{\omega_p} \right)^2, \quad \Delta\varepsilon = a\omega_p. \quad (211)$$

The hole Green function corresponding to the above spectra is given by

$$G(t < 0) = i \sum_{n=0}^{\infty} f_n e^{-i(\varepsilon + \Delta\varepsilon - n\omega_p)t} \theta(-t). \quad (212)$$

In the Vxc framework, the equation of motion is given by

$$[i\partial_t - \varepsilon - V_{xc}(t)]G(t) = \delta(t). \quad (213)$$

The exact Vxc can be calculated from the Green function yielding

$$V_{xc}(t < 0) = \Delta\varepsilon (1 - e^{i\omega_p t}). \quad (214)$$

This expression offers a very simple interpretation: the first term corrects the noninteracting core-electron energy, whereas the second term describes the bosonic mode interacting with the core electron, exchanging multiple quanta of ω_p with the field. The result means that the simplified Holstein model can be understood as a system driven by a periodic complex potential (Floquet system).

It is interesting to note that the exact spectra can be obtained using the cumulant expansion [69–71] in which the cumulant is calculated within the *GW* approximation of the self-energy. Had the exact self-energy been used in the cumulant expansion, the exact spectra would presumably be not reproduced. This illustrates the subtle cancellation of error in the diagrammatic approach in the traditional self-energy formalism.

C. The Hubbard dimer

Although it is very simple, the half-filled Hubbard dimer with total $S_z = 0$ contains some of the essential physics of correlated electrons, and it has the merit of being analytically solvable. It also illustrates that the concept of xc hole is not restricted to continuous systems but can be carried over to lattice models.

The Hamiltonian of the Hubbard dimer in standard notation is given by

$$\hat{H} = -\Delta \sum_{i \neq j, \sigma} \hat{c}_{i\sigma}^\dagger \hat{c}_{j\sigma} + U \sum_i \hat{n}_{i\uparrow} \hat{n}_{i\downarrow}. \quad (215)$$

It is convenient to define

$$\hat{c}_i = \hat{c}_{i\uparrow}, \quad \hat{a}_i = \hat{c}_{i\downarrow}, \quad \hat{n}_i = \hat{c}_i^\dagger \hat{c}_i, \quad \hat{m}_i = \hat{a}_i^\dagger \hat{a}_i. \quad (216)$$

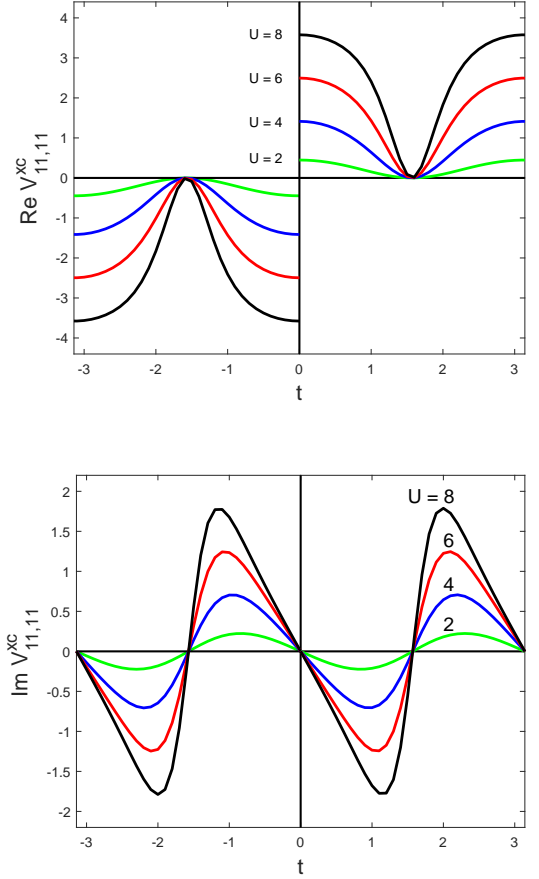


FIG. 2. The real and imaginary parts of $V_{11,11}^{xc}$ of the Hubbard dimer as functions of time for $U = 2, 4, 6$, and 8 with $\Delta = 1$ [44]. Due to the particle-hole symmetry, $V_{xc}(-t) = -V_{xc}(t)$.

To compare with the continuous case, one may define the Hubbard interaction as $U_{ij} = U\delta_{ij}$ and the Hamiltonian can be rewritten as

$$\hat{H} = -\Delta \sum_{i \neq j} \left(\hat{c}_i^\dagger \hat{c}_j + \hat{a}_i^\dagger \hat{a}_j \right) + \sum_{ij} \hat{n}_i U_{ij} \hat{n}_j. \quad (217)$$

The up-spin time-ordered Green function is defined as

$$iG_{ij}(t) = \langle \Psi_0 | T \hat{c}_i(t) \hat{c}_j^\dagger | \Psi_0 \rangle, \quad (218)$$

which is identical to the down-spin one. The Heisenberg equation of motion of $\hat{c}_i(t)$ is given by

$$i\partial_t \hat{c}_i(t) = [\hat{c}_i(t), \hat{H}] = \sum_k (h_{ik}^0 \hat{c}_k(t) + U_{ik} \hat{m}_k(t) \hat{c}_i(t)), \quad (219)$$

where

$$h^0 = \begin{pmatrix} 0 & -\Delta \\ -\Delta & 0 \end{pmatrix}. \quad (220)$$

The equation of motion of the Green function is then

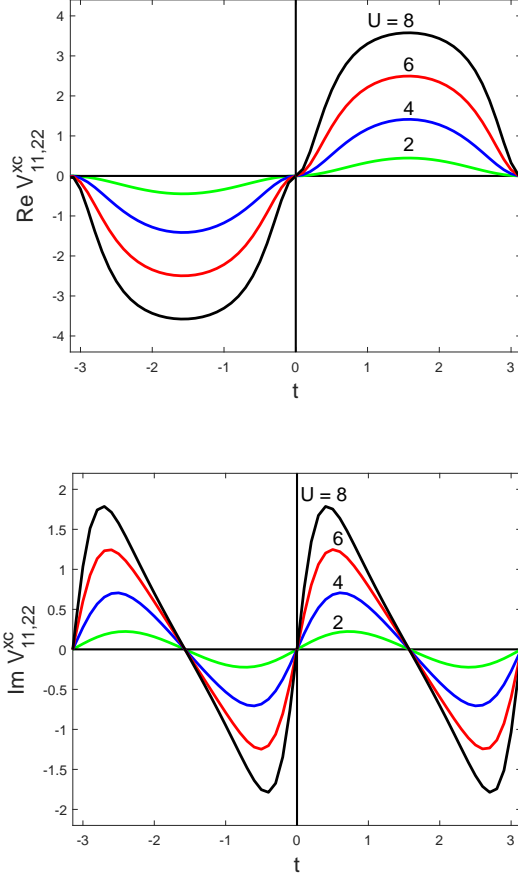


FIG. 3. The real and imaginary parts of $V_{11,22}^{xc}$ of the Hubbard dimer as functions of time for $U = 2, 4, 6$, and 8 with $\Delta = 1$ [44]. Due to the particle-hole symmetry, $V_{xc}(-t) = -V_{xc}(t)$.

given by

$$i\partial_t G_{ij}(t) - \sum_k \left[h_{ik}^0 G_{kj}(t) + U_{ik} G_{ijk}^{(2)}(t) \right] = \delta_{ij} \delta(t), \quad (221)$$

where

$$\begin{aligned} G_{ijk}^{(2)}(t) &= -i \langle \Psi_0 | T \hat{m}_k(t) \hat{c}_i(t) \hat{c}_j^\dagger | \Psi_0 \rangle \\ &= m_k g_{ijk}(t) G_{ij}(t), \end{aligned} \quad (222)$$

where $g_{ijk}(t)$ is the correlation function. Separating out the mean-field Hartree term $V_i^H = \sum_k U_{ik} m_k$ leads to the equation of motion,

$$(i\partial_t - V_i^H - V_{ij}^{xc}(t)) G_{ij}(t) - \sum_k h_{ik}^0 G_{kj}(t) = \delta_{ij} \delta(t), \quad (223)$$

where $V_{ij}^{xc}(t)$ is given by

$$V_{ij}^{xc}(t) = \sum_k U_{ik} \rho_{ijk}^{xc}(t), \quad \rho_{ijk}^{xc}(t) = [g_{ijk}(t) - 1] m_k. \quad (224)$$

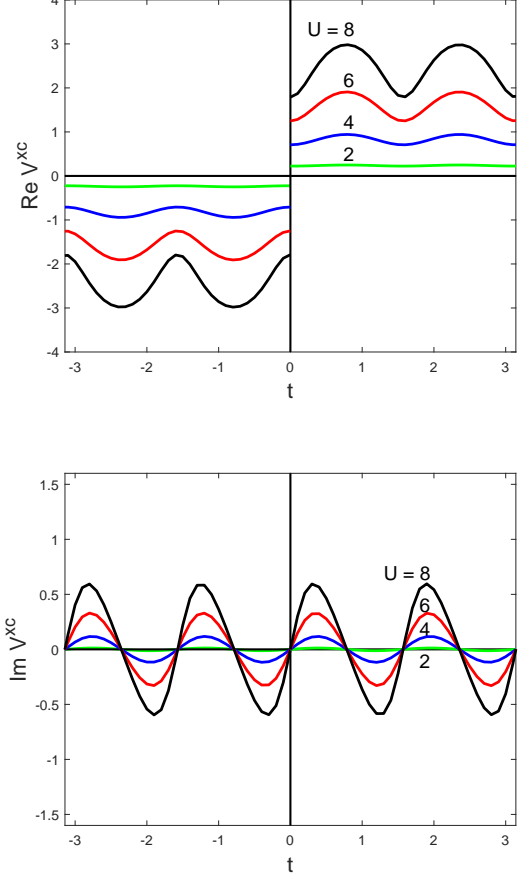


FIG. 4. The real and imaginary parts of $V_{BB}^{xc} = V_{AA}^{xc}$ as functions of time for $U = 2, 4, 6$, and 8 with $\Delta = 1$ [44].

Note that according to Eq. (49), $V_{ij}^{xc} = V_{ii,jj}^{xc}$, since the interaction has no off-site components and there is only one orbital per site.

The interaction term of the Hamiltonian of the Hubbard dimer explicitly takes into account exchange. For this reason, the sum rule for the xc hole integrates to zero. Since $\hat{M} = \sum_k \hat{m}_k$ counts the total number of down-spin electrons, one finds from the first line of Eq. (222)

$$\sum_k G_{ijk}^{(2)}(t) = M G_{ij}(t), \quad (225)$$

where M is the total number of down-spin electrons, which is one. This implies from the second line of Eq. (222) that

$$\sum_k m_k g_{ijk}(t) = M, \quad (226)$$

and from Eq. (224), it follows that

$$\sum_k \rho_{ijk}^{xc}(t) = 0. \quad (227)$$

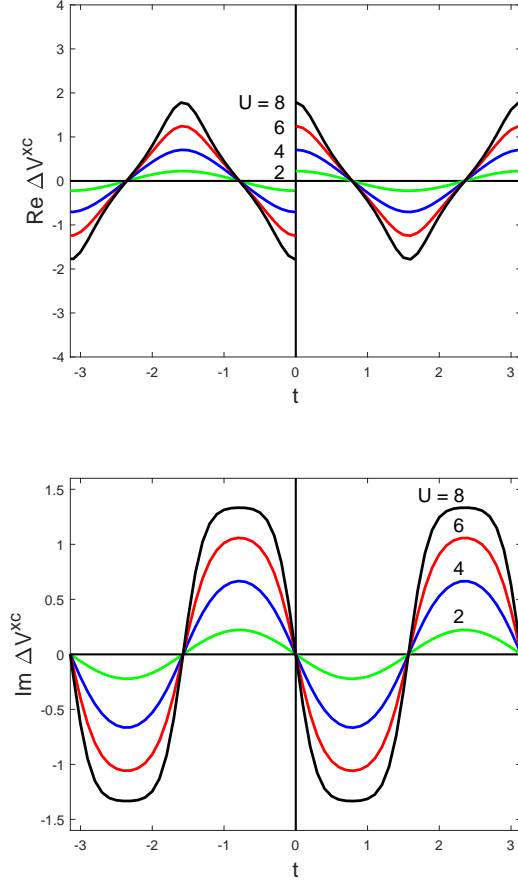


FIG. 5. The real and imaginary parts of V_{AB}^{xc} in as functions of time for $U = 2, 4, 6$, and 8 with $\Delta = 1$ [44].

This is consistent with the general sum rule in Eq. (40) since $\sigma \neq \sigma''$. Similarly, the exact constraint in Eq. (43) does not apply since in the present case $\sigma \neq \sigma''$.

The eigenvectors and eigenvalues corresponding to one-, two-, and three-electron fillings can be calculated analytically. V_{ij}^{xc} can be deduced from the equation of motion by calculating $G^{(2)}$ or G . The results, shown in Figs. 2 and 3, are given by [35, 44]

$$V_{11,11}^{\text{xc}}(t > 0) = \frac{\alpha U}{2} \frac{1 + e^{-i2\Delta t}}{1 + \alpha^2 e^{-i2\Delta t}}. \quad (228)$$

$$V_{11,22}^{\text{xc}}(t > 0) = \frac{\alpha U}{2} \frac{1 - e^{-i2\Delta t}}{1 - \alpha^2 e^{-i2\Delta t}}, \quad (229)$$

where

$$\alpha = \frac{1 - x}{1 + x}, \quad (230)$$

$$x = \frac{1}{4\Delta} \left(\sqrt{U^2 + 16\Delta^2} - U \right) \quad (231)$$

is the relative weight of double-occupancy configurations in the ground state with energy

$$E_0 = \frac{1}{2} \left(U - \sqrt{U^2 + 16\Delta^2} \right), \quad (232)$$

and

$$2\Delta = E_1^- - E_0^- = E_1^+ - E_0^+ > 0 \quad (233)$$

is the excitation energy of the $(N \pm 1)$ -systems. E_m^\pm are the m th eigenenergies of the $(N \pm 1)$ -systems:

$$E_0^- = -\Delta, \quad E_1^- = \Delta, \quad (234)$$

$$E_0^+ = U - \Delta, \quad E_1^+ = U + \Delta. \quad (235)$$

From symmetry, $V_{22}^{\text{xc}} = V_{11}^{\text{xc}}$ and $V_{21}^{\text{xc}} = V_{12}^{\text{xc}}$, i.e., V^{xc} is symmetric but not Hermitian, since it is complex. Due to the particle-hole symmetry, $V^{\text{xc}}(-t) = -V^{\text{xc}}(t)$. Note that the full V^{xc} carries four indices as in Eq. (49). Since there is only one orbital per site, it follows that $V_{11,11}^{\text{xc}} = V_{11}^{\text{xc}}$ and $V_{11,22}^{\text{xc}} = V_{12}^{\text{xc}}$.

In some cases, it is useful to choose the bonding and antibonding orbitals as the basis:

$$\phi_B = \frac{1}{\sqrt{2}} (\varphi_1 + \varphi_2), \quad \phi_A = \frac{1}{\sqrt{2}} (\varphi_1 - \varphi_2). \quad (236)$$

In this basis the Green function is diagonal and V^{xc} is given by

$$V_{BB,BB}^{\text{xc}} := V_{BB}^{\text{xc}} = V_{AA}^{\text{xc}} = \frac{1}{2} (V_{11}^{\text{xc}} + V_{12}^{\text{xc}}), \quad (237)$$

$$V_{AB,BA}^{\text{xc}} := V_{AB}^{\text{xc}} = V_{BA}^{\text{xc}} = \frac{1}{2} (V_{11}^{\text{xc}} - V_{12}^{\text{xc}}). \quad (238)$$

In the bonding-antibonding basis the equation of motion of the Green function becomes

$$[i\partial_t - \varepsilon_B - V_{BB}^{\text{xc}}(t)] G_B(t) - V_{BA}^{\text{xc}}(t) G_A(t) = \delta(t), \quad (239)$$

$$[i\partial_t - \varepsilon_A - V_{AA}^{\text{xc}}(t)] G_A(t) - V_{AB}^{\text{xc}}(t) G_B(t) = \delta(t), \quad (240)$$

where

$$\varepsilon_B = -\Delta, \quad \varepsilon_A = \Delta. \quad (241)$$

The Green functions in the bonding and antibonding orbitals can be solved analytically and are given by

$$iG_B(t > 0) = a_0^2 (1 - x)^2 \exp(-i\varepsilon_1^+ t), \quad (242)$$

$$iG_B(t < 0) = -a_0^2 (1 + x)^2 \exp(i\varepsilon_0^- t). \quad (243)$$

$$iG_A(t > 0) = a_0^2 (1 + x)^2 \exp(-i\varepsilon_0^+ t), \quad (244)$$

$$iG_A(t < 0) = -a_0^2 (1 - x)^2 \exp(i\varepsilon_1^- t), \quad (245)$$

where

$$a_0^2 = \frac{1}{2(1+x^2)}. \quad (246)$$

The orbital energies are defined as

$$\varepsilon_m^\pm = E_m^\pm - E_0. \quad (247)$$

For $t > 0$,

$$V_{BB}^{\text{xc}}(t > 0) = \frac{\alpha U}{2} \frac{1 - \alpha^2 e^{-i4\Delta t}}{1 - \alpha^4 e^{-i4\Delta t}}, \quad (248)$$

$$V_{AB}^{\text{xc}}(t > 0) = \frac{\alpha U}{2} \frac{(1 - \alpha^2) e^{-i2\Delta t}}{1 - \alpha^4 e^{-i4\Delta t}}, \quad (249)$$

shown in Figs. 4 and 5. Note the definition of V_{BB}^{xc} and V_{AB}^{xc} in Eqs. (237) and (238).

For a finite Δ one observes that $x = 1$ when $U = 0$, and x approaches zero as $U \rightarrow \infty$ so that $0 < x \leq 1$, which implies that $\alpha < 1$. It is therefore legitimate to expand the denominator in powers of α giving

$$\begin{aligned} V_{BB}^{\text{xc}}(t > 0) &= \frac{\alpha U}{2} (1 - \alpha^2 e^{-i4\Delta t}) (1 + \alpha^4 e^{-i4\Delta t} + \dots) \\ &= \frac{\alpha U}{2} \{1 - \alpha^2(1 - \alpha^2)e^{-i4\Delta t} - \alpha^6 e^{-i8\Delta t}\}, \end{aligned} \quad (250)$$

$$\begin{aligned} V_{AB}^{\text{xc}}(t > 0) &= \frac{\alpha U}{2} (1 - \alpha^2) e^{-i2\Delta t} (1 + \alpha^4 e^{-i4\Delta t} + \dots) \\ &= \frac{\alpha U}{2} (1 - \alpha^2) (e^{-i2\Delta t} + \alpha^4 e^{-i6\Delta t}) + \dots \end{aligned} \quad (251)$$

For a relatively strong correlation corresponding to $\frac{U}{4\Delta} = 2$, one finds $\alpha = 0.62$. This yields $1 - \alpha^2 = 0.62$ and $\alpha^2(1 - \alpha^2) = 0.24$. The dominating terms in V^{xc} are

$$V_{BB}^{\text{xc}}(t > 0) \approx \frac{\alpha U}{2}, \quad (252)$$

$$V_{AB}^{\text{xc}}(t > 0) = \frac{\alpha U}{2} (1 - \alpha^2) e^{-i2\Delta t}. \quad (253)$$

The first term shifts the one-particle energy, whereas the second gives rise to an incoherent or satellite feature. This approximate V_{xc} of the dimer will be extrapolated later to the infinite chain. The higher-energy excitations are multiples of 2Δ , which is the energy difference between the bonding and antibonding energies. This energy difference may be regarded as the bosonic excitation (particle-hole) energy.

An interesting feature of V_{xc} is the presence of a discontinuity at $t = 0$, reminiscent of the derivative discontinuity of the xc energy in DFT [55]. As alluded earlier in Sec. X, V_{xc} for the negative-time Green function is

expected to be more negative than the one for positive-time since the former is the Coulomb potential of an xc hole that integrates to -1 whereas the latter is to zero. This difference gives rise to the discontinuity and provides a physical explanation for the well-known band-gap underestimation in Kohn-Sham DFT. The xc potential in Kohn-Sham DFT corresponds to occupied orbitals only, that is, to the negative-time Green function (creation of a hole creation or removal of an electron). The unoccupied orbitals corresponding to the positive-time Green function should see an xc potential that is more positive than that of the occupied orbitals. However, the Kohn-Sham unoccupied and occupied orbitals see the same potential, which then leads to an underestimation of the band gap in semiconductors and insulators. Thus, even if the exact Kohn-Sham xc potential were known, it would likely give rise to a band-gap underestimation. In principle, there is nothing wrong with this since the Kohn-Sham scheme is not meant to describe excited states.

In terms of the effective potential defined in Eq. (170), the equations of motion in the bonding-antibonding basis can be recast as

$$[i\partial_t - \varepsilon_B - \Xi_B(t)] G_B(t) = \delta(t), \quad (254)$$

$$[i\partial_t - \varepsilon_A - \Xi_A(t)] G_A(t) = \delta(t), \quad (255)$$

where according to the definition in Eq. (170),

$$\Xi_B(t) = V_{BB}(t) + V_{BA}(t) \frac{G_A(t)}{G_B(t)}, \quad (256)$$

$$\Xi_A(t) = V_{AA}(t) + V_{AB}(t) \frac{G_B(t)}{G_A(t)}. \quad (257)$$

These yield

$$\Xi_B(t < 0) = -\frac{\alpha U}{2}, \quad \Xi_B(t > 0) = \frac{U}{2\alpha}. \quad (258)$$

$$\Xi_A(t > 0) = \frac{\alpha U}{2}, \quad \Xi_A(t < 0) = -\frac{U}{2\alpha}, \quad (259)$$

Note that the expressions for $\Xi_A(t < 0)$ and $\Xi_B(t > 0)$ are valid for $U > 0$ since if $U = 0$ then $G_A(t < 0) = G_B(t > 0) = 0$. The effective potential Ξ takes a very simple form, namely a constant in each time segment and in stark contrast to the traditional self-energy shown in Fig. 6 for the bonding orbital. The self-energy in the frequency domain $\Sigma_B(\omega)$ is defined as

$$G_B(\omega) = \frac{1}{\omega - \varepsilon_B - \Sigma_B(\omega)}. \quad (260)$$

In the V_{xc} formalism, $\Xi_B(t < 0)$ simply shifts the bonding energy ε_B by $-\frac{\alpha U}{2}$, and as a consequence of the many-electron interactions, $\Xi_B(t > 0)$ generates a new feature in the unoccupied part of the spectrum separated in energy from ε_B by $\frac{U}{2\alpha}$. The appearance of spectral

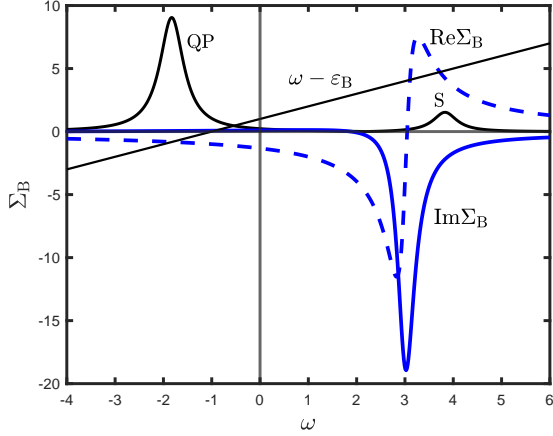


FIG. 6. The real and imaginary parts of the self-energy and the spectral function of the Hubbard dimer for $U = 4$ and $\Delta = 1$ in the bonding orbital. The energies at which the straight line $\omega - \varepsilon_B$ crosses the real part of the self-energy $\text{Re}\Sigma_B$ correspond to the main peak (QP) in the spectral function and an additional structure in the unoccupied region (S). Both of these peaks are magnified ten times for clarity and a broadening of 0.3 has been used for plotting purpose. The crossing at $\omega \approx 3$ does not yield any spectral feature since $\text{Im}\Sigma_B$ at that energy is very large. The spectral function for the antibonding orbital is the mirror image of that of the bonding-orbital with respect to $\omega = 0$.

weight above the chemical potential originating from the antibonding orbital compensates for the loss of spectral weight of the bonding orbital for $t < 0$, as can be seen in Eqs. (245) and (243), so that the sum of the spectral weights for $t < 0$ is equal to one. A similar consideration applies to the case $t > 0$.

XVII. EXCHANGE-CORRELATION HOLE AND VXC OF THE HOMOGENEOUS ELECTRON GAS

The homogeneous electron gas is an invaluable model of itinerant valence electrons in solids, which usually originate from s and p orbitals. It is also an indispensable reference system when employing LDA as an extrapolation scheme for application to real materials. It is therefore very important to study its xc hole and potential. A more detailed treatment of the present section can be found in Ref. [45].

The Green function of the noninteracting homogeneous electron gas is given by

$$iG_0(r, r'; t) = \frac{1}{\Omega} \sum_{k > k_F} e^{i\mathbf{k} \cdot (\mathbf{r} - \mathbf{r}')} e^{-i\varepsilon_k t} \theta(t) - \frac{1}{\Omega} \sum_{k \leq k_F} e^{i\mathbf{k} \cdot (\mathbf{r} - \mathbf{r}')} e^{-i\varepsilon_k t} \theta(-t), \quad (261)$$

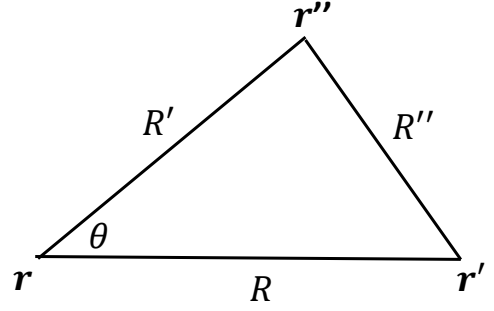


FIG. 7. Definition of the radial variables R , R' , and R'' . They are related to the angle θ by $R''^2 = R^2 - 2RR' \cos \theta + R'^2$. The corresponding vectors are defined as $\mathbf{R} = \mathbf{r}' - \mathbf{r}$, $\mathbf{R}' = \mathbf{r}'' - \mathbf{r}$, and $\mathbf{R}'' = \mathbf{r}'' - \mathbf{r}'$.

where $\varepsilon_k = \frac{1}{2}k^2$, k_F is the Fermi wave vector, and Ω is the space volume. For the paramagnetic case considered here $\sigma = \sigma'$.

For the homogeneous electron gas, it is convenient to introduce the variable $\mathbf{R} = \mathbf{r}' - \mathbf{r}$. The Green function as well as Vxc depend only on the spatial separation R . In spherical coordinates, the δ -function is given by

$$\delta(\mathbf{R}) = \frac{1}{R^2} \delta(R) \delta(y) \delta(\phi), \quad (262)$$

where $y = \cos \theta$ (θ is the polar angle in spherical coordinates). For a radial function $f(R)$ without angular dependence,

$$\nabla^2 f = \frac{1}{R} \frac{\partial^2}{\partial R^2} (Rf). \quad (263)$$

After integrating over the solid angle, the equation of motion becomes

$$\left(i \frac{\partial}{\partial t} - h(R) - V_{xc}(R, t) \right) \tilde{G}(R, t) = \frac{1}{4\pi R} \delta(R) \delta(t), \quad (264)$$

where

$$h(R) = -\frac{1}{2} \frac{\partial^2}{\partial R^2}, \quad \tilde{G}(R, t) = R G(R, t). \quad (265)$$

A. Exchange hole

Using the noninteracting Green function in Eq. (261) the exchange hole in Eq. (71) can be calculated analytically, and for the case $t < 0$ one finds

$$\rho_x(r, r', r''; t < 0) \sum_{k \leq k_F} e^{i\mathbf{k} \cdot (\mathbf{r} - \mathbf{r}')} e^{-i\varepsilon_k t} = -\frac{1}{\Omega} \sum_{k' \leq k_F} e^{i\mathbf{k}' \cdot (\mathbf{r} - \mathbf{r}'')} \times \sum_{k \leq k_F} e^{i\mathbf{k} \cdot (\mathbf{r}'' - \mathbf{r}')} e^{-i\varepsilon_k t}. \quad (266)$$

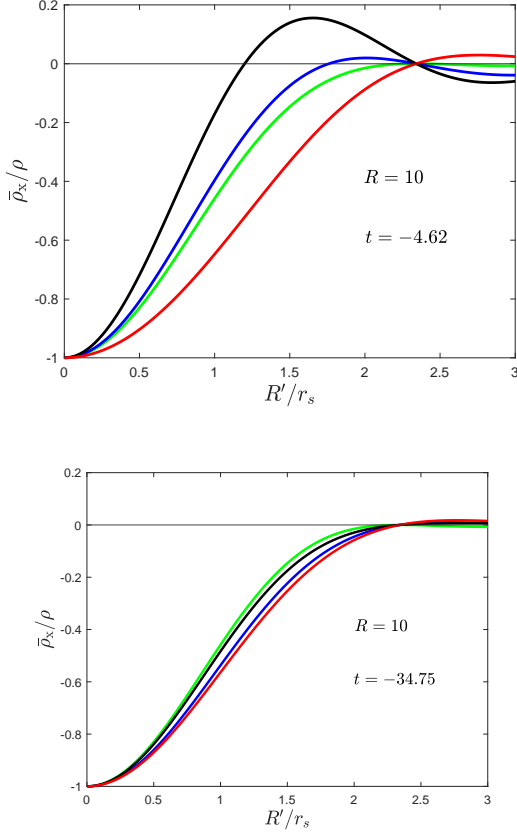


FIG. 8. The spherical average of the exchange hole of the electron gas scaled with the density with Wigner-Seitz radius $r_s = 3$ (blue), 4 (black), and 5 (red) plotted against R'/r_s for the case $R = 10$ and $t = -4.62$ (top) and -34.75 (bottom), corresponding to the inverse of the plasmon energy and the Fermi energy, respectively. The green curve is the static exchange hole, which is independent of r_s .

For $t > 0$,

$$\begin{aligned} \rho_x(r, r', r''; t > 0) &= \sum_{k > k_F} e^{i\mathbf{k} \cdot (\mathbf{r} - \mathbf{r}')} e^{-i\varepsilon_k t} \\ &= -\frac{1}{\Omega} \sum_{k' \leq k_F} e^{i\mathbf{k}' \cdot (\mathbf{r} - \mathbf{r}'')} \times \sum_{k > k_F} e^{i\mathbf{k} \cdot (\mathbf{r}'' - \mathbf{r}')} e^{-i\varepsilon_k t}. \end{aligned} \quad (267)$$

It can be immediately seen that by setting $r'' = r$ the exact constraint in Eq. (43) is satisfied and by integrating over r'' the sum rule in Eq. (40) is fulfilled. Expressed in terms of the radial variables R , R' , R'' and the angle θ as defined in Fig. 7,

$$\rho_x(R, R', \theta; t) = iG_0(R', 0^-) \frac{G_0(R'', t)}{G_0(R, t)} \quad (268)$$

where R'' depends on θ .

$G_0(R, t)$ can be calculated from Eq. (261) by perform-

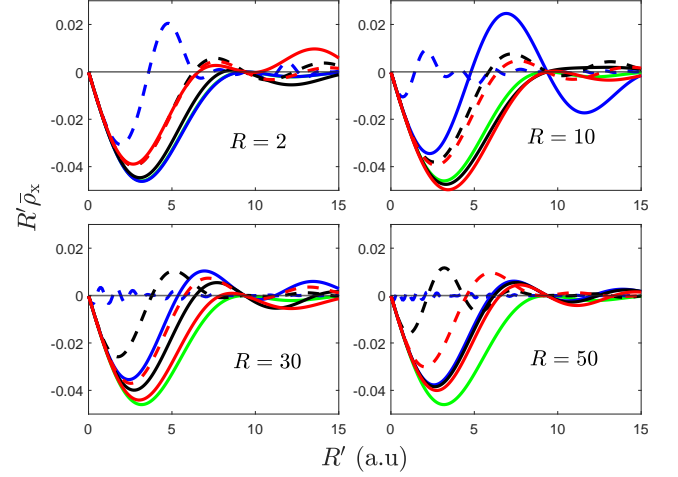


FIG. 9. The real part of the spherical average of the exchange hole multiplied by R' for $t = \pm 4.62$ (blue), ± 34.75 (black), ± 69.5 (red), and $R = 2, 10, 30, 50$. The solid and dashed curves correspond to $t < 0$ and $t > 0$, respectively. The green curve is the static exchange hole from the Hartree-Fock approximation. For $t = -4.62$ (solid blue) and $R = 2$ the exchange hole is virtually indistinguishable from the static one [45].

ing the integral over the solid angle in \mathbf{k} , yielding

$$iG_0(R, t < 0) = -\frac{1}{2\pi^2} \frac{1}{R} \int_0^{k_F} dk k \sin(kR) e^{-ik^2 t/2}, \quad (269)$$

$$iG_0(R, t > 0) = \frac{1}{2\pi^2} \frac{1}{R} \int_{k_F}^{\infty} dk k \sin(kR) e^{-ik^2 t/2}, \quad (270)$$

$$iG_0(R, 0^-) = -\frac{1}{2\pi^2} \frac{1}{R^3} [\sin(k_F R) - k_F R \cos(k_F R)]. \quad (271)$$

$G_0(R, t < 0)$ can be expressed in terms of the complex error function or calculated numerically using a standard quadrature.

To calculate $G_0(R, t > 0)$ requires more care. The integral over k can be decomposed as follows:

$$iG_0(R, t > 0) = \frac{1}{2\pi^2 R} [I(0, \infty) - I(0, k_F)], \quad (272)$$

where

$$I(a, b) = \int_a^b dk k \sin(kR) e^{-ik^2 t/2}. \quad (273)$$

The integral $I(0, \infty)$ can be performed analytically resulting in

$$I(0, \infty) = \sqrt{\frac{\pi}{2it}} \frac{R}{it} e^{iR^2/2t}. \quad (274)$$

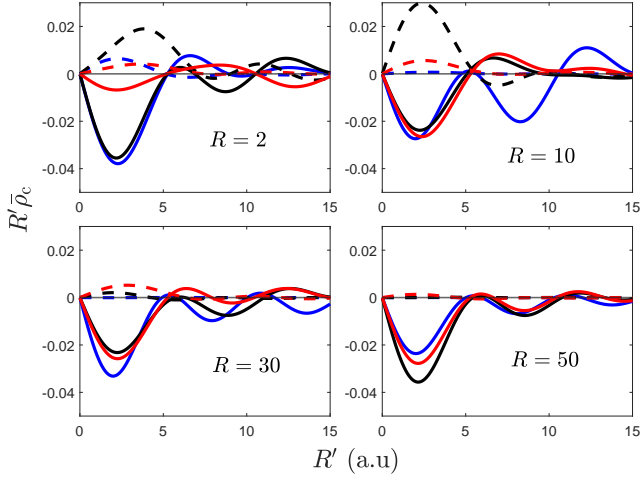


FIG. 10. The real part of the spherical average of the correlation hole multiplied by R' for $t = \pm 4.62$ (blue), ± 34.75 (black), ± 69.5 (red), and $R = 2, 10, 30, 50$. The solid and dashed curves correspond to $t < 0$ and $t > 0$, respectively [45].

1. Spherical average of the exchange hole

For the homogeneous electron gas, \mathbf{r} may be chosen as the origin of coordinate and set to zero. Defining $\mathbf{R} = \mathbf{r}' - \mathbf{r} = \mathbf{r}'$ and $\mathbf{R}' = \mathbf{r}'' - \mathbf{r} = \mathbf{r}''$ as illustrated in Fig. 7 the exchange hole in Eq. (266) becomes for $t < 0$

$$\begin{aligned} \rho_x(R, R', \theta; t < 0) \times iG_0(R, t < 0) \\ = -\frac{1}{\Omega^2} \sum_{\mathbf{k} \leq k_F} e^{-i\mathbf{k} \cdot \mathbf{R}} e^{-i\varepsilon_k t} \sum_{\mathbf{k}' \leq k_F} e^{i\mathbf{q} \cdot \mathbf{R}'}, \end{aligned} \quad (275)$$

where $\mathbf{q} = \mathbf{k} - \mathbf{k}'$. The spherical averaging of ρ_x amounts to performing a solid-angle integration over \mathbf{R}' ,

$$\int d\Omega_{R'} e^{i\mathbf{q} \cdot \mathbf{R}'} = 4\pi \frac{\sin(qR')}{qR'}, \quad (276)$$

yielding for $t < 0$

$$\begin{aligned} \bar{\rho}_x(R, R', t < 0) iG_0(R, t) \\ = \frac{1}{\Omega^2} \sum_{\mathbf{k}, \mathbf{k}' \leq k_F} e^{-i\mathbf{k} \cdot \mathbf{R}} e^{-i\varepsilon_k t} \times 4\pi \frac{\sin(qR')}{qR'}. \end{aligned} \quad (277)$$

Fig. 8 illustrates the spherical average of the exchange hole for $r_s = 3, 4, 5$, $R = 10$, and a couple of typical times. Fig. 9 shows examples of the spherical average of the exchange hole multiplied by the radial distance R' for $r_s = 4$ and for several values of R . As anticipated, the exchange holes for positive times are noticeably more oscillatory than those for negative times. For negative times, the exchange holes closely follow the static Hartree-Fock exchange hole.

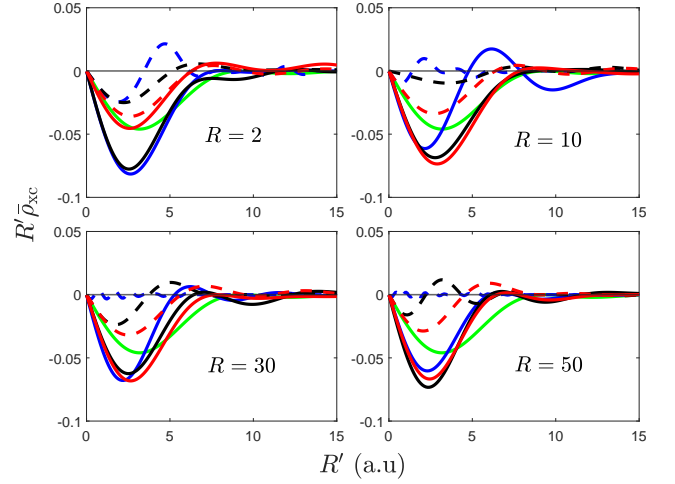


FIG. 11. The real part of the spherical average of the xc hole multiplied by R' for $t = \pm 4.62$ (blue), ± 34.75 (black), ± 69.5 (red), and $R = 2, 10, 30, 50$ [45]. The solid and dashed curves correspond to $t < 0$ and $t > 0$, respectively. The green curve is the static exchange hole from the Hartree-Fock approximation. For $t = -4.62$ (solid blue) and $R = 2$ the exchange hole is virtually indistinguishable from the static one.

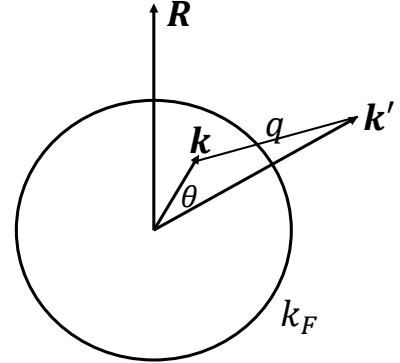


FIG. 12. Integration over \mathbf{k} and \mathbf{k}' for the correlation hole. The angle between \mathbf{k} and \mathbf{k}' is labelled by θ . The angle between \mathbf{k}' and \mathbf{R} is θ' (not labelled in the figure). $q = \sqrt{k'^2 + k^2 - 2kk'y}$ in which $y = \cos \theta$.

B. Correlation hole

The density-response contribution to ρ_{xc} is given by the second term on the right-hand side of Eq. (64):

$$\rho_c(1, 2, 3)G(1, 2) = i \int d4 G(1, 4)K(4, 3)G(4, 2) \quad (278)$$

where $K = \delta V_H / \delta \varphi = vR$ as defined earlier in Eq. (66). For the homogeneous electron gas, G and K depend only

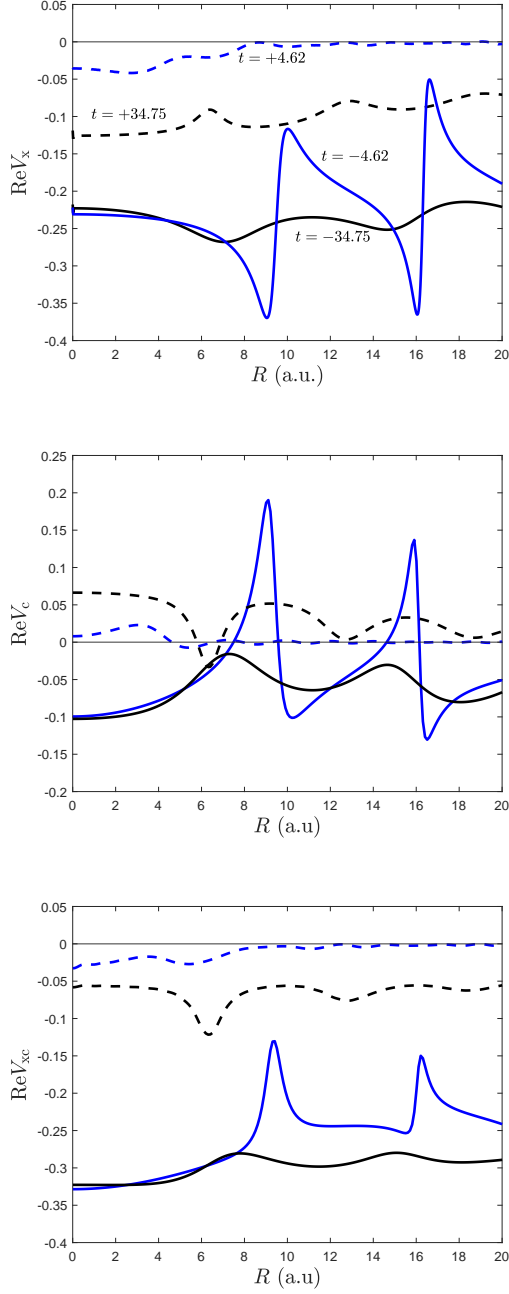


FIG. 13. The real part of the exchange potential (top), the correlation potential (middle), and V_{xc} for $t = \pm 4.62$ (blue) and ± 34.75 (black). The solid and dashed curves correspond to $t < 0$ and $t > 0$, respectively [45].

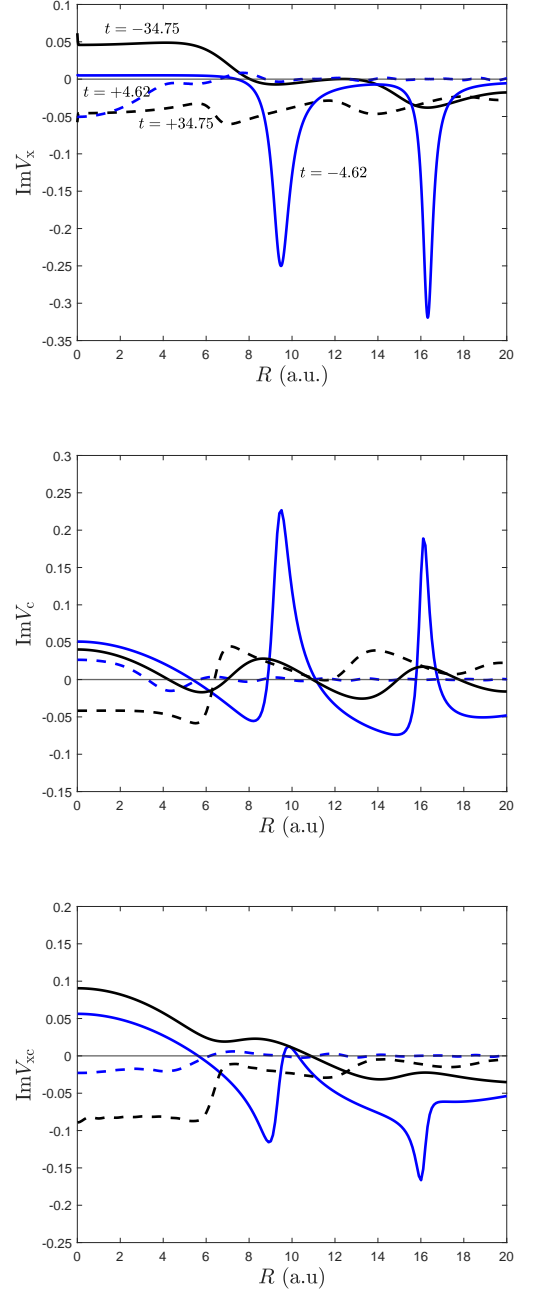


FIG. 14. The imaginary part of the exchange potential (top), the correlation potential (middle), and V_{xc} for $t = \pm 4.62$ (blue) and ± 34.75 (black). The solid and dashed curves correspond to $t < 0$ and $t > 0$, respectively [45].

$r_1 = r$, $r_2 = r'$, and $r_3 = r''$, one finds

$$\begin{aligned}
 & \rho_c(r, r', r''; t) G(r - r'; t) \\
 &= i \int dr_4 dt_4 G(r - r_4, t - t_4) K(r_4 - r'', t_4 - t) \\
 & \quad \times G(r_4 - r', t_4). \tag{279}
 \end{aligned}$$

on the separation of the spatial and time coordinates. Keeping in mind that $t_3 = t_1 = t$, $t_2 = 0$ and setting

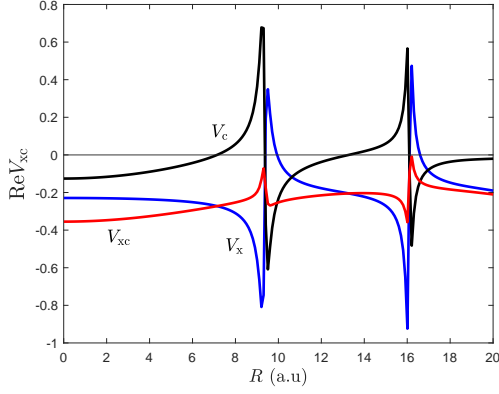


FIG. 15. The real part of the exchange potential (blue), the correlation potential (black), and V_{xc} (red) for $t = -1$. The large cancellation between exchange and correlation can be clearly seen [45].

To calculate ρ_c , a noninteracting G_0 as in Eq. (261) will be used. K is written in terms of its Fourier components,

$$K(r_4 - r'', t_4 - t) = \frac{1}{\Omega} \sum_q \int \frac{d\omega}{2\pi} e^{-i\mathbf{q} \cdot (\mathbf{r}_4 - \mathbf{r}'')} e^{-i\omega(t_4 - t)} K(q, \omega). \quad (280)$$

Within RPA, $K(q, \omega)$ is known analytically. Due to the time ordering, the product of two Green functions appearing on the right-hand side of Eq. (279) yields only two nonzero terms. Consider the case $t < 0$. The first nonzero term is (note the additional factor of i from $iGKG$)

$$A_1 = \frac{1}{\Omega^2} \sum_{k \leq k_F} \sum_{k' > k_F} e^{-i\mathbf{k}' \cdot \mathbf{R}} e^{i\mathbf{q} \cdot \mathbf{R}'} \times \int \frac{d\omega}{2\pi} K(q, \omega) \frac{e^{i(\omega - \varepsilon_k)t}}{\omega - \varepsilon_k + \varepsilon_{k'} - i\eta}, \quad (281)$$

where \mathbf{R} and \mathbf{R}' are defined in Fig. 7 and $\mathbf{q} = \mathbf{k}' - \mathbf{k}$.

The spectral representation of K ,

$$K(q, \omega) = \int_{-\infty}^0 d\omega' \frac{L(q, \omega')}{\omega - \omega' - i\delta} + \int_0^{\infty} d\omega' \frac{L(q, \omega')}{\omega - \omega' + i\delta}, \quad (282)$$

where

$$L(q, \omega) = -\frac{1}{\pi} \text{sign}(\omega) \text{Im}K(q, \omega), \quad (283)$$

is used to perform the integral over ω . The spectral function $L(q, \omega)$ is an odd function in ω .

For the case $t < 0$, the contour integral for A_1 in the

complex ω plane is closed in the lower quadrants, yielding

$$\int \frac{d\omega}{2\pi} \frac{1}{\omega - \omega' + i\delta} \times \frac{e^{i(\omega - \varepsilon_k)t}}{\omega - \varepsilon_k + \varepsilon_{k'} - i\eta} = \frac{-ie^{i(\omega' - \varepsilon_k - i\delta)t}}{\omega' - \varepsilon_k + \varepsilon_{k'} - i\eta}. \quad (284)$$

Using $L(q, -\omega) = -L(q, \omega)$, one finds

$$A_1 = \frac{1}{\Omega^2} \sum_{k \leq k_F} \sum_{k' > k_F} e^{-i\mathbf{k}' \cdot \mathbf{R}} e^{i\mathbf{q} \cdot \mathbf{R}'} e^{-i\varepsilon_k t} \times \int_0^{\infty} d\omega' L(q, \omega') \frac{-ie^{i\omega' t}}{\omega' + \varepsilon_{k'} - \varepsilon_k}. \quad (285)$$

The integral over ω' can be parametrised for each t as follows:

$$M(q, \omega, t) = \int_0^{\infty} d\omega' L(q, \omega') \frac{-ie^{i\omega' t}}{\omega' + \omega}, \quad (286)$$

A_1 together with the other nonzero $t < 0$ term, A_2 , and the two nonzero terms corresponding to $t > 0$, B_1 and B_2 , become

$$A_1 = \frac{1}{\Omega^2} \sum_{k \leq k_F} \sum_{k' > k_F} e^{-i\mathbf{k}' \cdot \mathbf{R}} e^{i\mathbf{q} \cdot \mathbf{R}'} e^{-i\varepsilon_k t} M(q, \varepsilon_{k'} - \varepsilon_k, t), \quad (287)$$

$$A_2 = \frac{1}{\Omega^2} \sum_{k \leq k_F} \sum_{k' > k_F} e^{-i\mathbf{k} \cdot \mathbf{R}} e^{i\mathbf{q} \cdot \mathbf{R}'} e^{-i\varepsilon_k t} M(q, \varepsilon_{k'} - \varepsilon_k, 0), \quad (288)$$

$$B_1 = \frac{1}{\Omega^2} \sum_{k \leq k_F} \sum_{k' > k_F} e^{-i\mathbf{k}' \cdot \mathbf{R}} e^{i\mathbf{q} \cdot \mathbf{R}'} e^{-i\varepsilon_{k'} t} M(q, \varepsilon_{k'} - \varepsilon_k, 0), \quad (289)$$

$$B_2 = \frac{1}{\Omega^2} \sum_{k \leq k_F} \sum_{k' > k_F} e^{-i\mathbf{k} \cdot \mathbf{R}} e^{i\mathbf{q} \cdot \mathbf{R}'} e^{-i\varepsilon_{k'} t} M(q, \varepsilon_{k'} - \varepsilon_k, -t). \quad (290)$$

The correlation hole is then given by

$$\rho_c(R, R', \theta; t < 0) = \frac{A_1 + A_2}{G_0(R, t < 0)}, \quad (291)$$

$$\rho_c(R, R', \theta; t > 0) = \frac{B_1 + B_2}{G_0(R, t > 0)}. \quad (292)$$

The correlation hole involves coupled integrals over momenta below and above k_F leading to a six-dimensional integral, which cannot be easily performed with standard quadratures. However, only the spherical average is needed to determine the correlation potential and the six-dimensional integral can be reduced to a three-dimensional one.

1. Spherical average of the correlation hole

Spherical averaging A_1 in Eq. (287) over $\mathbf{R}' = \mathbf{r}''$ yields

$$\bar{A}_1 = \frac{4\pi}{\Omega^2} \sum_{k' > k_F} e^{-i\mathbf{k}' \cdot \mathbf{R}} \sum_{k \leq k_F} \frac{\sin(qR')}{qR'} e^{-i\varepsilon_k t} \times M(q, \varepsilon_{k'} - \varepsilon_k, t). \quad (293)$$

It can be seen from Fig. 12 that for a fixed \mathbf{k}' , the integration over \mathbf{k} is independent of the azimuthal angle so that

$$\bar{A}_1 = \frac{1}{\pi\Omega} \sum_{k' > k_F} e^{-i\mathbf{k}' \cdot \mathbf{R}} \int_0^{k_F} dk k^2 \times \int_{-1}^1 dy \frac{\sin(qR')}{qR'} e^{-i\varepsilon_k t} M(q, \varepsilon_{k'} - \varepsilon_k, t). \quad (294)$$

It can also be seen that the integration over \mathbf{k} is independent of the direction of \mathbf{k}' so that the total integral reduces to three dimensions:

$$\bar{A}_1 = \frac{1}{2\pi^3 R} \int_{k_F}^{\infty} dk' k' \sin(k' R) \times \int_0^{k_F} dk k^2 e^{-i\varepsilon_k t} Q(k, k', R', t), \quad (295)$$

$$\bar{A}_2 = \frac{1}{2\pi^3 R} \int_0^{k_F} dk k \sin(k R) e^{-i\varepsilon_k t} \times \int_{k_F}^{\infty} dk' k'^2 Q(k, k', R', 0), \quad (296)$$

$$\bar{B}_1 = \frac{1}{2\pi^3 R} \int_{k_F}^{\infty} dk' k' \sin(k' R) e^{-i\varepsilon_{k'} t} \times \int_0^{k_F} dk k^2 Q(k, k', R', 0), \quad (297)$$

$$\bar{B}_2 = \frac{1}{2\pi^3 R} \int_0^{k_F} dk k \sin(k R) \times \int_{k_F}^{\infty} dk' k'^2 e^{-i\varepsilon_{k'} t} Q(k, k', R', -t), \quad (298)$$

where

$$Q(k, k', R', t) = \int_{-1}^1 dy \frac{\sin(qR')}{qR'} M(q, \varepsilon_{k'} - \varepsilon_k, t). \quad (299)$$

The dependence of the integrand on the variable y enters through q as defined in Fig. 12.

The spherical average of the correlation hole is then given by

$$\bar{\rho}_c(R, R'; t < 0) = \frac{\bar{A}_1 + \bar{A}_2}{G_0(R, t < 0)}, \quad (300)$$

$$\bar{\rho}_c(R, R'; t > 0) = \frac{\bar{B}_1 + \bar{B}_2}{G_0(R, t > 0)}. \quad (301)$$

C. Plasmon-pole approximation

Great simplification results if a plasmon-pole approximation independent of q is used for $L(q, \omega)$ defined in Eq. (283):

$$L(q, \omega) = \frac{\omega_p}{2} [\delta(\omega - \omega_p) - \delta(\omega + \omega_p)], \quad (302)$$

which corresponds to

$$K(q \rightarrow 0, \omega) = \frac{\omega_p^2}{\omega^2 - \omega_p^2}. \quad (303)$$

The approximation is valid for $q \leq q_c$ and for $r_s = 3, 4, 5$ the critical momenta are $q_c = 0.86, 0.82$, and $0.73 k_F$, respectively. These cover most of the average valence densities in real materials,

Within the plasmon-pole approximation, the quantity M defined in Eq. (286) can be calculated analytically:

$$M(q, \omega, t) = \frac{\omega_p}{2} \frac{-ie^{i\omega_p t}}{\omega_p + \omega}. \quad (304)$$

The interdependence between \mathbf{k} and \mathbf{k}' is partially unlock. The plasmon-pole approximation imparts error to the correlation contribution. This error can be minimised by treating the upper limit of the integral over unoccupied states (k') as a parameter. For $r_s = 4$, an upper limit of $\approx 1.5k_F$ approximately reproduces the static correlation hole [72].

Fig. 10 shows examples of the spherical average of the correlation hole multiplied by the radial distance R' for $r_s = 4$ and for several values of R calculated using the plasmon-pole approximation. Fig. 11 is similar to Fig. 10 but for the xc hole. It is interesting to observe that the xc hole is more localised than the exchange hole, as can be seen by comparing Figs. 9 and 11. A similar behaviour is known in DFT.

D. Exchange-correlation potential

As described in Section IX, the change of variable $\mathbf{R}' = \mathbf{r}'' - \mathbf{r}$ reduces V_{xc} in Eq. (46) to the first radial moment of the spherical average of ρ_{xc} :

$$V_{xc}(r, r'; t) = \int dR' R' \bar{\rho}_{xc}(r, r', R'; t), \quad (305)$$

where $\bar{\rho}_{xc}(r, r', R'; t)$, for given r, r' , and t , depends only on the radial distance $R' = |\mathbf{r}'' - \mathbf{r}|$,

$$\bar{\rho}_{xc}(r, r', R'; t) = \int d\Omega_{R'} \rho_{xc}(r, r', \mathbf{r} + \mathbf{R}'; t). \quad (306)$$

1. Exchange potential

The exchange potential is the first moment of $\bar{\rho}_x$ in R' , which from Eq. (277) is given by for $t < 0$

$$V_x(R, t < 0) = \frac{1}{iG_0(R, t)} \frac{4\pi}{\Omega^2} \sum_{k, k' \leq k_F} e^{-i\mathbf{k} \cdot \mathbf{R}} e^{-i\varepsilon_k t} \times \int dR' \frac{\sin(qR')}{q}. \quad (307)$$

Consider the integral over R' with positive $\alpha \rightarrow 0$:

$$\lim_{\alpha \rightarrow 0} \int_0^\infty dR' \sin(qR') e^{-\alpha R'} = \frac{1}{q}. \quad (308)$$

One finds

$$V_x(R, t < 0) = \frac{1}{iG_0(R, t)} \frac{4\pi}{\Omega^2} \sum_{k, k' \leq k_F} e^{-i\mathbf{k} \cdot \mathbf{R}} e^{-i\varepsilon_k t} \frac{1}{q^2}. \quad (309)$$

The integral over k' is given by

$$f(k) = \frac{1}{\Omega} \sum_{k' \leq k_F} \frac{1}{q^2} = \frac{1}{4\pi^2 k} \int_0^{k_F} dk' k' \ln \left| \frac{k+k'}{k-k'} \right|, \quad (310)$$

which can be performed analytically yielding

$$f(k) = \frac{k_F}{2\pi^2} F(k/k_F), \quad (311)$$

where

$$F(x) = \frac{1}{2} + \frac{1-x^2}{4x} \ln \left| \frac{1+x}{1-x} \right|. \quad (312)$$

This function is identical to the one appearing in the static Hartree-Fock theory for the electron gas [38]. More explicitly, as a function of k ,

$$f(k) = \frac{k_F}{2\pi^2} \left(\frac{1}{2} + \frac{k_F^2 - k^2}{4k_F k} \ln \left| \frac{k_F + k}{k_F - k} \right| \right). \quad (313)$$

There remains the integral over \mathbf{k} , which is a one-dimensional integral over radial k :

$$V_x(R, t < 0) = \frac{1}{iG_0(R, t)} \times \frac{2}{\pi R} \int_0^{k_F} dk k \sin(kR) e^{-i\varepsilon_k t} f(k). \quad (314)$$

For $t > 0$, the result is given by

$$V_x(R, t > 0) = -\frac{1}{iG_0(R, t)} \times \frac{2}{\pi R} \int_{k_F}^\infty dk k \sin(kR) e^{-i\varepsilon_k t} f(k). \quad (315)$$

2. Correlation potential

Similarly, the correlation potential is given by the first moment in R' of the spherical average of the correlation hole in Eqs. (300) and (301). The integral to be evaluated is

$$I(k, k', t) = \int dR' R' Q(k, k', R', t) = \int dR' \int_{-1}^1 dy \frac{\sin(qR')}{q} M(q, \varepsilon_{k'} - \varepsilon_k, t) = \int_{-1}^1 dy \frac{1}{q^2} M(q, \varepsilon_{k'} - \varepsilon_k, t), \quad (316)$$

where $q = |\mathbf{k} - \mathbf{k}'| = \sqrt{k^2 + k'^2 - 2kk'y}$ and Q is defined in Eq. (299). The result is given by

$$V_c(R, t < 0) = \frac{C_1 + C_2}{G_0(R, t < 0)}, \quad (317)$$

$$V_c(R, t > 0) = \frac{D_1 + D_2}{G_0(R, t > 0)}, \quad (318)$$

where

$$C_1 = \frac{1}{2\pi^3 R} \int_{k_F}^\infty dk' k' \sin(k'R) \int_0^{k_F} dk k^2 e^{-i\varepsilon_k t} I(k, k', t), \quad (319)$$

$$C_2 = \frac{1}{2\pi^3 R} \int_0^{k_F} dk k \sin(kR) e^{-i\varepsilon_k t} \int_{k_F}^\infty dk' k'^2 I(k, k', 0), \quad (320)$$

$$D_1 = \frac{1}{2\pi^3 R} \int_{k_F}^\infty dk' k' \sin(k'R) e^{-i\varepsilon_{k'} t} \times \int_0^{k_F} dk k^2 I(k, k', 0), \quad (321)$$

$$D_2 = \frac{1}{2\pi^3 R} \int_0^{k_F} dk k \sin(kR) \times \int_{k_F}^\infty dk' k'^2 e^{-i\varepsilon_{k'} t} I(k, k', -t). \quad (322)$$

Within the plasmon-pole approximation, Eq. (304),

$$M(q, \varepsilon_{k'} - \varepsilon_k, t'') = \frac{\omega_p}{2} \frac{-ie^{i\omega_p t''}}{\omega_p + \varepsilon_{k'} - \varepsilon_k}, \quad (323)$$

which partially decouples the interdependence of \mathbf{k} and \mathbf{k}' , allowing for analytical integration over the solid angles of both variables, yielding

$$C_1 = P_1(R, t, 0, t), \quad (324)$$

$$C_2 = P_2(R, t, 0, 0), \quad (325)$$

$$D_1 = P_1(R, 0, t, 0), \quad (326)$$

$$D_2 = P_2(R, 0, t, -t), \quad (327)$$

where

$$P_1(R, t, t', t'') = \frac{-i\omega_p e^{i\omega_p t''}}{4\pi^3 R} \int_0^{k_F} dk \int_{k_F}^{\infty} dk' k \sin(k'R) \\ \times \frac{e^{-i\varepsilon_k t} e^{-i\varepsilon_{k'} t'}}{\omega_p + \varepsilon_{k'} - \varepsilon_k} \ln \left| \frac{k + k'}{k - k'} \right|, \quad (328)$$

$$P_2(R, t, t', t'') = \frac{-i\omega_p e^{i\omega_p t''}}{4\pi^3 R} \int_0^{k_F} dk \int_{k_F}^{\infty} dk' k' \sin(kR) \\ \times \frac{e^{-i\varepsilon_k t} e^{-i\varepsilon_{k'} t'}}{\omega_p + \varepsilon_{k'} - \varepsilon_k} \ln \left| \frac{k + k'}{k - k'} \right|. \quad (329)$$

Due to the use of the plasmon-pole approximation, the upper limit of the integral over k' is restricted to $1.5k_F$ for $r_s = 4$ to reproduce approximately the static correlation hole, as described earlier in Sec. XVII C.

The real and imaginary parts of V_{xc} of the homogeneous electron gas with $r_s = 4$ for a couple of typical times corresponding to the plasmon energy and the Fermi energy are shown in Figs. 13 and 14. The strong cancellation between exchange and correlation potentials is illustrated in Fig. 15.

E. Effective potential Ξ_q in the homogeneous electron gas

In this section, the quasiparticle equation with effective potential Ξ_q derived in Sec. XIV B is worked out for the homogeneous electron gas [66]. Using the approximate form of the effective potential in Eq. (172) the static and dynamic terms are modelled with parameters determined from *GW* calculations. The parameters are functions of density, and the model provides a realisation of LDA.

For the homogeneous electron gas, the deviation potential defined in Eq. (168) is given by $\Delta V = V_{xc}$ since V_{xc}^0 is a constant and can be set to zero. Plane waves are the natural choice for the orbitals,

$$\varphi_k(r) = \frac{e^{i\mathbf{k}\cdot\mathbf{r}}}{\sqrt{\Omega}}. \quad (330)$$

The quasiparticle wave function for a given momentum k is given by

$$\psi_k^*(r, t) = G_k(t) \frac{e^{-i\mathbf{k}\cdot\mathbf{r}}}{\sqrt{\Omega}}. \quad (331)$$

Multiplying Eq. (166) by $e^{-i\mathbf{q}\cdot(\mathbf{r}-\mathbf{r}')}/\Omega$, integrating over r and r' , and using

$$\int d^3R e^{i\mathbf{q}\cdot\mathbf{R}} = (2\pi)^3 \delta(\mathbf{q}), \quad (332)$$

lead to the equation of motion for $t \neq 0$ and a given spin:

$$(i\partial_t - \varepsilon_q)G_q(t) - \frac{1}{\Omega} \sum_{\mathbf{k}} V_{|\mathbf{q}-\mathbf{k}|}^{\text{xc}}(t)G_k(t) = 0, \quad (333)$$

where

$$V_{|\mathbf{q}-\mathbf{k}|}^{\text{xc}}(t) = \frac{1}{\Omega^2} \int d^3r d^3r' e^{-i(\mathbf{q}-\mathbf{k})\cdot(\mathbf{r}-\mathbf{r}')} V^{\text{xc}}(|\mathbf{r}-\mathbf{r}'|, t) \\ = \frac{1}{\Omega} \int d^3R e^{-i(\mathbf{q}-\mathbf{k})\cdot\mathbf{R}} V^{\text{xc}}(R, t). \quad (334)$$

The equation of motion can be recast as

$$[i\partial_t - \varepsilon_q - \Xi_q(t)]G_q(t) = 0, \quad (335)$$

where

$$\Xi_q(t) = \frac{1}{\Omega} \sum_{\mathbf{k}} V_{|\mathbf{q}-\mathbf{k}|}^{\text{xc}}(t) \frac{G_k(t)}{G_q(t)}. \quad (336)$$

For $t < 0$, $\Xi_q(t)$ an approximate model as in Eq. (172) is

$$\Xi_q(t < 0) \approx \Xi_q^S + \Xi_q^D e^{i\omega_p t}, \quad (337)$$

where

$$\omega_p = \sqrt{4\pi\rho} \quad (338)$$

is the plasmon energy of the electron gas with density ρ . A simple model for Ξ_q^S is

$$\Xi_q^S = (1 - \gamma Z)(E_F - \varepsilon_q). \quad (339)$$

Here, Z is the quasiparticle renormalisation factor which reduces the bandwidth and $\gamma > 1$ is a factor which takes into account band broadening due to the momentum-dependence of the self-energy. Both Z and γ are assumed to be momentum independent. The model ensures that the noninteracting occupied bandwidth is reduced by a combined factor γZ , and the new and the noninteracting Fermi levels have been realigned.

The solution is given by

$$G_q(t) = G_q(0) e^{-iE_q t} e^{-i \int_0^t dt' \Xi_q^D e^{i\omega_p t'}} \\ = G_q(0) e^{-iE_q t} (A_0 + A_1 e^{i\omega_p t} + A_2 e^{i2\omega_p t} + \dots), \quad (340)$$

where

$$E_q = \varepsilon_q + \Xi_q^S \quad (341)$$

is the quasiparticle energy. Expanding the second exponent up to two plasmon energies and defining

$$\lambda = -\frac{\Xi_q^D}{\omega_p}, \quad (342)$$

one finds

$$A_0 = 1 - \lambda + \frac{1}{2}\lambda^2, \quad (343)$$

$$A_1 = \lambda(1 - \lambda), \quad (344)$$

$$A_2 = \frac{1}{2}\lambda^2. \quad (345)$$

Note that $A_0 + A_1 + A_2 = 1$. It is straightforward to include higher-order plasmon excitations. In this simple model, it is assumed that for $q \leq k_F$ the spectrum does not have weight above the Fermi level. It is possible to construct a model that includes a weight transfer above the Fermi level [45]. This assumption implies that $G_q(0) = 1$ and Ξ_q^D is then determined by the renormalization of the quasiparticle $Z = A_0$, resulting in

$$\lambda = 1 - \sqrt{2Z - 1}. \quad (346)$$

In general, Ξ_q^S is complex, and its imaginary part gives a life-time broadening of the quasiparticle and the plasmon satellite. A model for the life-time broadening, which depends linearly on the inverse lifetime, is given by

$$\eta(q) = \eta_0 + (\eta_1 - \eta_0) \frac{E_F - \varepsilon_q}{E_F - \varepsilon_0}. \quad (347)$$

In theory, η_0 should be zero at $q = k_F$ but it is taken as finite to give a broadened δ -function.

With $G_q(0) = 1$ the Fourier transform of $G_q(t)$ in Eq. (340) is given by

$$G_q(\omega) = \frac{A_0}{\omega - E_q - i\eta(q)} + \frac{A_1}{\omega - E_q + \omega_p - i\eta(q)} + \frac{A_2}{\omega - E_q + 2\omega_p - i\eta(q)}. \quad (348)$$

The spectrum, which is proportional to the imaginary part of $G_q(\omega)$, exhibits the expected peaks at the quasiparticle energy E_q and at multiples of the plasmon satellite energy below the quasiparticle energy, $E_q - \omega_p$, $E_q - 2\omega_p$, ..., in agreement with the result obtained from the cumulant expansion [70, 71, 73–75]. Fig. 16 and Fig. 17 show the parametrized γ and Z and the life-time broadening η_1 , respectively, as functions of r_s . They are extracted from one-shot *GW* [17] calculations for the homogeneous electron gas. The combined factor γZ provides a measure of band narrowing. As anticipated, the lower the density (larger r_s), the stronger the band narrowing.

The model given in Eq. (348) is now applied to solid Na. Na is bcc with lattice constant $a = 4.29$ Å and one s valence electron per unit cell, which corresponds to $r_s = 4.0$ (a.u.). The energy dispersion corresponding to $r_s = 4.0$ is shown in Fig. 18 and compared with the noninteracting dispersion. The total and $q = 0$ spectral functions are shown in Figs. 19 and 20. The calculated total spectral function of Na is in close agreement with the measured photoemission spectrum [76] and the result obtained using the cumulant expansion method [73]. Note that the model does not take into account the effects of band structure. The spectrum exhibits the characteristic main quasiparticle peak followed by plasmon satellites separated by multiples of the plasmon energy. An additional plasmon lifetime tends to shift the plasmon peak to a slightly lower energy.

Fig. 20 shows the calculated spectral function at the Γ point ($q = 0$), which is compared with the one obtained from a standard one-shot *GW* calculation. The

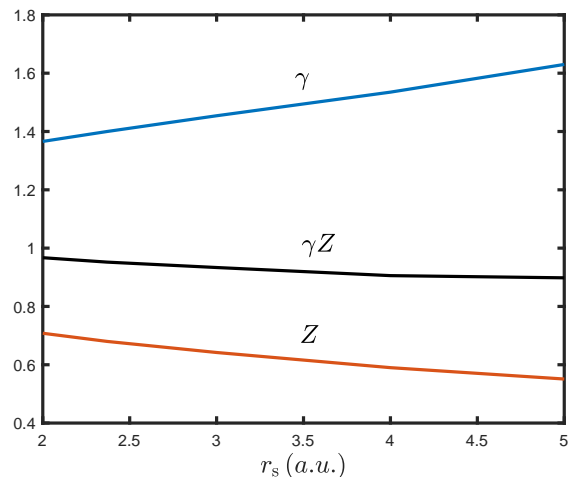


FIG. 16. The momentum-broadening factor γ and the quasiparticle renormalization factor Z as described in the text extracted from *GW* calculations of the homogeneous electron gas. γZ corresponds to the band narrowing. The renormalization factor Z is taken to be the average of the values at $q = 0$ and $q = k_F$.

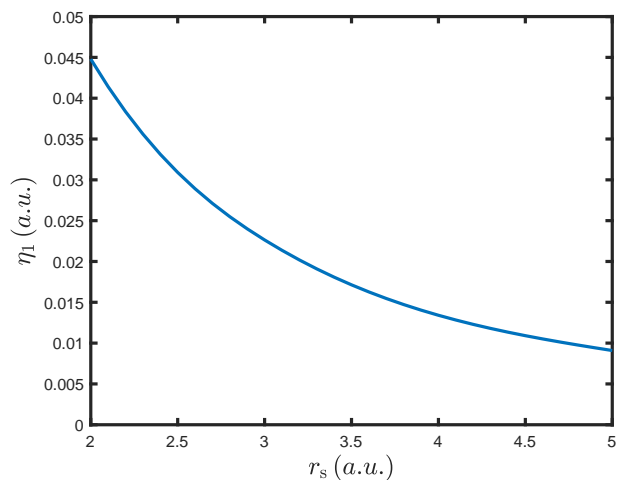


FIG. 17. The lifetime broadening factor (η_1 in Eq. (347)) obtained from *GW* calculations of the homogeneous electron gas as a function of r_s .

GW spectral function suffers from the well-known overestimation of the plasmon binding energy.

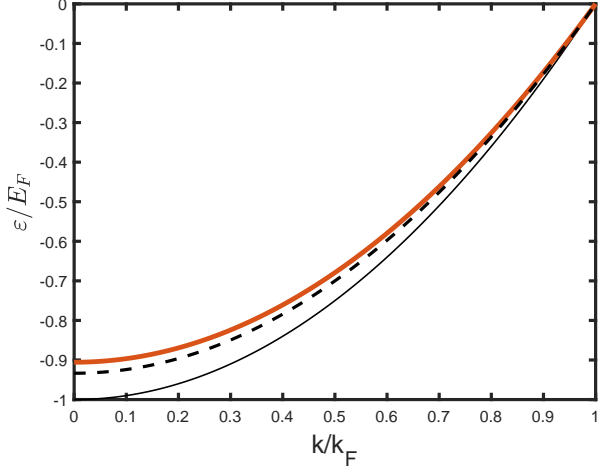


FIG. 18. The energy dispersion of the homogeneous electron gas with $r_s = 4.0$ a.u. corresponding to Na (thick solid line) and $r_s = 2.37$ a.u. corresponding to Al (dashed line) calculated using the model described in the text. For comparison, the dispersion of the noninteracting electron gas is also shown (thin solid line).

1. Local-density approximation

From the ansatz in Eq. (339), a possible local-density approximation [2–4] for simple metals is

$$\Xi_q^S(r) = [1 - \gamma(\bar{\rho})Z(\bar{\rho})] \left(\frac{1}{2} [3\pi^2 \rho(r)]^{2/3} - \varepsilon_q \right), \quad (349)$$

where

$$\bar{\rho} = \frac{1}{\Omega} \int dr \rho(r) \quad (350)$$

is the average density. Both γ and Z can be calculated as functions of the electron gas density $\bar{\rho}$ within the *GW* approximation [17] or using more accurate approximations [77, 78]. Alternatively, they can also be treated as fitting parameters. The plasmon energy ω_p is given by Eq. (338) with $\rho = \bar{\rho}$ which together with Z determines Ξ_q^D using Eq. (346).

XVIII. APPLICATIONS TO MODEL HAMILTONIANS

A. One-dimensional Hubbard model

The first application of the V_{xc} formalism is to calculate the Green function for the half-filled one-dimensional (1D) Hubbard chain [44] with the Hamiltonian given by

$$\hat{H} = -\Delta \sum_{i \neq j} \hat{c}_{i\sigma}^\dagger \hat{c}_{j\sigma} + U \sum_i \hat{n}_{i\uparrow} \hat{n}_{i\downarrow}. \quad (351)$$

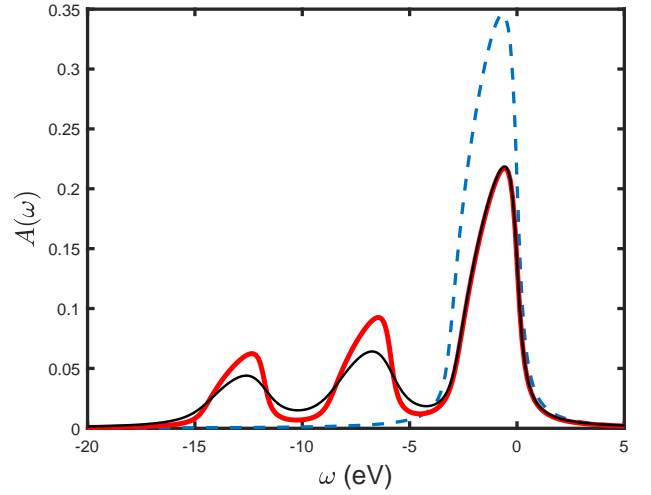
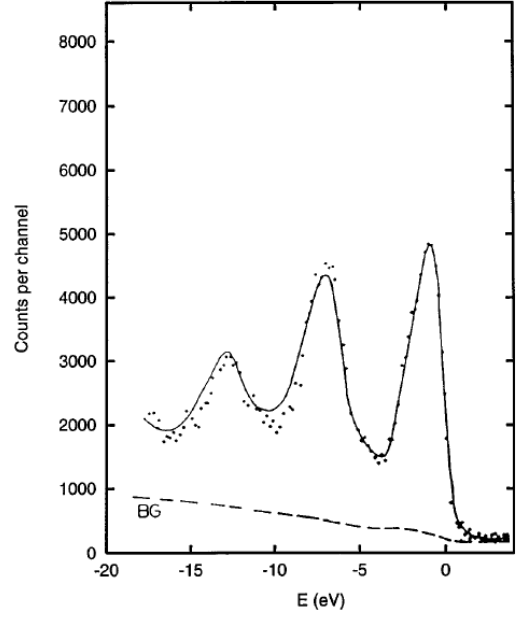


FIG. 19. The total spectral function of Na: experiment [76] (top) and calculated using the model described in the text with $r_s = 4.0$ (bottom). The thin solid line includes a plasmon broadening of 0.55 eV, which tends to shift the peak to lower energy. The noninteracting electron gas total spectrum corresponding to $r_s = 4.0$ is also shown (dashed line). The figure is taken from [66].

V_{xc} derived analytically for the Hubbard dimer will be used and extrapolated to the lattice case. Since V_{xc} of the Hubbard dimer only contains information about the onsite and nearest-neighbour sites, this approximation clearly neglects components of V_{xc} beyond nearest neighbours.

For the Hubbard chain which possesses lattice translation symmetry, it is convenient to introduce Bloch base

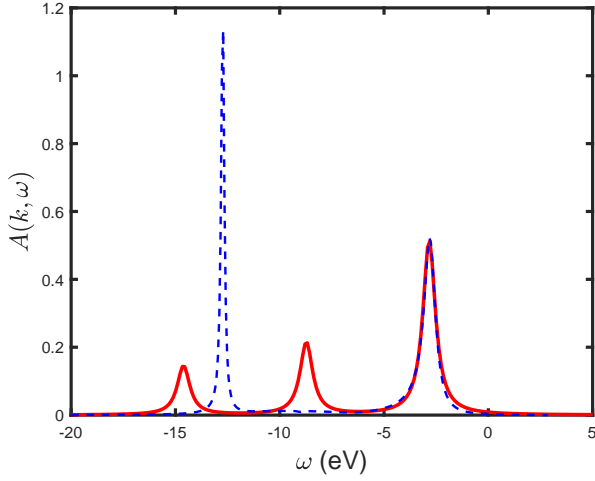


FIG. 20. The spectral function $A(k, \omega) = \frac{1}{\pi} \text{Im}G(k, \omega)$ of Na at the Γ -point ($k = 0$) calculated using the model described in the text (solid line). The dashed line is the GW spectral function of the homogeneous electron gas with $r_s = 4.0$. It shows the well-known overestimation of the plasmon binding energy in the GW approximation.

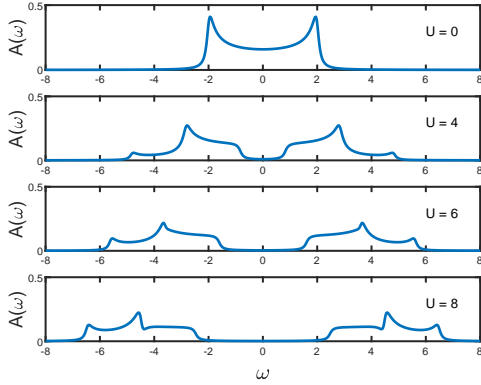


FIG. 21. The calculated total spectral functions of the 1D Hubbard model for $U = 0, 4, 6$, and 8 using approximations described in the text. A broadening of 0.1 has been used [44].

functions,

$$\varphi_k(r) = \frac{1}{\sqrt{N}} \sum_T e^{ikT} \varphi(r - T), \quad (352)$$

where T denotes a lattice site. The Green function expressed in these Bloch functions takes the form

$$G(r, r'; t) = \sum_k \varphi_k(r) G(k, t) \varphi_k^*(r'), \quad (353)$$

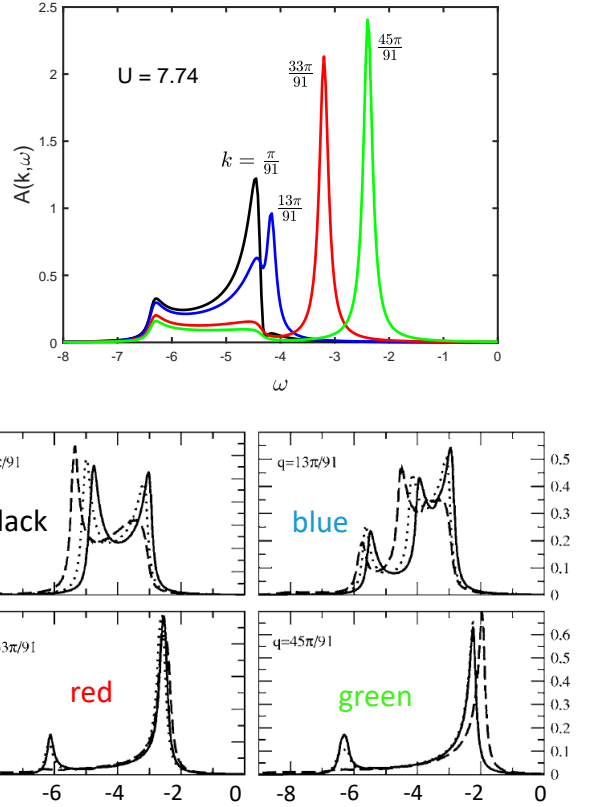


FIG. 22. The k -resolved spectral functions of the 1D Hubbard chain for $U = 7.74$ (upper figure) [44]. The U and k values have been chosen to facilitate comparison with Fig. 11 of Benthien and Jeckelmann [79], reproduced in the lower figure. For ease of comparison, the corresponding colour of each curve in the upper figure is indicated in the lower figure. A broadening of 0.1 has been used.

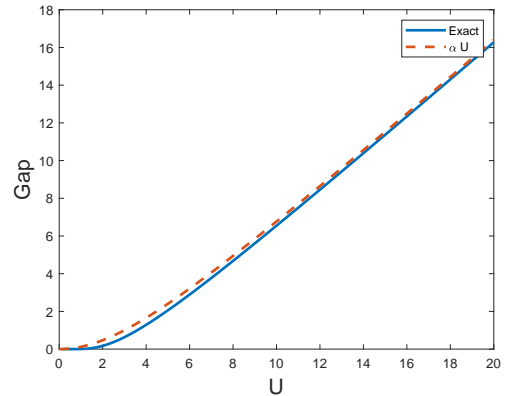


FIG. 23. The calculated band gap, αU , compared with the exact gap obtained from the Bethe ansatz as a function of U . The calculated gap approaches the exact result as U increases [44].

where

$$G(k, t) = \int dr dr' \varphi_k^*(r) G(r, r'; t) \varphi_k(r'). \quad (354)$$

The equation of motion in the Bloch base functions is obtained by inserting the expansion in Eq. (353) in Eq. (44), yielding

$$(i\partial_t - \varepsilon_q)G(q, t) - F(q, t) = \delta(t), \quad (355)$$

where

$$\begin{aligned} \varepsilon_q &= \int dr \varphi_q^*(r) h(r) \varphi_q(r) \\ &= \frac{1}{N} \sum_{TT'} e^{-ik(T-T')} \int dr \varphi^*(r-T) h(r) \varphi(r-T') \\ &= -2\Delta \cos q \end{aligned} \quad (356)$$

and

$$\begin{aligned} F(q, t) &= \sum_k \int dr dr' \\ &\times \varphi_q^*(r) \varphi_k(r) V_{xc}(r, r'; t) \varphi_k^*(r') \varphi_q(r') \times G(k, t). \end{aligned} \quad (357)$$

Because the site occupation number is uniform, the Hartree potential is constant and can be absorbed into the chemical potential. The terms $k \neq q$ in the summation over k in $F(q, t)$ describe the coupling between the propagator of momentum q and the rest of the propagators.

To utilise V^{xc} deduced for the Hubbard dimer, consider the equations of motion of the dimer Green function in the bonding and antibonding orbitals, which are given by

$$[i\partial_t - \varepsilon_A - V^{xc}(t)] G_A(t) - \Delta V^{xc}(t) G_B(t) = \delta(t), \quad (358)$$

$$[i\partial_t - \varepsilon_B - V^{xc}(t)] G_B(t) - \Delta V^{xc}(t) G_A(t) = \delta(t), \quad (359)$$

where

$$\varepsilon_A = \Delta, \quad \varepsilon_B = -\Delta, \quad (360)$$

are the one-particle antibonding and bonding energies. $V^{xc} = V_{BB}^{xc}$ and $\Delta V^{xc} = V_{AB}^{xc}$ are given in Eqs. (248) and (249), respectively. Eqs. (358) and (359) can be thought of as a special case of Eq. (355) with only two k points corresponding to the bonding and antibonding states. These two states may be regarded as the centre of the occupied and unoccupied bands of the one-dimensional Hubbard chain.

Comparison between Eq. (355) and Eq. (358) or (359) offers a physically motivated approximation: G_A or G_B is replaced by $G(q, t)$ and G_B or G_A by the average $\frac{1}{N} \sum_k G(k, t)$:

$$[i\partial_t - \varepsilon_q - V^{xc}(t)] G(q, t) - \frac{1}{N} \sum_k \Delta V^{xc}(t) G(k, t) = \delta(t). \quad (361)$$

The above equation can be rewritten as

$$[i\partial_t - \varepsilon_q - V^{xc}(t) - \Delta V^{xc}(q, t)] G(q, t) = \delta(t), \quad (362)$$

where

$$\Delta V^{xc}(q, t) = \frac{1}{N} \sum_k \Delta V^{xc}(t) \frac{G(k, t)}{G(q, t)}. \quad (363)$$

In terms of the effective potential Ξ defined in Eq. (170), it can be recognised that

$$\Xi(q, t) = V^{xc}(t) + \Delta V^{xc}(q, t). \quad (364)$$

The solution for the electron case ($t > 0$) is assumed to be given by

$$G^e(q, t) = -i\theta(t) e^{-i\varepsilon_q t - i \int_0^t dt' [V^{xc}(t') + \Delta V^{xc}(q, t')]} \quad (365)$$

This solution assumes that the weight is unity whereas in reality it should be renormalised to the quasiparticle weight. A similar result can be derived for the hole Green function, keeping in mind that $V^{xc}(-t) = -V^{xc}(t)$.

To proceed further, the following approximation is proposed:

$$\Delta V^{xc}(q, t) \approx \frac{1}{N} \sum_k \Delta V^{xc}(t) e^{-i(\varepsilon_k - \varepsilon_q)t}, \quad (366)$$

which corresponds to replacing G by a noninteracting G^0 . Furthermore, to facilitate analytical calculations $V^{xc} = V_{BB}^{xc}$ and $\Delta V^{xc} = V_{AB}^{xc}$ in Eqs. (248) and (249) are truncated as follows:

$$V^{xc}(t) \approx \frac{\alpha U}{2}, \quad (367)$$

$$\Delta V^{xc}(t) \approx \frac{\alpha U}{2} (1 - \alpha^2) e^{-i2\Delta t}. \quad (368)$$

The first term, which is a constant, shifts the one-particle energy whereas the second term, corresponding to the coupling between the propagator $G(q, t)$ and the rest of the system, gives rise to the main satellite. The higher excitation term $\exp(-i4\Delta t)$ is neglected.

To first order in ΔV^{xc} ,

$$\begin{aligned} G^e(q, t) &= -i\theta(t) e^{-i(\varepsilon_q + \frac{\alpha U}{2})t} \\ &\times \left\{ 1 - i \frac{\alpha U}{2} (1 - \alpha^2) \frac{1}{N} \sum_k \int_0^t dt' e^{-i(\varepsilon_k - \varepsilon_q + 2\Delta)t'} \right\}. \end{aligned} \quad (369)$$

Performing the time integral,

$$\begin{aligned} G^e(q, t) &= -i\theta(t) e^{-i(\varepsilon_q + \frac{\alpha U}{2})t} \\ &\times \left\{ 1 + \frac{\alpha U}{2} (1 - \alpha^2) \frac{1}{N} \sum_k \frac{e^{-i(\varepsilon_k - \varepsilon_q + 2\Delta)t} - 1}{\varepsilon_k - \varepsilon_q + 2\Delta} \right\}. \end{aligned} \quad (370)$$

Its Fourier transform is given by

$$G^e(q, \omega) = \frac{A_0^e(q)}{\omega - (\varepsilon_q + \frac{\alpha U}{2}) + i\eta} + \frac{1}{N} \sum_k \frac{A^e(q, k)}{\omega - (\varepsilon_k + \frac{\alpha U}{2} + 2\Delta) + i\eta}, \quad (371)$$

where

$$A_0^e(q) = 1 - \frac{\alpha U}{2}(1 - \alpha^2) \frac{1}{N} \sum_k \frac{1}{\varepsilon_k - \varepsilon_q + 2\Delta}, \quad (372)$$

$$A^e(q, k) = \frac{\alpha U}{2}(1 - \alpha^2) \frac{1}{\varepsilon_k - \varepsilon_q + 2\Delta}. \quad (373)$$

A similar derivation for the hole Green function yields

$$G^h(q, t) = i\theta(-t)e^{-i(\varepsilon_q - \frac{\alpha U}{2})t} \times \left\{ 1 - \frac{\alpha U}{2}(1 - \alpha^2) \frac{1}{N} \sum_k \frac{e^{-i(\varepsilon_k - \varepsilon_q - 2\Delta)t} - 1}{\varepsilon_k - \varepsilon_q - 2\Delta} \right\}, \quad (374)$$

$$G^h(q, \omega) = \frac{A_0^h(q)}{\omega - (\varepsilon_q - \frac{\alpha U}{2}) - i\eta} - \frac{1}{N} \sum_k \frac{A^h(q, k)}{\omega - (\varepsilon_k - \frac{\alpha U}{2} - 2\Delta) - i\eta}, \quad (375)$$

where

$$A_0^h(q) = 1 + \frac{\alpha U}{2}(1 - \alpha^2) \frac{1}{N} \sum_k \frac{1}{\varepsilon_k - \varepsilon_q - 2\Delta}, \quad (376)$$

$$A^h(q, k) = \frac{\alpha U}{2}(1 - \alpha^2) \frac{1}{\varepsilon_k - \varepsilon_q - 2\Delta}. \quad (377)$$

For the electron case, both ε_k and ε_q correspond to unoccupied states while for the hole case, to occupied states.

Fig. 21 shows the total spectral functions for $U = 0, 4, 6$, and 8 . Fig. 22 displays k -resolved spectra for a number of k -points for $U = 7.74$. For the purpose of comparison, the chosen values of k and U coincide with those of the benchmark results obtained using the dynamical density-matrix renormalisation group method [79]. Since in Eq. (363) the Green function is approximated by the noninteracting one, the electron Green function does not contribute to spectral weight below the chemical potential. Similarly, the hole Green function makes no contribution to spectral weight above the chemical potential. Furthermore, the use of the noninteracting Green function neglects life-time effects so that the peaks are sharp δ -functions with a renormalised weight due to weight transfer to lower or higher energy. The angle-resolved spectra consists of two branches; a spinless holon (antiholon) dispersion with a hole (electron) charge and a

charge-neutral spinon dispersion of spin $\frac{1}{2}$ [80]. Such an interpretation would probably require analysis in terms of state vectors, which are not accessible in Green function theory.

Despite the simplicity of the approximation used, the structure of the spectra of the benchmark results [79] is correctly reproduced as can be seen in Fig. 22. A major discrepancy is that for small k the peak positions are lower than the benchmark results, resulting in a wider dispersion for both the spinon and holon branches. This discrepancy can be traced back to the use of a noninteracting G^0 . A further factor that contributes to the discrepancy is the neglect of long-range correlations, which are expected to narrow the band dispersion. Evidently, the Hubbard dimer V^{xc} used in the approximation does not contain these long-range correlations beyond the nearest neighbours.

The analytic expression for the hole Green function in Eq. (375) provides a valuable means of understanding the structure of the calculated k -resolved hole spectra in Fig. 22. The first term gives rise to the main peak centred at $\omega = \varepsilon_q - \frac{\alpha U}{2}$ weighted by $A_0^h(q)$ and this peak corresponds to the spinon excitation. The second term is the noninteracting occupied density of states shifted by $-(\frac{\alpha U}{2} + 2\Delta)$ and weighted by $A^h(q, k)$. Taking the spectrum corresponding to $q = \frac{45\pi}{91}$ (green curve) as an example, the peak at around -2.4 is the spinon excitation. The low-energy spectra from -6.5 to -4.5 is the shifted occupied density of states weighted by $A^h(q, k)$, which indeed mimics the curve in Fig. 21 for $U = 0$. The feature at -6.5 is interpreted as the holon excitation. The structure at around -4.5 is largest for small q close to the bottom of the noninteracting band since the main peak merges with the shifted density of states. For $q = \frac{13\pi}{91}$ the main peak separates from the shifted density of states resulting in a three-peak structure, which is also found in the benchmark results [79].

The calculated band gap, αU , is shown Fig. 23 and in strikingly good agreement with the exact result obtained from the Bethe ansatz [81],

$$E_{\text{gap}} = \frac{16\Delta^2}{U} \int_1^\infty dy \frac{\sqrt{y^2 - 1}}{\sinh\left(\frac{2\pi\Delta y}{U}\right)}. \quad (378)$$

In the large- U limit the calculated gap reproduces the exact gap. The calculated gap is nonzero for any finite U as in the exact case. At small values of U , it is larger than the exact one. This discrepancy could be attributed to the lack of long-range correlations in the dimer V^{xc} discussed earlier, resulting in a too large effective U and consequently a larger band gap.

It is interesting to make a comparison with the result obtained from the dynamical mean-field theory (DMFT) [82]. Within the single-site approximation, the system remains metallic until $U > 6$. This is not inconsistent with the present result since V^{xc} is based on the Hubbard dimer. Indeed, a cluster DMFT with an even number of sites produces a gap for any finite U . With an

odd number of sites, there exists a coexistence region in which the system remains metallic before entering the Mott insulating regime after exceeding a certain value of U [83].

To improve the calculated angle-resolved spectra, V_{xc} derived from a larger cluster with six sites is used [84]. The results are shown in Fig. 24. The agreement with the benchmark density matrix renormalisation group (DMRG) results shown in Fig. 22 is markedly improved compared with the one based on the dimer V_{xc} .

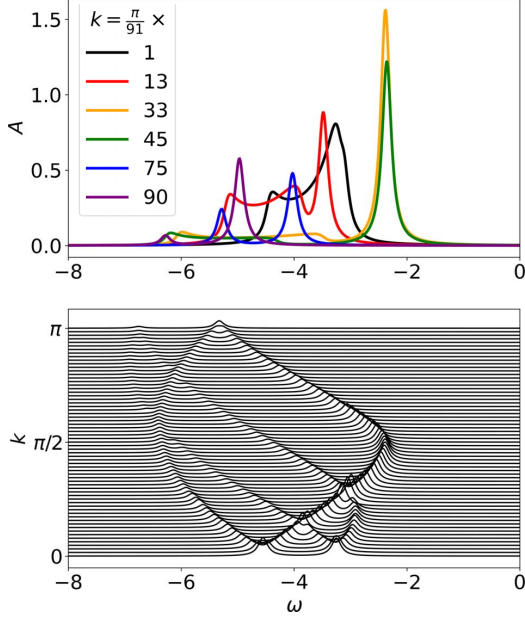


FIG. 24. The calculated angle-resolved spectra with improved V_{xc} obtained from a six-site cluster. The bottom figure shows a two-dimensional plot of k versus ω . The agreement with the benchmark DMRG result is clearly much improved compared with the one based on the dimer V_{xc} [84].

B. One-dimensional Heisenberg model

The V_{xc} formalism has also been extended to spin systems and applied to the paradigmatic 1D antiferromagnetic (AF) Heisenberg model with encouraging results [84].

The 1D Heisenberg spin model with a nearest-neighbour coupling is given by

$$\begin{aligned}\hat{H} &= -J \sum_i \hat{\mathbf{S}}_i \cdot \hat{\mathbf{S}}_{i+1} \\ &= -J \sum_i \left\{ \frac{1}{2} (\hat{S}_i^+ \hat{S}_{i+1}^- + \text{h.c.}) + \hat{S}_i^z \hat{S}_{i+1}^z \right\},\end{aligned}\quad (379)$$

where

$$\hat{S}_i^\pm = \hat{S}_i^x \pm i\hat{S}_i^y. \quad (380)$$

Experimentally of particular interest is the transverse-spin dynamical structure factor,

$$S^{+-}(k, \omega) = \frac{1}{N} \sum_{mn} \int dt \langle \hat{S}_m^+(t) \hat{S}_m^-(0) \rangle e^{i\omega t} e^{-ik(m-n)}, \quad (381)$$

where the expectation value is taken with respect to the ground state, and $\hat{S}_m^\pm(t)$ are the spin field operators in the Heisenberg picture. Here, m and n are site labels, and k is a momentum label. The transverse-spin Green function is defined as

$$iG_{ij}(t) = \langle \hat{S}_i^+(t) \hat{S}_j^-(0) \rangle \theta(t) + \langle \hat{S}_j^-(0) \hat{S}_i^+(t) \rangle \theta(-t). \quad (382)$$

Its equation of motion reads

$$i\partial_t G_{ij}(t) - F_{ij}(t) = 2\delta_{ij}\delta(t) \langle \hat{S}_i^z \rangle, \quad (383)$$

where the interaction term is given by

$$F_{ij}(t) = -i \sum_m J_{im} [\langle m, ij \rangle - \langle i, mj \rangle]. \quad (384)$$

Note that this definition differs slightly from the one in Ref. [84]. Here

$$\langle m, ij \rangle = \langle T \hat{S}_m^z(t) \hat{S}_i^+(t) \hat{S}_j^-(0) \rangle, \quad (385)$$

$$J_{im} = J(\delta_{m,i+1} + \delta_{m,i-1}). \quad (386)$$

In analogy with the charge case, the spin V_{xc} can be defined as

$$V_{ii,jj}^{xc}(t) G_{ij}(t) = F_{ij}(t) - V_i^H G_{ij}(t) - \sum_m V_{im}^F G_{mj}(t), \quad (387)$$

where V^H and V^F are the analogue of the Hartree and Fock potentials:

$$V_i^H = \sum_m J_{im} \langle \hat{S}_m^z \rangle, \quad (388)$$

$$V_{im}^F = -J_{im} \langle \hat{S}_i^z \rangle. \quad (389)$$

A spin correlator $g_{mij}(t)$ can now be defined such that

$$\begin{aligned}-i\langle m, ij \rangle &= \langle \hat{S}_m^z \rangle g_{mij}(t) G_{ij}(t) \\ &= [\rho_{mij}^{xc}(t) + \langle \hat{S}_m^z \rangle] G_{ij}(t),\end{aligned}\quad (390)$$

where the spin xc hole is given by

$$\rho_{mij}^{xc}(t) = \langle \hat{S}_m^z \rangle [g_{mij}(t) - 1]. \quad (391)$$

Since

$$\begin{aligned}\langle m, ij \rangle &= \theta(t) \langle \hat{S}_m^z(t) \hat{S}_i^+(t) \hat{S}_j^-(0) \rangle \\ &\quad + \theta(-t) \langle \hat{S}_j^-(0) \hat{S}_m^z(t) \hat{S}_i^+(t) \rangle,\end{aligned}\quad (392)$$

it follows that

$$-i \sum_m \langle m, ij \rangle = [\theta(-t) + S^z] G_{ij}(t), \quad (393)$$

where $S^z = \sum_m \langle \hat{S}_m^z \rangle$ is the total z component of the spin. The sum rule for the spin xc hole is then given by

$$\sum_m \rho_{mij}^{\text{xc}}(t) = \theta(-t). \quad (394)$$

$$V_{11,11}^{\text{xc}}(t > 0) = -J \frac{(\frac{(xy+x)(xy+x+2y)}{a_+^2})f_1 + (x^2+x)f_2 + (\frac{(xy-3x)(xy-3x+2y-4)}{a_-^2})f_3}{(\frac{xy+x+2y}{a_+})^2 f_1 + x^2 f_2 + (\frac{xy-3x+2y-4}{a_-})^2 f_3} \quad (395)$$

where $x = 1 + \sqrt{3}$, $y = 1 + \sqrt{2}$, $a_{\pm} = \sqrt{8 \pm 4\sqrt{2}}$, and $f_{i=1,2,3}$ are time oscillation factors determined by the difference between the spin excitation energies and the ground state energy. The rest of the matrix elements of V^{xc} can be found in Ref. [84].

As in the dimer case, it is fruitful to work in the bonding-antibonding-like orbitals ϕ_{μ} in view of an extrapolation to the infinite lattice case. These are linear combinations of the site-orbitals

$$\phi_{\mu} = \sum_i \varphi_i U_{i\mu}, \quad (396)$$

where $\mu = A, B, C, D$, $i = 1, 2, 3, 4$, and the unitary transformation matrix U is

$$U = \frac{1}{2} \begin{pmatrix} 1 & 1 & 1 & 1 \\ 1 & -1 & 1 & -1 \\ 1 & 1 & -1 & -1 \\ 1 & -1 & -1 & 1 \end{pmatrix}. \quad (397)$$

For the Green function, the transformation reads

$$G_{\mu\nu} = \sum_{ij} U_{\mu i}^{\dagger} G_{ij} U_{j\nu}, \quad (398)$$

The corresponding V^{xc} in the new basis is given by

$$V_{\mu\alpha, \beta\nu}^{\text{xc}}(t) := \sum_{mn} U_{\mu m}^{\dagger} U_{m\alpha} V_{mm, nn}^{\text{xc}}(t) U_{\beta n}^{\dagger} U_{n\nu} \quad (399)$$

so that the equation of motion is now

$$i\partial_t G_{\mu\nu}(t) - \sum_{\alpha\beta} V_{\mu\alpha, \beta\nu}^{\text{xc}}(t) G_{\alpha\beta}(t) = s_{\mu\nu} \delta(t), \quad (400)$$

where

$$s_{\mu\nu} = 2 \sum_i U_{\mu i}^{\dagger} \langle S_i^z \rangle U_{i\nu}. \quad (401)$$

Note that the xc hole is defined with opposite sign to that in Ref. [84].

1. A four-site spin chain

Before considering the infinite lattice, it is instructive to consider a minimal cluster with an even number of sites for which the V^{xc} is nonzero and can be calculated analytically. This simplest cluster reveals features which are likely to be generic. As an illustration, one of the diagonal elements is [84]

To compute the Green function for positive time,

$$G_{ij}(t) = \langle \Psi | e^{iHt} \hat{S}_i^+ e^{-iHt} \hat{S}_j^- | \Psi \rangle, \quad (402)$$

where $|\Psi\rangle$ is the ground state, one needs to use a complete set of eigenstates $|n\rangle$, which give nonzero weight elements $\langle n | \hat{S}_j^- | \Psi \rangle$. For an even number of sites and AF coupling, the total z -spin of $|\Psi\rangle$ is zero, which means that the states $\{|n\rangle\}$ are in the $S^z = -1$ sector. Labeling the eigenenergy corresponding to state $|n\rangle$ with E_n^- , the Green function can be written as

$$G_{ij}(t > 0) = \sum_n e^{-i(E_n^- - E^0)t} \langle \Psi | \hat{S}_i^+ | n \rangle \langle n | \hat{S}_j^- | \Psi \rangle, \quad (403)$$

and the high-order term for positive time is

$$\langle l, ij \rangle_{t>0} = \sum_n e^{-i(E_n^- - E^0)t} \langle \Psi | \hat{S}_l^z \hat{S}_i^+ | n \rangle \langle n | \hat{S}_j^- | \Psi \rangle. \quad (404)$$

By diagonalising the Hamiltonian in the $S^z = 0$ and $S^z = -1$ sectors, one gets $\{|\Psi\rangle; E^0\}$ and $\{|n\rangle; E_n^-\}$, respectively, and thus the weight elements $\langle n | \hat{S}_j^- | \Psi \rangle$ and $\langle \Psi | \hat{S}_l^z \hat{S}_i^+ | n \rangle$, respectively. Among the four states of $|n\rangle$, only three give nonzero $\langle n | \hat{S}_q^- | \Psi \rangle$. Explicitly, the time factors are

$$f_1 = e^{-i(E_0^- - E^0)t} = e^{iJ(\frac{\sqrt{3}-\sqrt{2}+1}{2})t}, \quad (405)$$

$$f_2 = e^{-i(E_1^- - E^0)t} = e^{iJ(\frac{\sqrt{3}+1}{2})t}, \quad (406)$$

$$f_3 = e^{-i(E_2^- - E^0)t} = e^{iJ(\frac{\sqrt{3}+\sqrt{2}+1}{2})t}. \quad (407)$$

The independent elements of V^{xc} in orbital basis can be calculated using $V_{ii,jj}^{\text{xc}}(t) = \frac{F_{ij}(t)}{iG_{ij}(t)}$.

Consider the equation of motion of the diagonal term

$G_{\mu\mu}$:

$$[i\partial_t - V_{\mu\mu,\mu\mu}^{\text{xc}}]G_{\mu\mu}(t) - \sum_{\gamma \neq \mu} V_{\mu\gamma,\gamma\mu}^{\text{xc}}(t)G_{\gamma\gamma}(t) - \sum_{\gamma \neq \delta} V_{\mu\gamma,\delta\mu}^{\text{xc}}(t)G_{\gamma\delta}(t) = s_{\mu\mu}\delta(t). \quad (408)$$

The contribution from fully off-diagonal terms $V_{\mu\nu,\delta\mu}^{\text{xc}}$ should be negligible and the higher excitation term f_3 can be neglected since the weight is relatively small. With these in mind, one arrives at an approximate expression for the matrix elements of $V_{\mu\gamma,\gamma\mu}^{\text{xc}}$:

$$V_{BD,DB}^{\text{xc}}(t > 0) \approx 0, \quad (409)$$

$$V_{BA,AB}^{\text{xc}}(t > 0) \approx 0, \quad (410)$$

$$V_{BB,BB}^{\text{xc}}(t > 0) \approx -J\alpha, \quad (411)$$

$$V_{BC,CB}^{\text{xc}}(t > 0) \approx -J\beta \exp\left[\frac{iJt}{\sqrt{2}}\right], \quad (412)$$

where

$$\alpha := \frac{xy+x}{xy+x+2y} = \frac{2x+2}{xy+x+2}, \quad (413)$$

$$\beta := \frac{1}{4} \left(\frac{a_+}{xy+x+2y} + \frac{a_+}{xy+x+2} \right)^2 (x^2 + x - \alpha x^2). \quad (414)$$

As in Eq. (395), $a_+ = \sqrt{8+4\sqrt{2}}$. The analytic spinon V^{xc} in the bonding-like basis and its approximation are shown in Fig. 25. Ignoring the high-excitation factor f_3 reduces the fine-structure details in V^{xc} . Consequently, $V_{BB,BB}^{\text{xc}}$ simplifies to a constant whereas $V_{BC,CB}^{\text{xc}}$ oscillates with a single frequency and a constant magnitude, and all other components are negligible.

2. Extrapolation to the infinite lattice

For the infinite lattice it is natural to use a Bloch basis:

$$G(k, t) = \frac{1}{N} \sum_{ij} G_{ij}(t) e^{-ik(i-j)}, \quad (415)$$

$$V^{\text{xc}}(k, t) = \frac{1}{N^2} \sum_{ij} V_{ii,jj}^{\text{xc}}(t) e^{-ik(i-j)}. \quad (416)$$

The equation of motion becomes

$$i\partial_t G(k, t) - \sum_q V^{\text{xc}}(k-q, t) G(q, t) = 2s\delta(t), \quad (417)$$

where $s = \langle \hat{S}_i^z \rangle$, which is independent of the lattice site due to translational symmetry.

The effect of V^{xc} on G can be decomposed into a static (S) and a dynamic (D) part:

$$\sum_q V^{\text{xc}}(k-q, t) G(q, t) = [V^{\text{S}}(k) + V^{\text{D}}(k, t)] G(k, t). \quad (418)$$

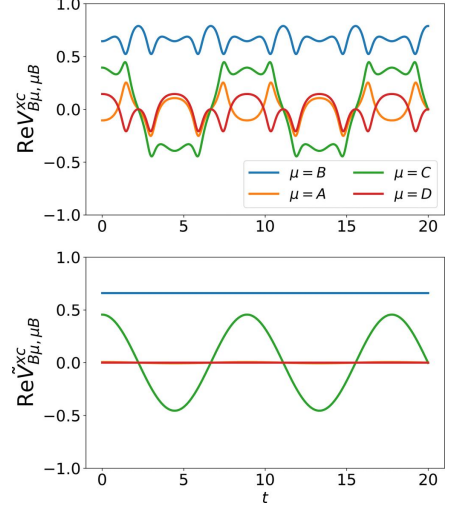


FIG. 25. Real part of V^{xc} of four-site spin- $\frac{1}{2}$ AF Heisenberg chain, in the unit of $|J|$ [84]. Top panel: exact. Bottom panel: results when the high-excitation contribution is ignored (see Eqs. (412-414) and related discussion).

The effective potential Ξ defined in Eq. (170) can be identified as

$$\Xi(k, t) = V^{\text{S}}(k) + V^{\text{D}}(k, t). \quad (419)$$

The solution to the equation of motion for $t > 0$ is then

$$G(k, t) = G(k, 0^+) e^{-iV^{\text{S}}(k)t} e^{-i \int_0^t dt' V^{\text{D}}(k, t')}. \quad (420)$$

The first term on the right-hand side of the above expression can be interpreted as the main quasiparticle excitation whereas the second to an incoherent or satellite feature.

For the antiferromagnetic case ($J < 0$) that will be considered here, it is known that the spinon dispersion has a lower (L) and an upper (U) boundary:

$$\Omega^{\text{L}}(k) = -J\frac{\pi}{2} |\sin k|, \quad (421)$$

$$\Omega^{\text{U}}(k) = -J\pi \sin \frac{k}{2}. \quad (422)$$

A reference Green function is constructed to reproduce the lower boundary by choosing $V^{\text{S}}(k) = \Omega^{\text{L}}(k)$ yielding

$$G^{\text{ref}}(k, \omega) = \frac{1}{\omega - \Omega^{\text{L}}(k)}. \quad (423)$$

To solve for the full G the dynamical component $V^{\text{D}}(k, t)$ is needed, which is obtained by extrapolation from a finite cluster.

Fig. 26 displays the real part of $V^{\text{D}}(k, t)$, which reveals that for each k , $\text{Re} V^{\text{D}}(k, t)$ oscillates in time around a

momentum-dependent term. This behaviour reflects a single quasiparticle-like main excitation. Based on this observation, a physically motivated ansatz for $V^D(k, t)$ in the infinite-chain case is

$$V^D(k, t) = \mathcal{A}(k)e^{-i\omega^{\text{sp}}(k)t} + \mathcal{B}(k), \quad (424)$$

where the amplitude \mathcal{A} , the spinon excitation energy ω^{sp} , and the shift term \mathcal{B} increase monotonically as k increases from 0 to π . Inserting this ansatz into Eq.(420) yields

$$G(k, t > 0) = G(k, 0^+)e^{-i[V^S(k) + \mathcal{B}(k)]t} \times e^{\frac{\mathcal{A}(k)}{\omega^{\text{sp}}(k)}(e^{-i\omega^{\text{sp}}(k)t} - 1)}, \quad (425)$$

where the static potential is $V^S(k) = -J\pi|\sin k|/2$.

Expanding the last term on the RHS of Eq.(425) to first order in $e^{-i\omega^{\text{sp}}(k)t}$ leads to

$$G(k, t > 0) \approx G(k, 0^+)e^{-i[V^S(k) + \mathcal{B}(k)]t} \times \left[1 + \frac{\mathcal{A}(k)}{\omega^{\text{sp}}(k)}(e^{-i\omega^{\text{sp}}(k)t} - 1)\right], \quad (426)$$

which in the frequency domain becomes

$$G(k, \omega) = G(k, 0^+) \left[\frac{1 - \frac{\mathcal{A}(k)}{\omega^{\text{sp}}(k)}}{\omega - [V^S(k) + \mathcal{B}(k)]} + \frac{\frac{\mathcal{A}(k)}{\omega^{\text{sp}}(k)}}{\omega - [V^S(k) + \mathcal{B}(k) + \omega^{\text{sp}}(k)]} \right]. \quad (427)$$

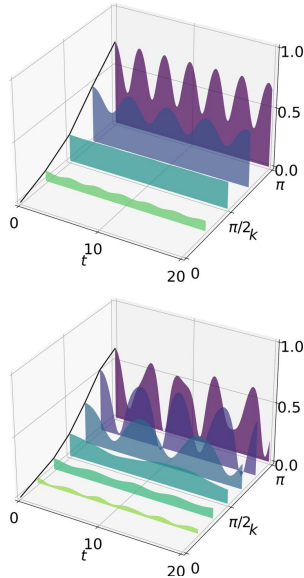


FIG. 26. Real part of V^D from a spin- $\frac{1}{2}$ AF Heisenberg ring [84]. Top (bottom) panel: results for a ring with 8 (12) sites. The number of available k -points is equal to half the number of sites.

The above equation shows that the dynamical structure factor consists of a main peak centred at $\omega = V^S + \mathcal{B}$ followed by a satellite peak separated from the main peak by the spinon energy ω^{sp} . Spectral weight in the amount of $\frac{\mathcal{A}(k)}{\omega^{\text{sp}}(k)}$ is transferred from the main peak to the satellite. Due to finite-size effects, the finite cluster solution gives nonzero \mathcal{B} at $k = \pi$, which opens a spin gap that is not present for the spin- $\frac{1}{2}$ lattice. To account for these finite-size effects, \mathcal{B} is adjusted to a smaller value in our extrapolation.

Based on the preceding discussion, the lattice V^{xc} is obtained by extrapolation from the cluster result. With V^D obtained by an exact diagonalisation of a cluster of 12 sites, the parameters \mathcal{A} , \mathcal{B} and $G(k, 0^+)$ are estimated by linear interpolation. The spinon excitation energy is estimated by fitting the cluster ω^{sp} to the two-spinon spectrum boundary,

$$\omega^{\text{sp}} \rightarrow (-J)\pi \left(\sin \frac{k}{2} - \frac{1}{2}|\sin k| \right). \quad (428)$$

The longitudinal and transverse spin dynamical structure factors are then calculated from the spinon Green function. For a spin-isotropic system S^{zz} and S^{+-} differ by a constant factor. For this reason only the spectral function of the Green function in Eq. (425) is calculated and the result is shown in Fig. 27. Comparison with the spin dynamical structure factor measured in inelastic neutron scattering for the 1D compound KCuF_3 [85] shows close agreement in both the peak locations and the relative weights.

A notable feature of the dynamical structure factor $S(k, \omega)$ shown in the bottom panel of Fig. 27 is that the weight of the main peak is close to zero at small k and increases with k reaching a maximum at $k \rightarrow \pi$. The spectrum with a broadening factor of 0.1 is gapless. The result agrees well with that calculated using DMRG shown in Fig. 28.

Although the extrapolation procedure may leave out fine details of the spectra, it captures most of the essential physical characteristics of the 1D AF Heisenberg model with a very low computational load. This appealing feature of the method is expected to also apply in more challenging situations, for example, in higher dimensions and realistic materials, where rigorous references such as the Bethe ansatz are not available.

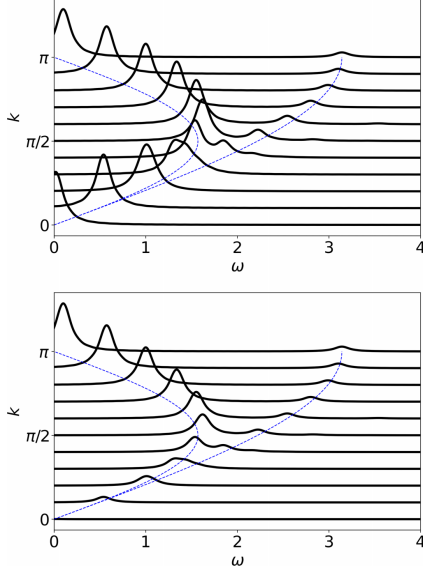


FIG. 27. Dynamic structure factor of 1D spin- $\frac{1}{2}$ AF Heisenberg lattice calculated with an extrapolated V^{xc} , with broadening 0.1 [84]. Top panel: weight factor $G(k, t=0)$ considered as unit. Bottom panel: weight renormalised with cluster $G(k, 0^+)$. Blue dashed curves are the boundaries for two-spinon processes.

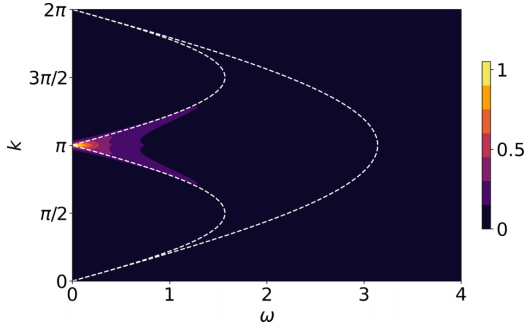


FIG. 28. Dynamic structure factor of a 100-site 1D spin- $\frac{1}{2}$ AF Heisenberg chain calculated within DMRG [84]. The weight is renormalised to be in the range 0-1.

C. The single-impurity Anderson model

The single-impurity Anderson model describes an impurity with a few discrete levels embedded in a bath of noninteracting conduction electrons with a continuous degree of freedom. Although it is seemingly a simple model, it is relevant in a wide range of physical phenomena such as the Kondo effect and quantum transport. In particular, it plays an important role as an auxiliary system in dynamical mean-field theory, a method of choice for treating strongly-correlated materials from first principles in combination with DFT and GW method.

The treatment in this section follows closely the work of Zhao [86]. The single-impurity Anderson model

(SIAM) is given by

$$\hat{H}_{\text{SIAM}} = \epsilon_f(\hat{n}_{f\uparrow} + \hat{n}_{f\downarrow}) + U\hat{n}_{f\uparrow}\hat{n}_{f\downarrow} + \sum_{k\sigma} \left[\epsilon_k \hat{c}_{k\sigma}^\dagger \hat{c}_{k\sigma} + (v_k \hat{f}_\sigma^\dagger \hat{c}_{k\sigma} + \text{h.c.}) \right]. \quad (429)$$

Here \hat{f}_σ^\dagger (\hat{f}_σ) creates (annihilates) an electron with spin σ on the impurity site, $\hat{n}_\sigma = \hat{f}_\sigma^\dagger \hat{f}_\sigma$ is the corresponding number operator, $\hat{c}_{k\sigma}^\dagger$ ($\hat{c}_{k\sigma}$) creates (annihilates) a bath electron with energy ϵ_k . The coupling between the impurity and bath electrons is given by the hybridisation amplitude v_k assumed to be spin independent, and ϵ_f and U are the impurity onsite energy and Coulomb interaction, respectively.

We consider a symmetric SIAM at half-filling, which means that the ensemble average

$$n_{f\sigma} = \text{Tr}\{\hat{\rho}_\beta \hat{n}_{f\sigma}\} = 0.5, \quad (430)$$

where the statistical operator and the partition function are given by, respectively,

$$\hat{\rho}_\beta = Z_\beta^{-1} e^{-\beta(\hat{H} - \mu \hat{N})}, \quad Z_\beta = \text{Tr}[e^{-\beta(\hat{H} - \mu \hat{N})}]. \quad (431)$$

β is the inverse temperature. The impurity level ϵ_f is chosen so that

$$\epsilon_f + \frac{U}{2} = 0. \quad (432)$$

In the limit of no hybridisation, the removal and addition impurity spectra consists of two peaks at ϵ_f and $\epsilon_f + U$. Setting the chemical potential in the middle of these two levels to zero leads to the choice in Eq. (432) yielding two peaks at $\pm \frac{U}{2}$. The hybridisation shifts and broadens the peaks and induces the Kondo peak at the chemical potential. The number of fermionic sites (impurity + bath) L is chosen to be even.

The equilibrium finite-temperature time-ordered Green function is given by

$$iG_{ff,\sigma}(t, \beta) = \langle T \hat{f}_\sigma(t) \hat{f}_\sigma^\dagger(0) \rangle := \text{Tr}\{\hat{\rho}_\beta [T \hat{f}_\sigma(t) \hat{f}_\sigma^\dagger(0)]\}, \quad (433)$$

where T is the time-ordering symbol. Its spectral decomposition is given by

$$\begin{aligned} iG_{ff,\sigma}(t, \beta) &= \theta(t) \frac{1}{Z_\beta} \sum_{mn} e^{-\beta E_m} e^{-i(E_n^+ - E_m)t} |\langle n^+ | \hat{f}_\sigma^\dagger | m \rangle|^2 \\ &\quad - \theta(-t) \frac{1}{Z_\beta} \sum_{mn} e^{-\beta E_m} e^{i(E_n^- - E_m)t} |\langle n^- | \hat{f}_\sigma | m \rangle|^2, \end{aligned} \quad (434)$$

where $|n^\pm\rangle$ are the $(L \pm 1)$ -electron eigenstates with eigenenergies E_n^\pm . Due to particle-hole symmetry of half-filling, it is only necessary to consider the case $t > 0$. The equation of motion of the Green function in the V^{xc} formalism is given by

$$[i\partial_t - \epsilon_f - V^{\text{H}} - V_\sigma^{\text{xc}}(t, \beta)] G_{ff,\sigma}(t, \beta) = \delta(t), \quad (435)$$

where the Hartree term

$$V^H = U n_{f\bar{\sigma}} = \frac{U}{2} \quad (436)$$

is due to the impurity electron with opposite spin $\bar{\sigma} = -\sigma$. The xc field V_{σ}^{xc} in the above equation of motion includes the hybridisation effects. The formal solution is given by

$$G_{ff,\sigma}(t, \beta) = G_{ff,\sigma}(0, \beta) e^{-i(\epsilon_f + V^H)t - i \int_0^t dt' V_{\sigma}^{\text{xc}}(t', \beta)}. \quad (437)$$

To investigate the effects of the hybridisation, it is useful to consider the noninteracting case ($U = 0$) at zero temperature. In this case the Green function can be solved analytically yielding

$$G_{ff,\sigma}(\omega) = \frac{1}{\omega - \epsilon_f - \Delta(\omega)}, \quad (438)$$

where

$$\Delta(\omega) = \sum_k \frac{|v_k|^2}{\omega - \epsilon_k} \quad (439)$$

is the hybridisation function. By modeling the continuous bath as a tight-binding ring with N_c sites and hopping strength t_h , and the impurity site couples to one site with strength V , $\Delta(\omega)$ can be calculated analytically. In this model, the SIAM parameters are given by

$$\epsilon_k = 2t_h \cos(k), \quad v_k = \frac{V}{\sqrt{N_c}}. \quad (440)$$

When $|\epsilon_f|, V \ll 2|t_h|$, we approach the so-called wide-band limit (WBL) so that the hybridisation function can be treated as a constant,

$$\Delta(\omega) = i\Gamma = i \frac{\pi V^2}{4t_h}. \quad (441)$$

This yields

$$V_{\text{nonint,WBL}}^{\text{xc}}(t) = i\Gamma\theta(-t). \quad (442)$$

The infinitely wide bath band results in a purely imaginary hybridisation field, leading to a broadening of the impurity level ϵ_f . This hybridisation effect persists in non-WBL or interacting cases.

Consider now the case of a finite but low temperature. Vxc can be obtained from Eqs. (434) and (435), yielding for $t > 0$

$$V_{\sigma}^{\text{xc}}(t > 0, \beta) = \frac{\sum_m e^{-\beta E_m} \sum_n a_{n,m}^+ \omega_{n,m}^+ e^{-i\omega_{n,m}^+ t}}{\sum_m e^{-\beta E_m} \sum_n a_{n,m}^+ e^{-i\omega_{n,m}^+ t}}, \quad (443)$$

where

$$\omega_{n,m}^+ = E_n^+ - E_m, \quad a_{n,m}^+ = |\langle n^+ | \hat{f}_{\sigma}^{\dagger} | m \rangle|^2. \quad (444)$$

At low temperature $e^{-\beta E_m}$ is negligible except for the two lowest eigenstates $m = 1, 2$. Vxc can be written as [86]

$$V_{\sigma}^{\text{xc}}(t, \beta) = V_{\sigma}^{\text{xc}}(t, T = 0) + \tilde{V}(t) e^{-\beta(E_2 - E_1)}. \quad (445)$$

The second term on the right-hand side is a thermal correction.

1. Impurity model with a single-site bath (dimer)

Before considering the full SIAM, it is instructive to study a dimer with U only on one site and the other site treated as a bath. This model can be solved analytically, providing valuable physical insights into some of the key features of the SIAM. In this highly simplified model, in which the bath is represented by one site, the Hamiltonian is given by

$$\hat{H}_{\text{dimer}} = \epsilon_f \sum_{\sigma} \hat{n}_{f\sigma} + U \hat{n}_{f\uparrow} \hat{n}_{f\downarrow} + V \sum_{\sigma} (\hat{f}_{\sigma}^{\dagger} \hat{c}_{\sigma} + \text{h.c.}). \quad (446)$$

Consider first the case of $T = 0$. In the Kondo regime ($U \gg V$), the particle part of Vxc ($t > 0$) has an approximate form [86]

$$V_{\sigma}^{\text{xc}}(t > 0, T = 0) \approx \omega_1 - \lambda \Omega e^{i\Omega t}, \quad (447)$$

where

$$\omega_1 = \sqrt{\frac{U^2}{16} + 4V^2} + \sqrt{\frac{U^2}{16} + V^2}, \quad (448)$$

$$\lambda \approx \frac{36V^2}{U^2}, \quad (449)$$

$$\Omega = \sqrt{\frac{U^2}{4} + 4V^2}. \quad (450)$$

Keeping in mind the condition in Eq. (436) and that for half-filling $V^H = \frac{U}{2}$, the impurity Green function according to Eq. (437) is given by

$$\begin{aligned} G_{ff,\sigma}(t, T = 0) &= g^+ e^{-i\omega_1 t + \lambda \Omega i \int_0^t dt' e^{i\Omega t'}} \\ &\approx g^+ e^{-i\omega_1 t} \left[1 + i\lambda \Omega \int_0^t dt' e^{i\Omega t'} \right] \\ &\approx g^+ [(1 - \lambda) e^{-i\omega_1 t} + \lambda e^{-i\omega_0 t}], \end{aligned} \quad (451)$$

where

$$g^+ = G_{ff,\sigma}(0, T = 0) = -0.5i, \quad (452)$$

$$\omega_0 = \omega_1 - \Omega \approx \frac{6V^2}{U}. \quad (453)$$

The particle-hole symmetric spectral function is then given by

$$\begin{aligned} A_{\text{dimer}}(\omega, T = 0) &= \frac{1 - \lambda}{2} [\delta(\omega + \omega_1) + \delta(\omega - \omega_1)] \\ &\quad + \frac{\lambda}{2} [\delta(\omega + \omega_0) + \delta(\omega - \omega_0)]. \end{aligned} \quad (454)$$

Some important features of SIAM can be deduced: for large U , there are two peaks ($\omega = \pm\omega_1$) corresponding to impurity levels ϵ_f and $\epsilon_f + U$. The excitation associated with energy Ω induces two central peaks at $\omega = \pm\omega_0 \approx 0$, which may be regarded as a harbinger of the Kondo resonance. However, for the dimer the spectral weight given in Eq. (449), $\frac{\lambda}{2} \sim (\frac{V}{U})^2$, vanishes as U increases. This can also be seen from V_{xc} in Eq. (447): with increasing U , the exponential term with amplitude $\lambda\Omega \sim \frac{V^2}{U}$ becomes negligible. The vanishing of the Kondo resonance is a consequence of having a single site instead of a continuous bath.

Consider now the case of a finite but low temperature. At low temperature, the term that oscillates with time in Eq. (445) can be written as [86]

$$\frac{\tilde{V}(t)}{V_{\sigma}^{xc}(t, T=0)} \approx \lambda_1 e^{i\Omega_1 t} - \lambda_2 e^{i\Omega_2 t}, \quad (455)$$

where

$$\lambda_1, \lambda_2 \sim \frac{V^2}{U^2}, \quad \Omega_1 \sim U, \quad \Omega_2 \sim \frac{V^2}{U}. \quad (456)$$

V_{xc} is then

$$V_{\sigma}^{xc}(t, \beta) \approx \omega_1 - \lambda\Omega e^{i\Omega t} + e^{-\beta\Delta_0} \omega_1 (\lambda_1 e^{i\Omega_1 t} - \lambda_2 e^{i\Omega_2 t}), \quad (457)$$

where $\Delta_0 \sim \frac{V^2}{U}$. At low temperature, the condition $e^{-\beta\Delta_0} \ll 1$ is valid. The particle ($\omega > 0$) spectral function is given by

$$\begin{aligned} A_{\text{dimer}}(\omega > 0, \beta) &\approx \frac{1 - \lambda - e^{-\beta\Delta_0} \omega_1 (\frac{\lambda_2}{\Omega_2} - \frac{\lambda_1}{\Omega_1})}{2} \delta(\omega - \omega_1) + \frac{\lambda}{2} \delta(\omega - \omega_0) \\ &+ \frac{e^{-\beta\Delta_0} \omega_1}{2} \left[\frac{\lambda_2}{\Omega_2} \delta(\omega - \tilde{\omega}_1) - \frac{\lambda_1}{\Omega_1} \delta(\omega - \tilde{\omega}_0) \right], \end{aligned} \quad (458)$$

where

$$\tilde{\omega}_0 = \omega_1 - \Omega_1, \quad \tilde{\omega}_1 = \omega_1 - \Omega_2. \quad (459)$$

The first two terms on the right-hand side of Eq. (458) correspond to the original zero-temperature peaks, while the last two terms, with weights proportional to $e^{-\beta\Delta_0}$, are referred to as thermal peaks, which are close to the original zero-temperature peaks. The mixture of a zero-temperature peak and a thermal peak which are close in energy induces a broadening of the zero-temperature peak with width given effectively by the energy difference between the two peaks.

2. Impurity coupled to a finite cluster

After studying the simplest impurity model, a dimer, we are in the position to consider a more realistic model in which the impurity is coupled to a bath with a finite

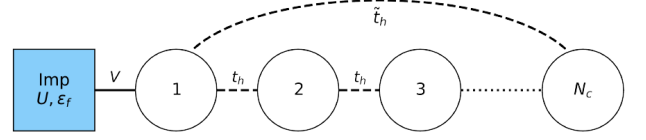


FIG. 29. Illustration of the single-impurity Anderson model with a bath of N_c sites. When a periodic boundary condition is applied ($\tilde{t}_h = t_h$) the SIAM parameters become $\epsilon = 2t_h \cos k$ and $v_k = \frac{V}{\sqrt{N_c}}$. The figure is taken from [86].

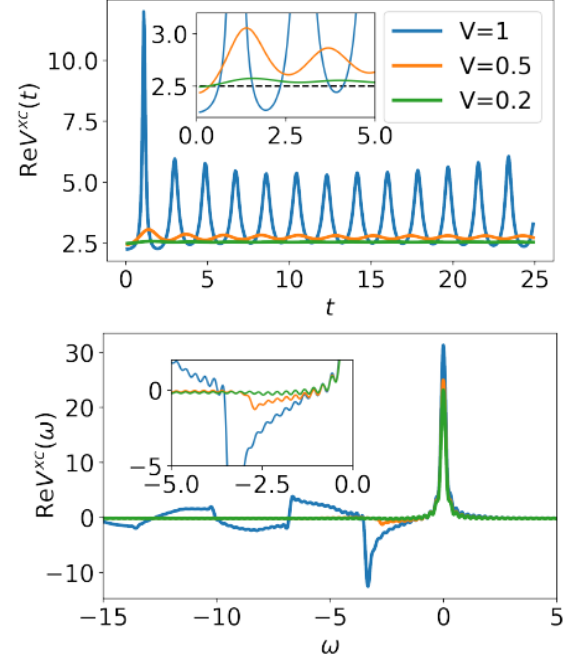


FIG. 30. Top: The real part of V_{xc} as a function of time. Bottom: The real part of V_{xc} as a function of frequency calculated with a broadening factor $\eta = 0.1$. The calculations have been performed at zero temperature with parameters $\epsilon_f = -2.5$, $U = 5$, and $t_h = -1$. The figure is taken from [86].

number N_c of noninteracting sites as illustrated in Fig. 29. The SIAM defined in Eq. (429) with

$$\epsilon_k = 2t_h \cos k, \quad v_k = \frac{V}{\sqrt{N_c}} \quad (460)$$

is reproduced in the limit $N_c \rightarrow \infty$.

Fig. 30 shows the numerically exact V_{xc} of the SIAM obtained with a bath consisting of a cluster of 50 sites [86]. $\text{Re}V_{xc}(t)$ exhibits the characteristic oscillating behaviour, of the form

$$V^{xc}(t) = \mathcal{A}e^{-i\omega_1 t} + \mathcal{C} \quad (461)$$

The hybridisation between the impurity and the bath requires a complex \mathcal{C} : $\text{Re } \mathcal{C}$ and $\text{Im } \mathcal{C}$ determine the peak position and the width of the Hubbard band, respectively. Moreover, unlike the dimer, ω_1 can be complex.

To develop an ansatz for V_{xc} , it is necessary to consider its limiting behaviour for large t . Since time and frequency are reciprocal variables, the large-time behaviour is determined by the low-frequency structure of the Green function. If Γ_K is the half-width of the Kondo resonance at low frequency, then at large time one expects

$$G_{ff,\sigma}(t > 0, \beta) \propto e^{-i\Gamma_K t}. \quad (462)$$

According to the formal solution in Eq. (437), the corresponding large- t V_{xc} is proportional to Γ_K . This together with the finite-cluster result leads to

$$V^{xc}(t > 0, \beta) \approx \begin{cases} \lambda \omega_1 e^{-i\omega_1 t} + \mathcal{C}, & \text{small } t \\ -i\Gamma_K, & \text{large } t \end{cases} \quad (463)$$

3. Ansatz for SIAM V_{xc}

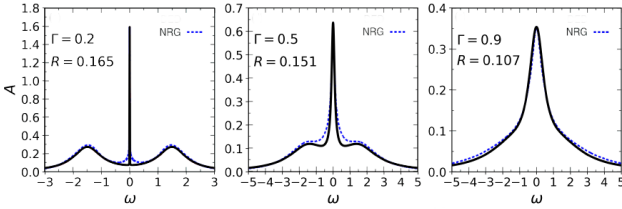


FIG. 31. The zero-temperature particle-hole symmetric SIAM spectra calculated with $U = 3$ and $t_h = 50$ to approach the wide-band limit and compared with benchmark results obtained using the numerical renormalisation group (NRG) method [86]. Γ is related to the height of the Kondo resonance as $A(\omega = 0) = \frac{1}{\pi\Gamma}$ and R is the ratio between the Hubbard and Kondo peaks. For details of the determination of the parameters defining the ansatz see Zhao [86].

An ansatz that fulfils the large- and small-time behaviour of V_{xc} is [86]

$$V^{xc}(t > 0, \beta) = \frac{\lambda(\omega_1 + \mathcal{C}) + (1 - \lambda)\mathcal{C}e^{i\omega_1 t}}{\lambda + (1 - \lambda)e^{i\omega_1 t}}. \quad (464)$$

Here, λ is real, ω_1 and \mathcal{C} are complex, and $\omega_1 + \mathcal{C} = -i\Gamma_K$ is temperature dependent. The fractional form follows the general solution in Eq. (443). The particle-hole symmetry implies that

$$V^{xc}(-t, \beta) = -V^{xc}(t, \beta). \quad (465)$$

According to the formal solution in Eq. (437) with $\epsilon_f + V^H = 0$,

$$G_{ff,\sigma}(t > 0, \beta) = -\frac{i}{2} \left[(1 - \lambda)e^{-i\mathcal{C}t} + \lambda e^{-i(\mathcal{C} + \omega_1)t} \right] \quad (466)$$

with the corresponding spectral function

$$A(\omega > 0, \beta) = \frac{1 - \lambda}{2\pi} \frac{|\text{Im } \mathcal{C}|}{(\omega - \text{Re } \mathcal{C})^2 + (\text{Im } \mathcal{C})^2} + \frac{\lambda}{2\pi} \frac{|\text{Im } (\mathcal{C} + \omega_1)|}{[\omega - \text{Re } (\mathcal{C} + \omega_1)]^2 + [\text{Im } (\mathcal{C} + \omega_1)]^2}. \quad (467)$$

The particle-hole symmetry provides the relation

$$A(\omega > 0, \beta) = A(-\omega, \beta). \quad (468)$$

The first term on the right-hand side of Eq. (467) can be recognised as the Hubbard side band located at $\omega = \text{Re } \mathcal{C}$ with a half width $\Gamma_H = |\text{Im } \mathcal{C}|$. The second term is the Kondo resonance located at $\omega = \text{Re } (\mathcal{C} + \omega_1) = 0$ with a half width $\Gamma_K = |\text{Im } (\mathcal{C} + \omega_1)|$.

The parameters defining the ansatz can be determined from cluster calculations with a bath consisting of fifty sites [86]. The calculated spectral functions are shown in Fig. 31 and compared with the benchmark results obtained using the numerical renormalisation group method. The close agreement attests to the correctness of the ansatz.

XIX. SUMMARY AND OUTLOOK

The V_{xc} formalism is complementary to the traditional self-energy approach. In contrast to the self-energy, which is usually expressed in momentum and frequency domains, V_{xc} is more naturally formulated in space and time domains. In the V_{xc} formalism, the xc hole is a fundamental quantity that generates V_{xc} as the Coulomb potential, and it is directly related to the ground-state electron density. This is similar to the Slater exchange hole, whose Coulomb potential is the Slater exchange potential. Thus, in the V_{xc} formalism, the many-electron problem associated with addition and removal of an electron is reduced to constructing for given r , r' , and t an approximate radial charge distribution (xc hole), which integrates to -1 (sum rule) and whose value at the origin is equal to the negative of the ground-state electron density (exact constraint). It is worth noting that only the spherical average of the xc hole is needed and only its first radial moment is relevant. This property suggests that V_{xc} is not sensitive to the detailed structure of the xc hole, which is known to partially explain the success of LDA in DFT. This opens the possibility of approximating V_{xc} as a functional of the electron density, for example, within LDA. The V_{xc} formalism can therefore be regarded as a density-functional approach to calculating the Green function from which one-particle excitation spectra can be extracted.

The V_{xc} formalism has been applied to a number of generic model Hamiltonians representing strongly correlated systems. These are the 1D half-filled Hubbard model, the 1D antiferromagnetic Heisenberg model, and the half-filled single-impurity Anderson model. By far,

these applications are based on an extrapolation procedure in which V_{xc} of a small cluster is calculated using an accurate numerical tool and the resulting V_{xc} is extrapolated to the model V_{xc} by means of a parametrisation. The results are in rather good agreement with benchmark results and suggest that it may be feasible to parametrise V_{xc} as a functional of the model parameters for a general filling. Such a parametrised V_{xc} is highly advantageous from the numerical point of view, since it would circumvent expensive computations in solving, for example, the impurity problem in DMFT.

To apply the local-density approximation, the xc hole and V_{xc} of the homogeneous electron gas have been calculated within the random-phase approximation. Due to the sum rule and the exact constraint, it is found that the xc hole is rather robust in the sense that it does not deviate drastically from the static xc hole. An encouraging finding is that there is a large cancellation between exchange and correlation potentials resulting in a generally smooth V_{xc} , rendering a local-density approximation may well be reasonable.

The equation of motion of the Green function in the V_{xc} formalism can be recast into a quasiparticle equation of motion. Each quasiparticle interacts with the rest of the quasiparticles through a (residual) xc field, thus providing a quantitative description of a many-electron system as a set of interacting quasiparticles as in Landau's phenomenological theory. The coupling between the quasiparticles can be absorbed into an effective field. An important finding is that this effective field, for systems that have been investigated so far, has a simple form consisting of a static term and a dynamic term. From the quasiparticle picture, the static term corrects the reference mean-field quasiparticle energy, while the dynamic term induces a coupling to the main collective excitation in the system, for example, plasmon, giving rise to an incoherent or a satellite feature. This simple physical

picture is very appealing, and in strong contrast to the self-energy picture.

One of the main challenges of the V_{xc} formalism is to construct simple but accurate approximations for V_{xc} or the effective field $\Xi_q(r, t)$. The availability of such approximations would avoid costly calculations of traditional self-energy. For systems with itinerant valence electrons as in alkali metals, the effective field is modelled as a functional of electron density, and the parameters are determined from GW calculations. A local-density approximation, which reproduces the results of the homogeneous electron gas in the limit of constant density, is then proposed. For more general systems and materials, machine learning and artificial intelligence can potentially play a crucial role in the search for accurate V_{xc} as a functional of density or model parameters. There is a large amount of data available in the literature on self-energy calculations based on the GW approximation and DMFT, which can be exploited to help construct the desired V_{xc} . This V_{xc} can be used to study complex systems that are too complicated to be treated using traditional self-energy methods.

The V_{xc} formalism originally developed for fermions can be extended to systems of bosons. Model systems describing a coupling between fermions and bosons can also be formulated in the V_{xc} language. The V_{xc} formalism may offer an alternative and simpler description of the many-body problem than traditional approaches.

ACKNOWLEDGMENTS

Financial support from the Swedish Research Council (Vetenskapsrådet, VR, Grant No. 2021.04498) is gratefully acknowledged.

-
- [1] P. Hohenberg and W. Kohn, Inhomogeneous electron gas, *Phys. Rev.* **136**, B864 (1964).
 - [2] W. Kohn and L. J. Sham, Self-consistent equations including exchange and correlation effects, *Phys. Rev.* **140**, A1133 (1965).
 - [3] R. O. Jones and O. Gunnarsson, The density functional formalism, its applications and prospects, *Rev. Mod. Phys.* **61**, 689 (1989).
 - [4] A. D. Becke, Fifty years of density functional theory in chemical physics, *J. Chem. Phys.* **140**, 18A301 (2014).
 - [5] R. O. Jones, Density functional theory: Its origins, rise to prominence, and future, *Rev. Mod. Phys.* **87**, 897 (2015).
 - [6] L. H. Thomas, The calculation of atomic fields, *Mathematical Proceedings of the Cambridge Philosophical Society* **23**, 542–548 (1927).
 - [7] E. Fermi, Eine statistische Methode zur Bestimmung einiger Eigenschaften des Atoms und ihre Anwendung auf die Theorie des periodischen Systems der Elemente, *Z. Physik* **48**, 73 (1928).
 - [8] A. D. Becke, A new mixing of Hartree–Fock and local density-functional theories, *J. Chem. Phys.* **98**, 1372 (1993).
 - [9] J. P. Perdew and M. Ernzerhof, Rationale for mixing exact exchange with density functional approximations, *J. Chem. Phys.* **105**, 9982 (1996).
 - [10] J. P. Perdew, K. Burke, and M. Ernzerhof, Generalized gradient approximation made simple, *Phys. Rev. Lett.* **77**, 3865 (1996).
 - [11] J. Heyd, G. E. Scuseria, and M. Ernzerhof, Hybrid functionals based on a screened Coulomb potential, *J. Chem. Phys.* **118**, 8207 (2003).
 - [12] K. Burke, J. P. Perdew, and M. Ernzerhof, Why the generalized gradient approximation works and how to go beyond it, *International Journal of Quantum Chemistry* **61**, 287 (1997).
 - [13] R. Nagai, R. Akashi, and O. Sugino, Completing density functional theory by machine learning hidden messages from molecules, *npj Comput Mater* **6**, 43 (2020).

- [14] L. Fiedler, K. Shah, M. Bussmann, and A. Cangi, Deep dive into machine learning density functional theory for materials science and chemistry, *Phys. Rev. Mater.* **6**, 040301 (2022).
- [15] L. J. Sham and W. Kohn, One-particle properties of an inhomogeneous interacting electron gas, *Phys. Rev.* **145**, 561 (1966).
- [16] D. Pines and D. Bohm, A collective description of electron interactions: II. Collective vs individual particle aspects of the interactions, *Phys. Rev.* **85**, 338 (1952).
- [17] L. Hedin, New method for calculating the one-particle Green's function with application to the electron-gas problem, *Phys. Rev.* **139**, A796 (1965).
- [18] L. Hedin and S. Lundqvist, Effects of electron-electron and electron-phonon interactions on the one-electron states of solids, in *Solid State Physics*, Vol. 23, edited by D. T. F. Seits and H. Ehrenreich (Academic Press, New York, 1969).
- [19] F. Aryasetiawan and O. Gunnarsson, The *GW* method, *Reports on Progress in Physics* **61**, 237 (1998).
- [20] G. Onida, L. Reining, and A. Rubio, Electronic excitations: Density-functional versus many-body Green's-function approaches, *Rev. Mod. Phys.* **74**, 601 (2002).
- [21] C. S. Wang and W. E. Pickett, Density-functional theory of excitation spectra of semiconductors: Application to Si, *Phys. Rev. Lett.* **51**, 597 (1983).
- [22] R. W. Godby, M. Schlüter, and L. J. Sham, Trends in self-energy operators and their corresponding exchange-correlation potentials, *Phys. Rev. B* **36**, 6497 (1987).
- [23] E. K. U. Gross, L. N. Oliveira, and W. Kohn, Density-functional theory for ensembles of fractionally occupied states. I. Basic formalism, *Phys. Rev. A* **37**, 2809 (1988).
- [24] L. N. Oliveira, E. K. U. Gross, and W. Kohn, Density-functional theory for ensembles of fractionally occupied states. II. Application to the He atom, *Phys. Rev. A* **37**, 2821 (1988).
- [25] T. Gould, G. Stefanucci, and S. Pittalis, Ensemble density functional theory: Insight from the fluctuation-dissipation theorem, *Phys. Rev. Lett.* **125**, 233001 (2020).
- [26] T. R. Scott, J. Kozłowski, S. Crisostomo, A. Pribram-Jones, and K. Burke, Exact conditions for ensemble density functional theory, *Phys. Rev. B* **109**, 195120 (2024).
- [27] M. J. Stott and E. Zaremba, Linear-response theory within the density-functional formalism: Application to atomic polarizabilities, *Phys. Rev. A* **21**, 12 (1980).
- [28] A. Zangwill and P. Soven, Density-functional approach to local-field effects in finite systems: Photoabsorption in the rare gases, *Phys. Rev. A* **21**, 1561 (1980).
- [29] E. Runge and E. K. U. Gross, Density-functional theory for time-dependent systems, *Phys. Rev. Lett.* **52**, 997 (1984).
- [30] C. A. Ullrich, *Time-Dependent Density-Functional Theory* (Academic, Oxford University Press, 2011).
- [31] in *Time-Dependent Density Functional Theory*, edited by M. Marques, C. Ullrich, F. Nogueira, A. Rubio, K. Burke, and E. K. U. Gross (Springer-Verlag (Lecture Notes in Physics), Berlin Heidelberg, 2006).
- [32] N. T. Maitra, Perspective: Fundamental aspects of time-dependent density functional theory, *The Journal of Chemical Physics* **144**, 220901 (2016).
- [33] D. Jacob and S. Kurth, Many-body spectral functions from steady state density functional theory, *Nano Letters* **18**, 2086 (2018).
- [34] S. Kurth and G. Stefanucci, Time-dependent i-DFT exchange-correlation potentials with memory: Applications to the out-of-equilibrium Anderson model, *Eur. Phys. J. B* **91**, 118 (2018).
- [35] F. Aryasetiawan, Time-dependent exchange-correlation potential in lieu of self-energy, *Phys. Rev. B* **105**, 075106 (2022).
- [36] J. C. Slater, A simplification of the Hartree-Fock method, *Phys. Rev.* **81**, 385 (1951).
- [37] J. C. Slater, Exchange in spin-polarized energy bands, *Phys. Rev.* **165**, 658 (1968).
- [38] N. W. Ashcroft and N. D. Mermin, *Solid State Physics* (Saunders College Publishing, Forth Worth, 1976).
- [39] B. Holm and U. von Barth, Fully self-consistent *GW* self-energy of the electron gas, *Phys. Rev. B* **57**, 2108 (1998).
- [40] R. van Leeuwen, O. Gritsenko, and E. J. Baerends, Step structure in the atomic Kohn-Sham potential, *Zeitschrift für Physik D Atoms, Molecules and Clusters* **33**, 229 (1995).
- [41] A. L. Fetter and J. D. Walecka, *Quantum Theory of Many-Particle Systems* (Dover, Mineola, New York, 2003).
- [42] J. W. Negele and H. Orland, *Quantum Many-Particle Systems* (Westview Press, Boulder, Colorado, 1998).
- [43] F. Aryasetiawan, *Elements of Green Function and Density Functional Theory* (World Scientific, Singapore, 2025).
- [44] F. Aryasetiawan and T. Sjöstrand, Spectral functions of the half-filled one-dimensional Hubbard chain within the exchange-correlation potential formalism, *Phys. Rev. B* **106**, 045123 (2022).
- [45] K. Karlsson and F. Aryasetiawan, Time-dependent exchange-correlation hole and potential of the electron gas, *Phys. Rev. B* **107**, 115172 (2023).
- [46] O. Gunnarsson and B. I. Lundqvist, Exchange and correlation in atoms, molecules, and solids by the spin-density-functional formalism, *Phys. Rev. B* **13**, 4274 (1976).
- [47] W. Kohn, Density functional and density matrix method scaling linearly with the number of atoms, *Phys. Rev. Lett.* **76**, 3168 (1996).
- [48] E. Prodan and W. Kohn, Nearsightedness of electronic matter, *Proceedings of the National Academy of Sciences* **102**, 11635 (2005).
- [49] E. Prodan, Nearsightedness of electronic matter in one dimension, *Phys. Rev. B* **73**, 085108 (2006).
- [50] O. Gunnarsson, M. Jonson, and B. I. Lundqvist, Descriptions of exchange and correlation effects in inhomogeneous electron systems, *Phys. Rev. B* **20**, 3136 (1979).
- [51] J. A. Alonso and L. A. Girifalco, Nonlocal approximation to the exchange potential and kinetic energy of an inhomogeneous electron gas, *Phys. Rev. B* **17**, 3735 (1978).
- [52] L. J. Sham and M. Schlüter, Density-functional theory of the energy gap, *Phys. Rev. Lett.* **51**, 1888 (1983).
- [53] D. Langreth and J. Perdew, The exchange-correlation energy of a metallic surface, *Solid State Communications* **17**, 1425 (1975).
- [54] R. van Leeuwen and E. J. Baerends, Exchange-correlation potential with correct asymptotic behavior, *Phys. Rev. A* **49**, 2421 (1994).
- [55] J. P. Perdew, R. G. Parr, M. Levy, and J. L. Balduz, Density-functional theory for fractional particle number: Derivative discontinuities of the energy, *Phys. Rev. Lett.* **49**, 1691 (1982).
- [56] M. Gatti, V. Olevano, L. Reining, and I. V. Tokatly,

- Transforming nonlocality into a frequency dependence: A shortcut to spectroscopy, *Phys. Rev. Lett.* **99**, 057401 (2007).
- [57] S. Y. Savrasov and G. Kotliar, Spectral density functionals for electronic structure calculations, *Phys. Rev. B* **69**, 245101 (2004).
- [58] F. Aryasetiawan, Continuity equation for the many-electron spectral function, *Phys. Rev. B* **108**, 115110 (2023).
- [59] N. N. Lathiotakis, N. Helbig, and E. K. U. Gross, Open shells in reduced-density-matrix-functional theory, *Phys. Rev. A* **72**, 030501 (2005).
- [60] N. N. Lathiotakis, N. Helbig, and E. K. U. Gross, Performance of one-body reduced density-matrix functionals for the homogeneous electron gas, *Phys. Rev. B* **75**, 195120 (2007).
- [61] S. Sharma, J. K. Dewhurst, N. N. Lathiotakis, and E. K. U. Gross, Reduced density matrix functional for many-electron systems, *Phys. Rev. B* **78**, 201103 (2008).
- [62] D. Gibney, J.-N. Boyn, and D. A. Mazziotti, Density functional theory transformed into a one-electron reduced-density-matrix functional theory for the capture of static correlation, *The Journal of Physical Chemistry Letters* **13**, 1382 (2022).
- [63] T. L. Gilbert, Hohenberg-Kohn theorem for nonlocal external potentials, *Phys. Rev. B* **12**, 2111 (1975).
- [64] L. D. Landau, The theory of a Fermi liquid, *Sov. Phys. JETP* **3**, 920 (1957).
- [65] L. D. Landau, Oscillations in a Fermi-liquid, *Sov. Phys. JETP* **5**, 101 (1957).
- [66] F. Aryasetiawan and K. Karlsson, Quasiparticle wave function and its equation of motion, *Phys. Rev. B* **111**, 075139 (2025).
- [67] M. Dvorak, Particle conservation in the single-particle Green's function, *arXiv:2101.00704 [cond-mat.str.el]* (2021).
- [68] D. C. Langreth, Singularities in the X-ray spectra of metals, *Phys. Rev. B* **1**, 471 (1970).
- [69] B. Bergersen, F. W. Kus, and B. C., Single particle Green's function in the electron-plasmon approximation, *Can. J. Phys.* **51**, 102 (1973).
- [70] L. Hedin, Effects of recoil on shake-up spectra in metals, *Physica Scripta* **21**, 477 (1980).
- [71] C.-O. Almbladh and L. Hedin, Beyond the one-electron model. many-body effects in atoms, molecules, and solids, in *Handbook of Synchrotron Radiation*, Vol. 1b, edited by E. Koch (North-Holland, 1983) pp. 607–904.
- [72] Y. Wang and J. P. Perdew, Correlation hole of the spin-polarized electron gas, with exact small-wave-vector and high-density scaling, *Phys. Rev. B* **44**, 13298 (1991).
- [73] F. Aryasetiawan, L. Hedin, and K. Karlsson, Multiple plasmon satellites in Na and Al spectral functions from ab initio cumulant expansion, *Phys. Rev. Lett.* **77**, 2268 (1996).
- [74] J. J. Kas, J. J. Rehr, and L. Reining, Cumulant expansion of the retarded one-electron Green function, *Phys. Rev. B* **90**, 085112 (2014).
- [75] J. J. Kas, T. D. Blanton, and J. J. Rehr, Exchange-correlation contributions to thermodynamic properties of the homogeneous electron gas from a cumulant Green's function approach, *Phys. Rev. B* **100**, 195144 (2019).
- [76] P. Steiner, H. Höchst, and S. Hüfner, Photoemission in Solids II, in *Topics in Applied Physics*, Vol. 27, edited by L. Ley and M. Cardona (Springer-Verlag, Berlin, Heidelberg, 1979) pp. 349–372.
- [77] S. Huotari, J. A. Soininen, T. Pylkkänen, K. Hämäläinen, A. Issolah, A. Titov, J. McMinis, J. Kim, K. Esler, D. M. Ceperley, M. Holzmann, and V. Olevano, Momentum distribution and renormalization factor in sodium and the electron gas, *Phys. Rev. Lett.* **105**, 086403 (2010).
- [78] J. Li and T. Zhu, Interacting-bath dynamical embedding for capturing nonlocal electron correlation in solids, *Phys. Rev. Lett.* **133**, 216402 (2024).
- [79] H. Benthien and E. Jeckelmann, Spin and charge dynamics of the one-dimensional extended Hubbard model, *Phys. Rev. B* **75**, 205128 (2007).
- [80] T. Giamarchi, *Quantum Physics in One Dimension* (Oxford University Press, 2004).
- [81] A. A. Ovchinnikov, Excitation spectrum in the one-dimensional Hubbard model, *Sov. Phys., JETP* **30**, 1160 (1970).
- [82] A. Georges, G. Kotliar, W. Krauth, and M. J. Rozenberg, Dynamical mean-field theory of strongly correlated fermion systems and the limit of infinite dimensions, *Rev. Mod. Phys.* **68**, 13 (1996).
- [83] A. Go and G. S. Jeon, Properties of the one-dimensional Hubbard model: Cellular dynamical mean-field description, *Journal of Physics: Condensed Matter* **21**, 485602 (2009).
- [84] Z. Zhao, C. Verdozzi, and F. Aryasetiawan, Dynamical exchange-correlation potential formalism for spin- $\frac{1}{2}$ Heisenberg and Hubbard chains: The antiferromagnetic/half-filled case, *Phys. Rev. B* **108**, 235132 (2023).
- [85] B. Lake, D. A. Tennant, J.-S. Caux, T. Barthel, U. Schollwöck, S. E. Nagler, and C. D. Frost, Multispinon continua at zero and finite temperature in a near-ideal Heisenberg chain, *Phys. Rev. Lett.* **111**, 137205 (2013).
- [86] Z. Zhao, Kondo spectral functions at low-temperatures: A dynamical-exchange-correlation-field perspective, *SciPost Phys.* **18**, 002 (2025).